Studies on a new low calcium amorphous hydraulic binder

Álvaro José Lebres Mendes

Thesis to obtain the Master of Science Degree in

Chemical Engineering

Supervisors

Dr. Rodrigo Manuel Lino Santos

Dr. Patrizia Paradiso

Examination Committee

Chairperson: Prof. Carla Isabel Costa Pinheiro

Supervisor: Dr. Rodrigo Manuel Lino Santos

Members of the Committee: Eng. João Carlos Ferreira Chaves Pereira

January 2021

Declaration

I declare that this document is an original work of my own authorship and that it fulfils all the requirements of the Code of Conduct and Good Practices of the Universidade de Lisboa.

Acknowledgements

This dissertation represents the end of one of the most important cycles of my life and, if I am concluding it now, I have to thank many people for all the support they have given me so far.

I thank Professor Rogério Colaço for being the first person to introduce me this project and to convince me to join it, for all the valuable knowledge shared in the group meetings and for all the support and confidence that he gave me during this dissertation.

I thank Professor Bayão Horta for all the technical expertise he offered in the group meetings and for the advices and words of confidence he has given me, which, taking into account all his experience in the academic world, represent a lot to me.

I thank my supervisor Eng. João Pereira, for receiving me in the central laboratory of CIMPOR in the best possible way, always guaranteeing the best conditions in the laboratory so that my work could be developed without any problems and for all the opinions, suggestions and knowledge that gave me in the course of this work.

I thank my supervisor, Dr. Patrizia Paradiso, for being the first person to accompany me on my first visit to the CIMPOR laboratory, for always being available to help me with whatever was necessary, for all the effort, concern and patience to review my thesis, always giving advice on what could be improved.

I thank my supervisor, Dr. Rodrigo Santos, for being a role model in what it means to be an engineer, for being the person who, within the project group, accompanied me the most during this work, always available to, not only help me in all the activities that I had to perform, but also in ensuring that I had the best resources and that I learned as much as possible, for all the tireless work that he did so that all the objectives of this thesis were achieved and by all advice on how to improve this dissertation and for my future life.

I thank all my friends, particularly João Simões, João Pinto, Carlos Carlos and Vera Atanásio, with whom I shared my 5 years at IST and who filled this journey with some of the most memorable experiences of my life.

I thank Adriana Carrolino, the best partner I could ask to accompany me throughout this journey that was my academic life and for all the adventures that will come in the future, for being the person who gives me all the attention and affection and love I need, in the best and worst moments, and that it is always available to make me see the positive side and to make me smile.

I thank my whole family, particularly my brother Frederico Mendes, my mother Maria Lebres and my father Daniel Mendes, for being the greatest source of motivation and confidence I could wish for, for giving me the best possible conditions to see all my goals achieved and for all the love that a brother and son can ask for in a family.

Abstract

In this dissertation, different alkaline activators were studied to improve the mechanical performance of the new amorphous hydraulic binder with low calcium content. In addition, the effects that fineness, the type of mill used for grinding and the storage time after grinding have on the reactivity of this binder were also studied. Finally, the optimization of the water/cement (W/C) ratio in alkaline-activated mortars was also studied in order to optimize the compressive strength performance and evaluate the necessary conditions to obtain a workability equivalent to that of a traditional cement. It was concluded that fineness has a strong influence on the initial reactivity of the amorphous, with this binder presenting competitive compressive strengths for a fineness similar to that of the OPC. In addition, it was found that the type of mill used and the storage time after milling do not significantly influence the reactivity of the amorphous. It was found that the alkaline activation with sodium sulphate and calcium sulphate do not present competitive results and also, the necessary amount of sodium silicate in the alkaline activation was optimized, reducing, at least, 25% of the previously used amount without negatively impacting its mechanical performance. It was also found that the best workability in mortar is achieved for a W/C ratio of 0.38, while the best mechanical performance is achieved for a proportion of 0.365.

Keywords: Amorphous hydraulic binders, fineness, grinding, storage time, alkaline activators, water/cement ratio optimization

Resumo

Nesta dissertação foram estudados diferentes ativadores alcalinos para melhorar o desempenho mecânico do novo ligante hidráulico amorfo com baixo teor de cálcio. Além disso, foram estudados os efeitos que a finura, o tipo de moinho utilizado para a moagem e o tempo de armazenamento após a moagem têm sobre a reatividade desse ligante. Por fim, foi estudada a otimização da relação água/cimento em argamassas alcalina-ativadas com o objetivo de otimizar o desempenho de resistência à compressão e avaliar as condições necessárias para obter uma trabalhabilidade equivalente à de um cimento tradicional. Concluiu-se que a finura tem forte influência na reatividade inicial do amorfo, com este ligante a apresentar resistências à compressão competitivas para uma finura semelhante à do OPC. Além disso, verificou-se que o tipo de moinho utilizado e o tempo de armazenamento após a moagem não influenciam significativamente a reatividade do amorfo. Verificou-se que a ativação alcalina com sulfato de sódio e sulfato de cálcio não apresentam resultados competitivos e otimizou-se a quantidade necessária de silicato de sódio na ativação alcalina, reduzindo, no mínimo, 25% da quantidade utilizada anteriormente sem impactar negativamente o desempenho mecânico do ligante. Verificou-se também que a melhor trabalhabilidade em argamassa é alcançada para uma relação água/cimento de 0.38, enquanto o melhor desempenho mecânico é alcançado para uma proporção de 0.365.

Palavras-chave: ligantes hidráulicos amorfos, finura, moagem, tempo de armazenamento, ativadores alcalinos, otimização rácio água/cimento

Contents

List of Figures

List of Tables

Cement nomenclature

A	Al_2O_3
Ċ	CO_2
C	CaO
F	F_2O_3
H	H_2O
S	SiO_2
Ṡ	SO_3

List of abbreviations

AFm	Calcium Aluminate Monosulfate
AFNOR	Association Française de Normalisation
ATR	Attenuated Total Reflectance
BAT	Best Available Technology
C/S	CaO/SiO_2 molar ratio
$CaSO_4$	Calcium sulphate
C_3S	$3\ CaO \cdot SiO_2$ – Alite
C_2S	$2CaO \cdot SiO_2$ – Belite
C_3A	3 CaO · Al2O3 – Tricalcium aluminate
C_3S_2	$3\ CaO \cdot 2\ SiO_2$ – Rankinite
C_4AF	$4\ CaO \cdot Al_2O_3 \cdot Fe_2O_3$ – Tetracalcium alumino-ferrite
CH	$Ca(OH)_2$ – Portlandite
CS	$CaO \cdot SiO_2$ – Wollastonite
C–S–H	Calcium silicate hydrate without a well-defined stoichiometry
FTIR	Fourier Transform Infrared
H_2O	Water
LSF	Lime Saturation Factor

Na_2SO_4	Sodium sulphate
Na_2SiO_3	Sodium silicate
OPC	Ordinary Portland Cement
TGA	Thermogravimetry Analysis
W/C	Water/Cement
XRD	X–ray Diffraction
XRF	X–ray Fluorescence

1. General consideration

1.1. Main concept

This thesis focused on the study of the effects that fineness, the type of mill used during grinding and the storage time after grinding have on the reactivity of a new low calcium amorphous hydraulic binder, capable of lowering the environmental impact that cement has on CO_2 emissions. This dissertation is also dedicated to the study of different activators for the alkaline activation of the binder and the optimization of W/C ratio on mortar formulations.

1.2. Motivation

The production of Portland cement (OPC) stands today close to 4 billion tons per year and it is expected to grow to 5 billion tons per year by 2050 [1]. Despite this growth represents a positive socioeconomic event, its potential impact on the climate change is an issue that deserves particular attention. Nowadays, the production of OPC clinker releases an estimated of ~0.8 ton CO_2/ton clinker, representing 5-6% of total manmade greenhouse gases [2] [3] [4]. The major emissions of cement industries come from the kiln system. The industrial production of Portland clinker, requires heating a mixture of calcium, silica, alumina and iron sources in adequate proportions, in a kiln to a temperature up to 1400-1500ºC, to produce clinker nodules, with a typical mineralogical distribution around 50-70% C_3S, 15-30% C_2S, 5-10% C_4AF and 5-15% C_3A, resulting in a high energy demanding process with high amounts of CO_2 emitted [5]. Hence with increasing infrastructure and building demands in the near future, the development of a hydraulic binder that reduces the ecological footprint without jeopardizing the technical, economic and workability characteristics of the OPC is a challenge of the upmost importance for the cement industry [3] [6] [7].

Over the last few years, a lot of effort has been put towards the development of eco-friendly alternatives to traditional OPC, such as the increase of clinker replacement in cement mixtures using, for example supplementary cementitious materials (SCM) like clays rich in metakaolin and limestone [8] and the development of new types of cements like belite-rich cements [9] and alkali-activated cements [10], to reduce the amount of CO_2 emitted. Nevertheless, due to the lack of extensive availability in the desired qualities of the raw materials needed to produce these new cement types or due to the shortage of materials able to be alkali-activated, these solutions are still far from representing a real alternative to OPC.

Thus, in an attempt to develop an alternative to OPC that addresses the CO_2 emissions problem and making use of most of the existing clinker production technology, Santos *et. al* [11], proposed a new binder which would reduce about 25% of the CO_2 emissions registered in the production of typical OPC. The new process consists in fully melting and rapid cooling a mixture of conventional raw materials used

in cement manufacture, characterized by a final CaO/SiO_2 molar ratio of 1.1 in the final mix. The obtained amorphous calcium silicate binder revealed its hydraulic activity and demonstrated promising compressive strengths in pastes.

Following these promising results in pastes, the need to further investigate this amorphous binder, by studying mortars and concrete produced with it, was evidenced. The preparation of mortars and concrete require large volume of amorphous binders, and consequently the investigation of the effect of storage and large scale milling.

In another work, Santos *et. al* [12], explored the effects of using alkaline activation in the before mentioned amorphous calcium silicate binder. The prepared pastes of amorphous calcium silicate binder with alkaline activators solutions (Na_2CO_3 and Na_2SiO_3) revealed a faster development of compressive strength at early ages, than the ones without activation, surpassing typical values obtained for OPC clinker pastes, especially for the pastes activated with Na_2SiO_3, proving that, with the help of alkaline activators, this amorphous binder has the potential to develop similar, or even higher, compressive strengths to those of OPC, emitting lower amounts of CO_2.

1.3. Objectives

With the intention to continue the work developed by the CIMPOR/ADIST project "Nanocimento", the present thesis had three major objectives:

Objective 1 – Production of the low calcium amorphous binders with low and high alumina content and preparation of alkali-activated pastes. The produced binders were chemical and mineralogically characterized (eg. TGA, FRX, DRX, FTIR) and the activated pastes were characterized by isothermal calorimetry and compressive strength tests.

Objective 2 – Study the influence of the type of mill used, the fineness of the amorphous and the storage time have on the binder's reactivity and consequently on its mechanical performance (Chapter 4).

Objective 3 – Test different types and amounts of alkaline activators in the preparation of mortars, in order to improve the mechanical properties and decrease the setting time (Chapter 5). One of the purposes of this objective was to identify the minimum activator amount in order to obtain the desired mechanical performance. For this, three activators were tested:

- sodium metasilicate (Na_2SiO_3)
- a mixture of Na_2SiO_3 and gypsum ($CaSO_4 \cdot 2H_2O$)
- a mixture of Na_2SiO_3 and sodium sulphate (Na_2SO_4).

Objective 4 – Optimization of the water/cement ratio (W/C), in the alkaline activated mortars, in order to obtain a workability equivalent to a standard cement (Chapter 5). The following tests were performed:

- determination of the consistence of fresh mortar by flow table
- bending and compressive strengths at 2, 7, 28 and 90 days

1.4. Outline of the Thesis

This dissertation is structured in seven chapters.

The first chapter has an introductory character, revealing the main problems associated with cement production in the current conditions which served as a motivation for the development of alternative cements and, consequently, of this thesis.

The second chapter introduces the general aspects of traditional cement, namely its production process, the composition of its phases and its hydration mechanism, and the most prominent developments in “green” cements such as the use of alternative fuels, replacement of OPC clinker by SCM's, alternative low-carbon binders and the low calcium amorphous hydraulic binder.

The third chapter describes the materials used in the production of the binder and the techniques used for its characterization.

The fourth chapter is structured in the form of a scientific article including the experimental procedures used in the preparation of the samples and the results of which are divided into sub-chapters where the effects of fineness, the type of mill used in grinding and the storage time after grinding are revealed.

The fifth chapter is also structured in the form of a scientific article describing the experimental procedures used in preparing the samples and the results, divided into sub-chapters where the effects of sodium sulphate, calcium sulphate and sodium silicate on alkaline activation are revealed, together with optimization of the W/C ratio in mortars.

The sixth chapter presents the general conclusions of the entire dissertation.

The seventh chapter suggests future work so that the project can be further developed.

Figure 1 presents a diagram with the structure of this dissertation.

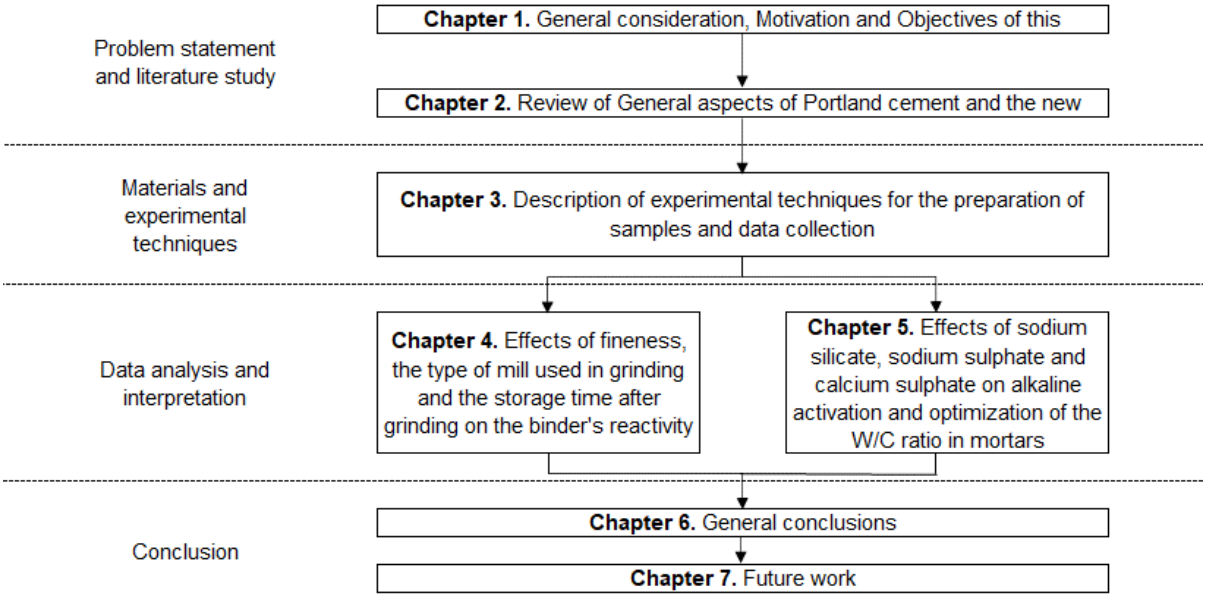

Figure 1 – Structure of dissertation.

2. Introduction

2.1. General aspects about cement

Cement can be defined, in the words of Cecil H. Desch, as an adhesive substance capable of uniting fragments or masses of solid matter to a compact whole [13]. The Egyptians, in 4000 BCE, used a predecessor of cement in the form of calcined gypsum and, the Greeks and Romans, since 500 BCE, mixed sand to heated limestone to make mortar, but only in 1824, modern cement was introduced and patented as Portland cement by Joseph Aspdin and nowadays plays a major role as the most important binding material in civil engineering construction [13].

Cement is a finely ground powder that, when combined with water, forms a paste that sets and hardens to a rock-like mass. This setting and hardening process results from a series of chemical reactions called hydration. A cement that increases in strength even when stored under water after setting is called hydraulic [14]. Currently, the most predominant cement is the Portland cement and the subsequent sections are dedicated to the description of the production of Portland cement and also to its main features, such as the composition, reactivity, hydration mechanisms and hydration products.

2.1.1. Portland Cement Production

Cement can be manufactured in four different process routes: dry, semi-dry, semi-wet and wet processes. The choice of process is determined, primarily, by the state of the raw materials (dry or wet). Currently, the Best Available Technology (BAT) for the production of OPC is the dry process, in which the raw materials are ground and dried to raw meal in the form of a fine powder and then fed to a kiln.

All the production process of Portland Cement can be split into four main steps: (i) quarrying; (ii) raw meal preparation; (iii) clinkering and (iv) grinding [15]. These 4 stages will be discussed in the following sections, and are evidenced in Figure 2, that displays the schematic of the production process used in CIMPOR's cement plant at Alhandra (dry process).

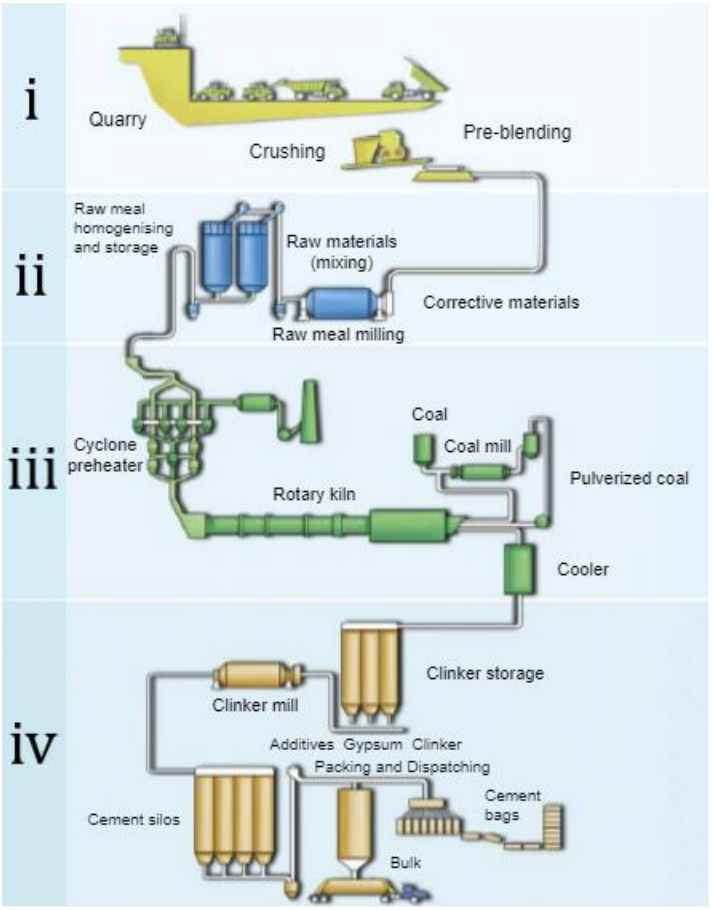

Figure 2 – Schematic of the production process of CIMPOR cement plant at Alhandra. Adapted from [16].

2.1.1.1. Quarrying and raw meal preparation

The essential raw materials needed for cement production are limestone, marl and clay that are used as the source for calcium carbonate, silica, alumina and iron oxide. These materials are obtained through mining and quarrying operations in quarries, that are located near the cement plants to drive the transportations costs to a minimum [15] [17].

After extraction, the raw materials are directed to a primary crushing facility and are later moved to the cement plant in order to be mixed and stored in blending beds. The raw meal should present a composition similar to 67% CaO, 22% SiO_2, 5% Al_2O_3, 3% Fe_2O_3 and 3% of other components [7]. To achieve this desired composition, additional raw materials, such as sand, blast furnace slag and iron ore may need to be added. The final mixture is fed to ball mills where it is ground to a fine powder of 90 µm particle size. Finally, this fine powder is sent to raw meal silos to be homogenised and stored [7] [15].

2.1.1.2. Clinkering

In the clinkering stage, which consists into a series of chemical reactions and sintering processes, the raw meal is converted into the clinker.

The raw meal is first dried and preheated in cyclone preheaters and then fed to a rotary kiln which works at 1450°C. The main reactions taking place at this stage are divided into three groups, reactions below 1300°C, reactions at 1300 – 1450°C (clinkering) and reactions during cooling.

Below 1300°C, the reaction that stands out is the decomposition of calcite (present into limestone) to give lime and carbon dioxide occurring between 525°C and 950°C (equation 1).

$$CaCO_3 \rightarrow CaO + CO_2 \quad (1)$$

Still below 1300°C, some liquid phase starts to form, lime reacts with silica to make belite (equation 2), and some aluminate and ferrite phases are also formed .

$$2CaO + SiO_2 \rightarrow Ca_2SiO_4 \quad (2)$$

Above 1300°C and up to 1450 °C, roughly 20–30 % of the mix is liquid, mainly from aluminate and ferrite. This liquid phase promotes the reaction between belite and lime in order to form alite (equation 3).

$$CaO + Ca_2SiO_4 \rightarrow Ca_3SiO_5 \quad (3)$$

At this point, the material nodulizes and starts forming clinker nodules, as seen in Figure 3, which are then directed to a cooler, where the residual liquid crystallizes, stabilizing the phases formed at high temperatures, producing a clinker with the final composition of 50–70% C_3S, 15–30% C_2S, 5–10% C_3A and 5–15% C_4AF [7].

Figure 3 – Clinker nodules.

2.1.1.3. Grinding

To produce Portland cement, the clinker nodules, after cooling, are ground in ball mills together with less than 5% in weight of gypsum. Gypsum is added to avoid the phenomenon of flash-setting, that is a rapid set with much evolution of heat and is related with increased early hydraulic reaction of the ferrite and aluminate phases and the formation of calcium aluminate monosulfate phase (AFm) throughout the paste [7]. In the end, the ground powder is homogenised and stored in cement silos.

2.1.2. Calcium silicate phases

In Figure 4, it is displayed the binary phase diagram for the CaO–SiO_2 (C–S) system, where the most important calcium silicate phases, alite, belite, rankinite and wollastonite, can be seen.

Wollastonite (CS), presents a C/S = 1, and successively increasing the calcium content leads to the formation of rankinite (C_3S_2), then belite (C_2S) and lastly, alite (C_3S). The hydraulic reactivity increases with increasing calcium content, therefore alite has the highest hydraulic reactivity, followed by belite. Rankinite and both allotropic forms of wollastonite (α–CS, β–CS) are stated as being hydraulically inactive [7].

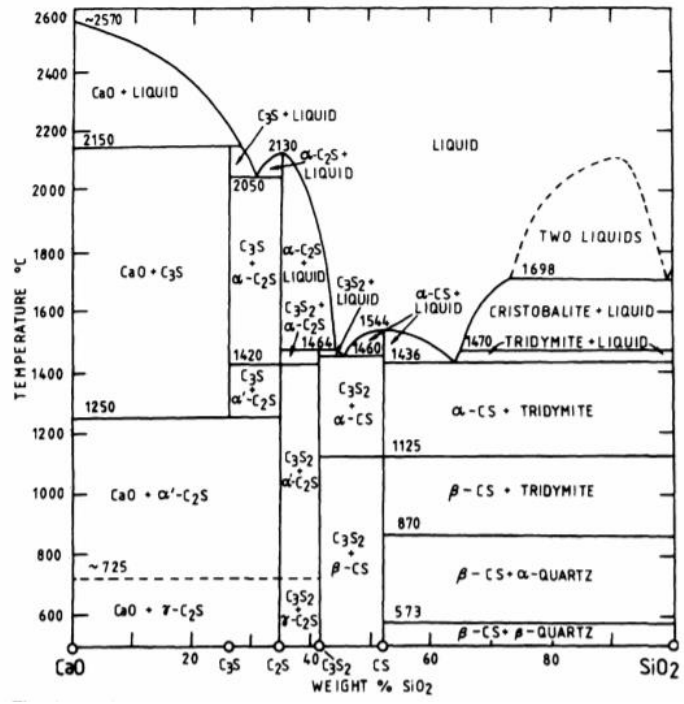

Figure 4 – CaO – SiO_2 phase diagram. Adapted from [7].

Figure 5 exhibits the development of compressive strength of the pure components of OPC along with hydration time. It is clear that alite and belite have the most influence on the increase of compressive strength in Portland cement.

Alite (C_3S), representing 50–70% of OPC, reacts relatively quick with water, making it the most important of the constituent phases for strength development at early ages. Belite (C_2S), constituting 15–30% of OPC, reacts slowly with water, having minimal contribution to the strength during the first 28 days, but, at later ages, leads to a substantial increase in strength. Aluminate (C_3A), accounting for 5–10% of OPC, reacts rapidly with water, and can cause undesirably rapid setting. Nonetheless, it can have some effect on the early growth of compressive strength of cement, more evidently in limestone cements, due to the formation of carboaluminates. Ferrite (C_4AF), making up 5–15% of OPC, reacts fairly quickly with water, but it doesn't significantly contribute to the development of strength in cement [7].

In the following sections alite, belite, rankinite, and wollastonite phases will be discussed.

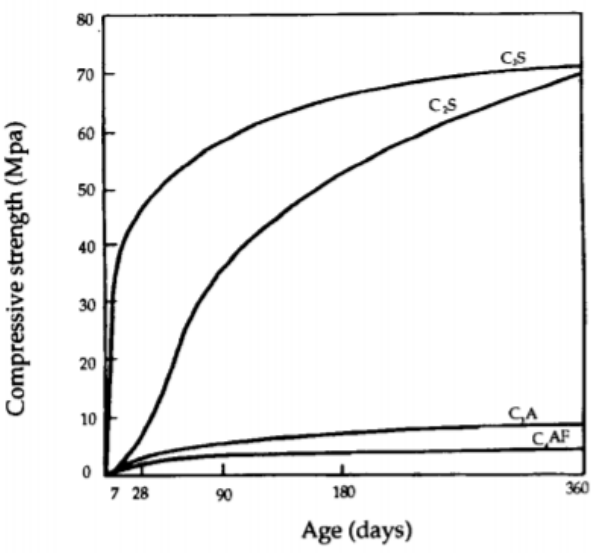

Figure 5 – Development of compressive strength of pure components. Adapted from [18].

2.1.2.1. Alite

Alite (C_3S) is a chemically modified form of pure tricalcium silicate phase (Ca_3SiO_5), formed at temperatures around 1450°C through the reaction between belite and lime. It is responsible for the development of compressive strength of OPC at early ages, upon hydration. From the CaO-SiO_2 phase diagram, it can be inferred that alite is metastable at room temperature, only occurring for temperatures above 1250°C.

When heated, alite undergoes a series of reversible phase transitions, being able to present seven different polymorphic forms, as shown in equation 4: triclinic (T1, T2 or T3), monoclinic (M1, M2 or M3) and rhombohedral (R), with increasing symmetry with increasing temperature [14].

$$T_1 \overset{620℃}{\Longleftrightarrow} T_2 \overset{920℃}{\Longleftrightarrow} T_3 \overset{980℃}{\Longleftrightarrow} M_1 \overset{990℃}{\Longleftrightarrow} M_2 \overset{1060℃}{\Longleftrightarrow} M_3 \overset{1070℃}{\Longleftrightarrow} R \quad (4)$$

When cooled to room temperature, pure alite assumes the triclinic polymorph T_1. In clinker production, thanks to incorporation of substituent ions, alite is stabilized, commonly, in M_1, M_3 or a mixture of these two polymorphs [7].

Thanks to the molecular dynamic simulation study developed by Freitas *et al.* [19], it's possible to see, in figure 6, the arrangement of alite's M_3 polymorph, where it stands out an obvious distinction among free calcium atoms as well as free oxygen atoms and those connected to isolated tetrahedra $[SiO_4]^{4-}$.

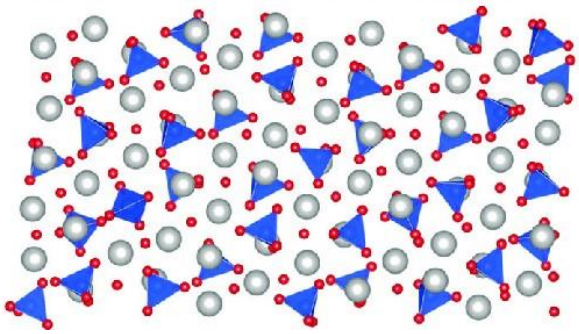

Figure 6 – Alite's M_3 polymorph. Calcium, silicon and oxygen atoms are represented as grey, blue and red spheres, respectively. Blue tetrahedra represent the $[SiO_4]^{4-}$ units. Adapted from [19].

2.1.2.2. Belite

Belite (C_2S) is a dicalcium silicate phase (Ca_2SiO_4) and may present five polymorph forms (α, α'_H, α'_L, β, γ), as shown in Figure 7. At room temperature, the γ polymorph is the only one that is stable, however it has minimal hydraulic reactivity. The β polymorph, the most common polymorph in industrial clinkers, is a metastable phase at room temperature that can be achieved by fast cooling and by the incorporation of stabilizer oxides, such as B_2O_3, Na_2O or K_2O, preventing the transition from the β to γ–C_2S. The transition of β to γ–C_2S can be easily identified since it's followed by the dusting phenomenon, that emerge from the difference in density of the two polymorphs. The α'_H, α'_L, γ polymorphs have an orthorhombic structure, β polymorph has a monoclinic structure and lastly, α has a hexagonal structure [20] [21].

$$\alpha \overset{1425°C}{\Longleftrightarrow} \alpha'_H \overset{1160°C}{\Longleftrightarrow} \alpha'_L \overset{630-680°C}{\Longleftrightarrow} \beta \overset{500°C}{\longrightarrow} \gamma$$

$$780 - 860°C$$

Figure 7 – Structures and transition temperatures for belite. Adapted from [7].

Figure 8 illustrates the atomic structure of belite's α polymorph, consisting primarily in silicate Q^0 units. The main difference in belite structure, comparing to alite, is the lack of free O^{2-} ions.

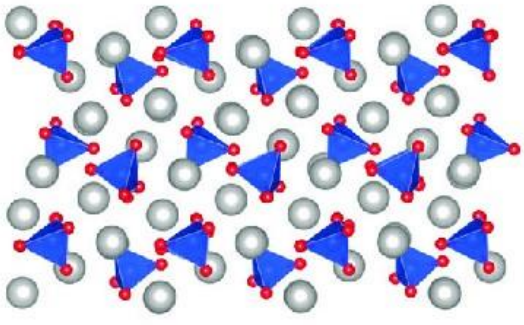

Figure 8 – Belite's α polymorph. Calcium, silicon and oxygen atoms are depicted as grey, blue and red spheres, respectively. Blue tetrahedra represent the $[SiO_4]^{4-}$ units. Adapted from [19].

All belite's polymorphs are made of Ca^{2+} ions and $[SiO_4]^{4-}$ tetrahedrons, presenting a similar structure for all of them, except for the γ polymorph. The α'_H, α'_L, β polymorph's structures derive from

α polymorph, diverging slightly in $[SiO_4]^{4-}$ tetrahedrons orientations and small movements of Ca^{2+} ions, causing progressive decreases in symmetry [7].

2.1.2.3. Rankinite

Rankinite (C_3S_2), $Ca_3Si_2O_7$, has a well-defined structure and doesn't present polymorphs, melting incongruently at 1464ºC. Moreover, rankinite is not found in OPC clinkers and has insignificant hydraulic reactivity [17].

Figure 9 represents rankinite's structure, indicating an arrangement of dimeric units of silicate tetrahedra (Q^1 groups).

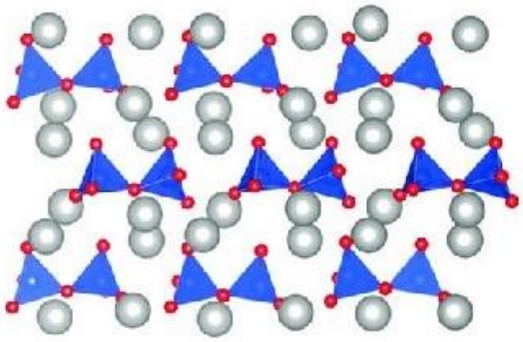

Figure 9 – Rankinite structure. Calcium, silicon and oxygen atoms are depicted as grey, blue and red spheres, respectively. Blue tetrahedra represent the $[SiO_4]^{4-}$ units. Adapted from [19].

2.1.2.4. Wollastonite

Wollastonite, $CaSiO_3$, presents two polymorphs, α–CS and β–CS. The α–CS polymorph, called pseudowollastonite, is the high-temperature form, occurring rarely in nature. The β–CS form exhibits two polytypes: 1T (wollastonite) and 2M (parawollastonite). β–CS polymorph melts congruently at 1544ºC, with the transition between the β → α form taking place at 1125ºC. This transition is reversible, however the transition α → β is slow, making the α–CS polymorph easily stabilized upon quenching [7] [17]. Like rankinite, wollastonite is not present in OPC clinkers and has no hydraulic reactivity [17].

Figure 10 illustrates a representation for the β–CS polymorph, showing an arrangement of parallel linear silicate chains (Q^2 groups) that creates wollastonite's structure.

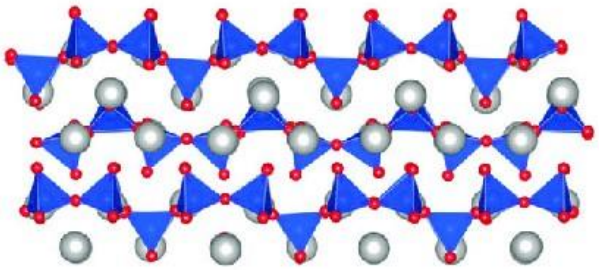

Figure 10 – Wollastonite β-polymorph. Calcium, silicon and oxygen atoms are depicted as grey, blue and red spheres, respectively. Blue tetrahedra represent the $[SiO_4]^{4-}$ units. Adapted from [19].

2.1.3. Hydration of Portland Cement

In cement chemistry, hydration takes place when a cement is mixed with water, forming a paste that sets and hardens. Setting refers to the stiffening of the paste without significant development of compressive strength and occurs during the first few hours upon hydration. Hardening means a substantial development of compressive strength and is generally a slower process [7].

Portland cement is, essentially, a mixture of alite (C_3S), belite (C_2S), aluminate (C_3A) and ferrite (C_4AF). To be considered as a hydraulic binder, any given substance has to react with water to an adequate extent and at an adequate rate, but also has to generate solid products of very low solubility and with a microstructure that can develop enough mechanical strength and volume stability. As such, and even though C_3A is hydraulically reactive, the products that are formed do not meet the described criteria, making its ability to act as a hydraulic cement very poor. In contrast, both C_3S and C_2S present good hydraulic reactivity, producing a nearly amorphous calcium silicate hydrate of variable composition (C–S–H) that meets all the conditions specified for a good hydration product, thus being the main responsible for the development of compressive strength through hydration of OPC [7].

2.1.3.1. Mechanism of hydration

With the intention of improving the sustainability of cement, many efforts have been made towards better understanding the basic mechanisms of hydration. A better knowledge of these hydration mechanisms can lower the environmental impact of cement by allowing the integration of higher amounts of supplementary cementitious materials (SCMs) or even the development of new clinkers [22]. Given that alite (C_3S) constitutes about 50–70% of OPC by mass and that it dominates the early hydration period, cement hydration investigation has been primarily focused on the understanding of the mechanism of hydration of C_3S [23].

The mechanism of hydration has, always, been a topic of intense debate. Nearly one hundred years ago, at the first Chemistry of Cement Conference, some supporters led by Le Chatelier suggested a “through solution” mechanism to explain the hydration of cement, while others defended the solid state theory [24]. At the moment, it is evident that hydration is a dissolution–precipitation process [22]. This dissolution–precipitation process proclaims that an anhydrous phase cannot transform to a hydrate

phase without the passage of ions through solution. As such, and for hydration to carry on, the anhydrous phases are required to have a higher solubility than the potential hydration products.

Figure 11 displays the solubility curves of silica (amorphous and quartz), anhydrous calcium silicates (alite, belite and wollastonite) and calcium silicate hydrate, the C–S–H, where it can be seen that alite presents a higher solubility than C–S–H for a [CaO] between 0 and 36 mmol/L, so C_3S always hydrates. Regarding belite, it only hydrates for [CaO] between 0 and 30 mmol/L. Lastly, wollastonite is less soluble than C–S–H for every concentration, thus it doesn't hydrate [22].

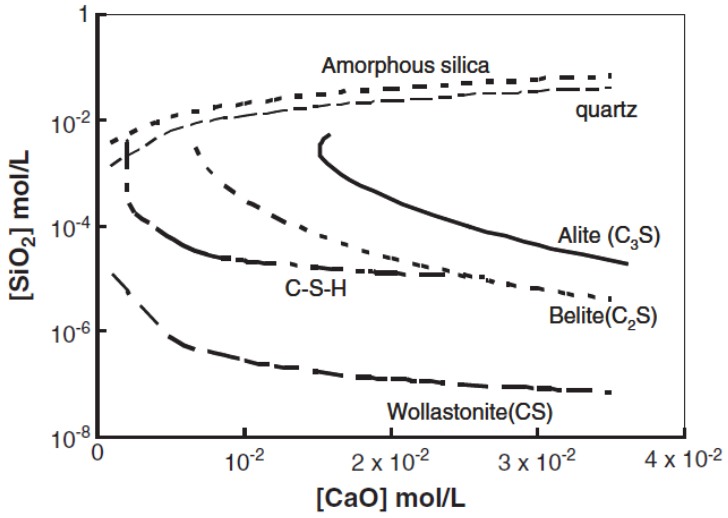

Figure 11 – Solubility curves of silica (amorphous and quartz) and anhydrous calcium silicates phases compared to the solubility of C–S–H. Adapted from [22].

The rate of hydration of cement, which can be translated into heat of hydration [23], varies substantially as time goes on, as seen in Figure 12, leading to a semi-arbitrary division of the mechanism of hydration in four different steps: initial reaction, period of slow reaction, acceleration period and deceleration period [23].

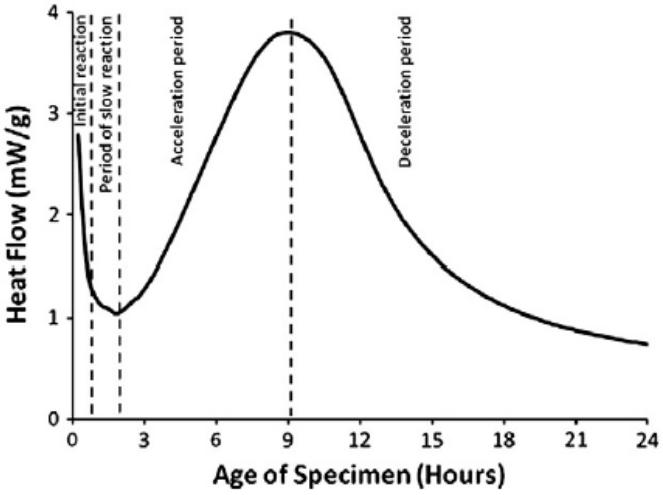

Figure 12 – Heat of hydration as a function of time by isothermal calorimetry results. Adapted from [23].

The initial reaction starts immediately after wetting and can be described as fast reactions between water and the hydraulic active phases of cement, primarily C_3S. These reactions between cement and water lead to the dissolution of C_3S (equation 5) releasing a large amount of heat, as depicted in Figure 12.

$$C_3S + 3H_2O \longrightarrow 3Ca^{2+} + H_2SiO_4^{2-} + 4OH^- \quad (5)$$

As time goes by, the hydration enters the period of slow reaction or induction period, where there is a decrease in heat released, due to a reduction in dissolution rate of C_3S. This decrease in heat released can be explained by the dissolution theory, proposed by Juilland *et al.* [25], that suggests that the dissolution is powered by the formation of defects on surfaces, named etch pits. When the level of undersaturation drops below the one required to provide enough energy for the nucleation of etch pits, the rate of dissolution becomes slow as atoms may dissolve only from preformed steps.

The induction period is followed by an acceleration period, where there is a large exothermic signal resulting from the precipitation of Portlandite (CH) and rapid growth of C–S–H. The initial dissolution of C_3S leads to a solution supersaturated in C–S–H [22], which leads to its nucleation. The nucleation depends on the rate of dissolution, the volume and the initial concentration of the solution, and takes place preferably in pre-existing surfaces, like anhydrous grains of alite. As the nuclei of C–S–H grow, so does the surface of precipitation and the rate of precipitation [22].

In the last stage of hydration, deceleration period, the amount of heat released decreases continuously, extending over a long period of time, during which a slow development of strength occurs. It is considered that this deceleration period is controlled by a diffusion process at later ages, nonetheless, the consumption of small particles, leaving only large particles to react and the lack of space and water also play a major role in the deceleration of heat released [23].

As the hydrated phases continue to expand, occupying the remaining available space, the space which other hydrated phases could occupy starts to be depleted, thus decreasing hydration rate. The lack of water causes the formation of gas-filled porosity after setting, and, as a result, leads to a decrease in internal relative humidity, that also decreases the hydration rate [23].

2.1.3.2. C–S–H Models

Calcium silicate hydrates (C–S–H) are the main responsible for the binding properties of Portland cement, thus understanding the structure of the C–S–H phase is crucial for the development of viable alternatives to OPC.

C–S–H is a nearly amorphous solid, formed upon hydration of Portland cement. Its composition can vary, and the dashes in the term ‘‘C–S–H’’ indicate that no specific composition is implied [26]. Their C/S ratio varies between 1.2 and 2.3 in Portland cement pastes, with an average C/S value of 1.7 being widely accepted [27].

Given its poorly crystalline form and variable composition, C–S–H structure has proven very difficult to study, however results have been obtained from samples of C–S–H synthesized in laboratory with controlled C/S ratios, that presented structural similarities with natural crystalline calcium silicate hydrated phases, specifically tobermorite and jennite. C–S–H can be presented as C–S–H (I) for C/S ratios lower than 1.4 and as C–S–H (II) for higher values. C-S-H(I) has been considered to be a structurally imperfect form of 14 Å tobermorite and C-S-H(II) to be related in a similar way to jennite [28]. Figure 13 depicts the chemical structures of 14 Å tobermorite and jennite.

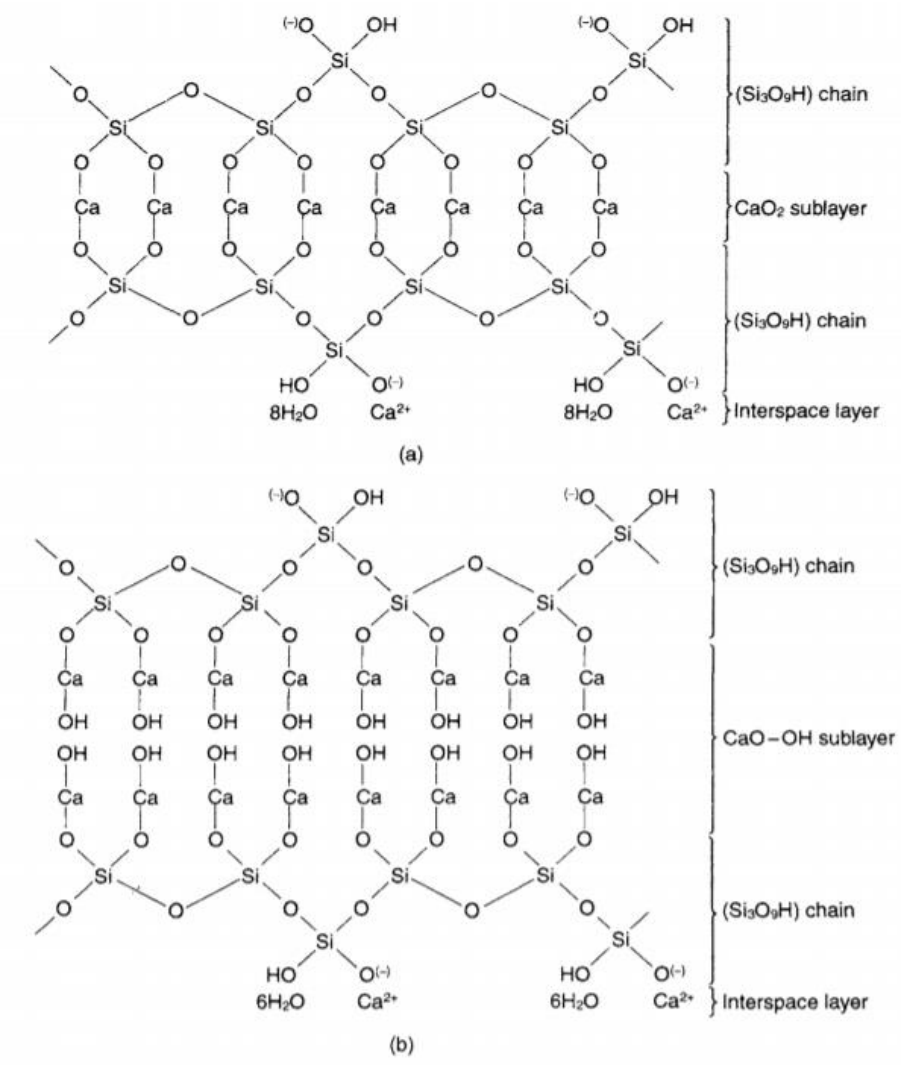

Figure 13 – Idealised chemical structure of (a) 14 Å Tobermorite and (b) Jennite. Adapted from [17].

Tobermorite has a layered structure. Each layer contains a central piece of CaO_2 connected to a SiO_4 tetrahedra of a SiO_4 chain in each side by their shared oxygen atoms. Each SiO_4 chain contains SiO_4 tetrahedra condensed into linear chains that are linked so that they repeat at intervals of three tetrahedra, an arrangement called ‘dreierketten’, in which only two of the SiO_4 tetrahedra, called ‘paired’ tetrahedra, share two of their oxygens with the oxygens of the CaO_2 sublayer. The third tetrahedron is a 'bridging' tetrahedron that is positioned between two pairs of paired tetrahedra to form a continuous SiO_4 chain. The interlayer space between the individual layers is loaded with Ca^{2+} ions, that balance out the negative charge of the layers, and water molecules. The number of water molecules in the interlayer

space determines the distance between the individual layers. The tobermorite with the highest interlayer water content is the 14 Å tobermorite with 8 water molecules per layer [17].

Jennite has an identical structure to that of tobermorite, with the main difference being the existence of OH groups connected to the Ca atoms present in the central region of the individual layers [17].

Even though tobermorite and jennite models were reported as a plausible approximation to the structure of C–S–H, their values of density (2.18 and 2.27 g/cm^3, respectively) and C/S ratio (0.83 and 1.5, respectively) don't quite resemble those obtained for C–S–H formed upon hydration of OPC (ρ=2.6 g/cm^3 and C/S=1.7) [29]. To design a more realistic C–S–H molecular model, Pellenq *et al.* [30] resorted to computational simulations using a defective structure of 11 Å tobermorite, where SiO_2 units were removed from the silicate chains, which increased the C/S ratio, allowing them to achieve density values and C/S ratios (ρ=2.56 g/cm^3 and C/S=1.65) similar to those observed in C–S–H formed upon hydration of OPC.

Qomi *et al.* [31] adopted the same strategy and further explored the resources of computational simulations, where they observed that removing the bridging SiO_4 tetrahedra from the silicate chains of 11 Å tobermorite, led to an increase in the disorder degree of C–S–H, as seen in Figure 14.

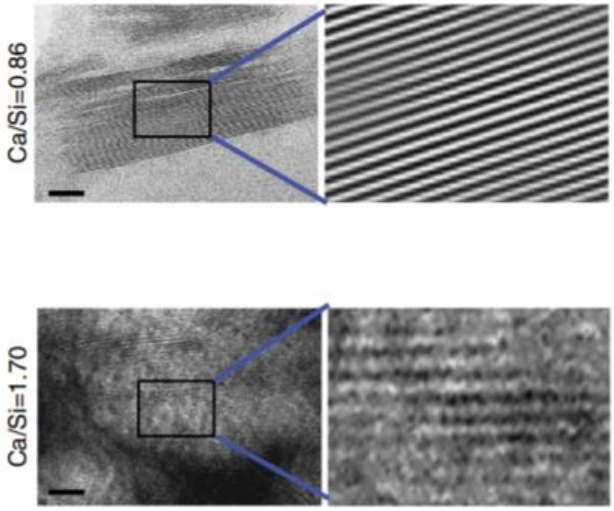

Figure 14 – TEM observations of C–S–H domains for different C/S ratios. Adapted from [31].

Another possible explanation for the unconformity in the values for the C/S ratio between C–S–H and those reported in tobermorite and jennite is that, in reality, C–S–H structure could comprise a mixture of these two structures instead of only one of them [32]. Even so, a final consensus that explains such disagreement in the C/S ratio and density values has not been achieved.

In their findings, Qomi *et al.* [31], also noticed that the C–S–H at C/S = 1 to 1.1 exhibited better mechanical properties than the C–S–H at a median C/S ratio of 1.7, common of OPC, showing on average 31% and 48% superior stiffness and hardness, respectively. The increase of C/S results in the formation of more defective calcium-silicate layers, causing a decline in mechanical stiffness and anisotropy.

2.2. Developments in “green” cements

The cement industry is one of the major sources of man-made CO_2 emissions [33]. The high amount of CO_2 emissions is due to the fact that concrete is the second most used substance in the world after water, and that the cement production is characterized by its high-energy and resource-intensive process, releasing high amounts of greenhouse gases through the combustion of fuels and the calcination of limestone in the production of clinker. Moreover, the cost increase in energy supply, the recent requirements to reduce CO_2 emissions, stated in the Paris Agreement [34], and finally the constant need of raw materials supply in sufficient qualities and quantities has led the cement industry to encourage the investigation of new sustainable alternatives to minimize the cement industry’s environmental impact [35].

In that regard, different strategies have already been implemented by the industry to reduce cement’s environmental impact, while others are still under research and can, possibly, account for large reductions in CO_2 emissions if implemented on a global scale. Those strategies can generally be classified as follows [36]:

A. Use of alternative fuels.
B. Substitution of Portland clinker by supplementary cementitious materials (SCMs).
C. Development of alternative low-carbon binders.

A more detailed overview consisting in the description as well as the benefits and limitations of each of these strategies is presented in the subsequent subsections.

2.2.1. Use of alternative fuels

The use of alternative fuels in the manufacture of cement is a strategy used since the mid–1980s [37], consisting in the utilization of waste materials as an energy source for heat generation. This recycling of waste materials allows cement producers to reduce energy requirement from fossil fuels, which cuts down the CO_2 emissions from combustion of fossil fuels and cement’s production cost [38].

The most frequently used alternative fuels in cement manufacture are waste tires, sewage sludge, waste oil, plastics, fabrics and biomass [36]. The replacement of traditional fuels like coal for alternative ones as biomass can account for a decline in the order of 20–25% of CO_2 emissions [37].

The use of alternative fuels has been an accepted strategy all over the world. In 2006, the alternative fuel ratio was around 16% in developed countries and 5% in developing countries. By 2030, the alternative fuel ratio is expected to reach 40–60% in developed countries and 10–20% in developing countries [36].

The major disadvantage in alternative fuels utilization is that the chemical properties of alternative fuels are different from the conventional fossil fuels. Given its different chemical composition, the use of alternative fuels can introduce undesirable components into the clinker, modifying its chemical

composition, which can impair cement's mechanical properties. This issue can be surpassed by controlling and monitoring the production process and ensuring that the raw materials are burned correctly, offsetting differences in composition [37].

2.2.2. Substitution of Portland clinker by SCMs

Another strategy to mitigate cement's environmental impact is based on the partial replacement of Portland clinker by SCMs in the formulation of cement and concrete. SCMs can act as a filler or used for their pozzolanic properties, meaning that they can react with the excessive hydrated lime produced during the hydration of cement, forming a calcium aluminosilicate phase (C–A–S–H) [37]. The use of SCMs has the advantages of lowering the production cost of cement and, more importantly, substantially reducing CO_2 emissions, since the clinker content in cement is reduced [39].

The most common SCMs in the industry are ground granulated blast furnace slag (GGBFS), pulverized fly ash (PFA) and silica fume (SF). GGBFS is a by-product of the iron and steel industry, comprising calcium and magnesium aluminosilicates and can present pozzolanic properties. Fly ash is produced from the combustion of coal in coal power plants, and is constituted by aluminium oxides, iron oxide, but mostly silicon oxides. It also presents pozzolanic properties, which allows for a replacement of around 30% in weight of OPC in concrete formulations. SF is a by-product of the manufacture of silicon alloys in electric arc furnaces. It is characterized for having a high pozzolanic activity, making it extremely useful for the production of high performance concretes [37] [40].

The main disadvantage across these SCMs is their very limited availability when compared to the much large amounts of cement clinker's raw materials, a problem that is amplified in developing countries. To address this problem, Scrivener [41], defended that the only materials that are present in the necessary quantities and can, successfully, reduce the clinker content in cement at a global scale, and therefore, CO_2 emissions, are calcined clays in combination with limestone (LC^3 technology) [42]. The potential of this ternary blend technology has been demonstrated in clays containing kaolinite, that become pozzolanic active when calcined between 700 and 850^{o}C, combined with limestone and clinker (50% in weight) can present similar mechanical strengths to those of a reference plain Portland cement [42].

2.2.3. Alternative low-carbon binders

The development of novel binders using different combinations of raw materials is an alternative method with the goal of increasing the sustainability of cement, reducing energy demands and CO_2 emissions in the cement industry without compromising the quality of cement.

A brief description of some of the most promising alternative binders to OPC is given below.

2.2.3.1. Belite-rich Portland cements

Belite-rich Portland cements present numerous similarities with Portland cements, in fact, the major difference from OPC is the alite/belite ratio in clinker composition. Typically, the belite content is above 40%, while alite stays between 35–20%, meaning that belite is the most abundant phase in this cement [9] [37].

Due to the reduced amount of alite phase needed in belite-rich cements, the energy consumption (clinkering temperature – 1350ºC) and the amount of limestone required in the clinker raw mix is diminished, resulting in a small reduction, around 10%, of CO_2 emissions in the manufacture of these cements relatively to OPC, which is not very ground-breaking. Other advantages of belite-rich cements are that, due to their higher belite content, higher compressive strengths at later ages and a lower heat of hydration than the typical OPC are achieved. Moreover, belite-rich cements present good resistance to sulphate attacks and are covered to a large extent by existing norms for OPC cements and that its manufacture can be carried out in existing OPC plants. However, to make belite reactive, a physical or chemical activation is necessary, namely rapid clinker cooling or element doping [43].

The main disadvantage of belite-rich cement consists in the much slower strength gain of these cements compared to the majority of Portland cements, making its use only feasible in applications where early strength development is not essential [44].

2.2.3.2. Belite–Ye'elimite–Ferrite (BYF) cements

Belite–Ye'elimite–Ferrite cements is a new and promising technology based, as the name implies, on clinkers containing belite, ye'elimite and ferrite as major phases. In this cement, belite is the most abundant phase, followed by ye'elimite and lastly, ferrite [45].

The BYF technology is considered as an intermediate approach between standard OPC and calcium sulfoaluminate (CSA) cements. BYF clinkers requires lower amounts of limestone in the kiln feed, when compared to OPC, resulting in CO_2 savings of around 20% per unit of clinker in the cement, while also needing smaller quantities of the expensive aluminium-rich raw materials used in CSA clinkers, allowing for a significant reduction of manufacture costs compared to CSA cements, but still higher than OPC [44]. Moreover, these clinkers can be produced in traditional Portland cement plants by only adjusting the mix proportion, which is an advantage in terms of investment cost [43].

BYF cements have the potential to substitute OPC in many applications, due to their higher resistance to chemical attacks, lower permeability, and the possibility for the addition of SCMs in concrete formulations, particularly industrial by-products, without affecting its performance, driving down even more the environmental impact of this cement [43].

The major restriction limiting a wider commercialisation of BYF cements still lies in its aluminium-rich raw materials like bauxite that represent higher manufacture costs than OPC, making the use of BYF technology as an alternative to OPC unjustifiable until the cost of emitting CO_2 increases

significantly or until the costs of BYF cements are sufficiently reduced through further research and development studies [44].

2.2.3.3. Alkali–activated cements

Alkali-activated cements are hydraulic cements characterized by a high content of aluminosilicates. Although these aluminosilicates present very low reactivity with water, given their high amorphous content, when mixed with an alkaline activating solution, they hydrolyse producing a gel of sodium/potassium aluminosilicate hydrate (N(K)–A–S–H) or calcium aluminosilicate hydrate (C–A–S–H) that have high strength performance [10].

The key difference between alkali-activated cement and OPC is that, instead of having limestone as a primary source of raw material, alkali-activated cements rely on waste-stream materials and industrial by-products, especially fly ashes and blast furnace slags as a source of solid components, granting alkali-activated cements an advantage in terms of cost, performance and significantly lower CO_2 emissions when compared to Portland cements [46]. It is estimated that by using alkali-activated cements instead of OPC, it is possible to save approximately 80% of the total CO_2 emissions, making this technology one of the most promising, in terms of environmental impact reduction in the cement industry [47].

The main setbacks for the application of alkali-activated cements are related to the difficulties in handling and the cost of concentrated caustic solutions used as activators and the lack of standards covering the use of alkali-activated cements, since most of the current standards for cementitious materials include prescriptive-based specifications instead of performance-based specifications, which is delaying a larger acceptance across the world [48].

2.2.3.4. Low calcium amorphous hydraulic binder

The new low calcium amorphous hydraulic binder developed by CIMPOR and IST is characterized for its lower requirement of CaO, working at a C/S = 1.1, allowing for a reduction of around 25% of CO_2 emissions in the decarbonating stage, compared to traditional OPC clinkers, and for its hydraulic behaviour resulting from its production process, which consists in fully melting and rapidly cooling the raw mix, resulting in a full amorphization of the clinker [11].

The reduction of CaO requirements compared to OPC means that less pure limestone can be used in the production of these amorphous binder, with the lime saturation factor (LSF) corresponding to the raw meal of this binder only being of around 45, while in the production of OPC, the LSF is usually around 100. This also has a positive effect on quarries, increasing its lifetime, since high quality requirements of limestone decrease [49].

Further investigations on this binder revealed that, with alkaline activation, pastes of this low calcium amorphous binder presented, not only a faster development of compressive strength at early ages, but also higher compressive strength values at later ages compared to OPC [12].

However, some minor setbacks are still to be completely overcome, as a type of refractory lining that can withstand the extremely high temperatures (1550^{o}C) and resist the acidic characteristics of the molten material (~45% SiO_2) is still to be discovered. In addition, the production process still needs to be completely clarified, since to produce this amorphous, it is necessary to have a fast and homogeneous cooling of all the material, which is a problem when the production takes place on a larger scale. However, as the investigation proceeds and moves to a continuous production line, these problems must be resolved.

The present thesis intends to follow up on this new and innovative alternative developed by CIMPOR and IST, a low calcium amorphous hydraulic binder, a material that already served as the basis for the publication of six scientific papers ([11], [12], [19], [50], [51], [52]), a PhD Thesis [49] and a patent application [53].

3. Materials and experimental techniques

In this chapter, the characteristics of the raw materials used to produce the hydraulic binder studied in this thesis, along with the experimental techniques implemented for the characterization and evaluation of all anhydrous binders and prepared pastes and mortars are described.

Further details about the experimental procedures can be found in chapter 4.1 and 5.1 regarding specific procedures followed in each study.

3.1. Raw materials and sample preparation

In this work, a mixture of three different raw materials was prepared to produce the low calcium hydraulic binder, comprising limestone as a source of calcium, sand as a source of silica and a cement raw meal as a source of alumina and calcium. The chemical composition of each raw material and amorphous calcium silicate hydraulic binder was obtained via wavelength-dispersive X-ray fluorescence spectrometry, using an Axios cement from Malvern Panalytical and is displayed in Table 1.

Table 1 – Raw materials composition and raw mix combination used for the production of the amorphous binders.

		Composition (wt.%)								
Raw materials	**% wt.**	**SiO_2**	**Al_2O_3**	**F_2O_3**	**CaO**	**MgO**	**K_2O**	**Na_2O**	**TiO_2**	**Others**
Limestone	≈ 50%	0,85	0,22	0,29	55,21	0,20	0,02	0,05	0,02	0,06
Sand	≈ 30%	96,95	1,29	0,17	0,07	0,00	0,53	0,10	0,04	0,01
Cement raw meal	≈ 20%	13,19	3,36	2,03	43,69	0,76	0,64	0,09	0,18	0,34
Amorphous	**C/S**									
A	1,006	49,63	2,32	0,73	46,58	0,35	0,34	0,11	0,09	0,10
B	1,059	48,33	1,99	0,51	47,75	0,32	0,24	0,14	0,09	0,15
C	1,022	47,97	3,58	0,96	45,76	0,32	0,35	0,20	0,10	0,05
D	1,046	47,64	3,34	1,02	46,49	0,31	0,36	0,15	0,10	0,07
E	1,044	48,55	2,15	0,72	47,29	0,31	0,32	0,13	0,09	0,11
F	1,038	47,88	3,15	0,96	46,38	0,31	0,31	0,14	0,10	0,13

The process to prepare the mixture of raw materials starts by milling sand in a ring mill, 65 grams (g) for about 40 seconds, then, it is mixed with limestone and cement raw meal, in their respective proportions (see Table 1) in a mixer, for 10 minutes, to ensure a good homogenization.

After mixing, 2 discs with approximately 10 cm diameter and 1.5 cm height were obtained by pressing 250 g of raw meal with a force of around 100 kN for each disc. Each disc was then broken into four pieces and placed in a silicon carbide (SiC) crucible which was moved inside and outside the furnace by means of a steel crucible holder.

The binder production thermal process is described below and is exemplified in Figure 15.

A. Heating the raw mix at a rate of 15°C/min to a temperature of 900°C
B. The temperature of 900°C was maintained constant for a period of 40 min to allow for the full decarbonation of the raw-mix and to increase CO_2 saturation in the heating chamber[1]
C. Heating mix at a rate of 15°C/min to a temperature of 1550°C
D. The temperature of 1550°C (in the liquid region) was maintained constant for a period of 60 min to ensure complete fusion of the mixture and homogenization of the composition
E. Cooling the sample to room temperature by quenching it directly in a water-cooling system with sieves integrated for a quick removal of the amorphous hydraulic binder.

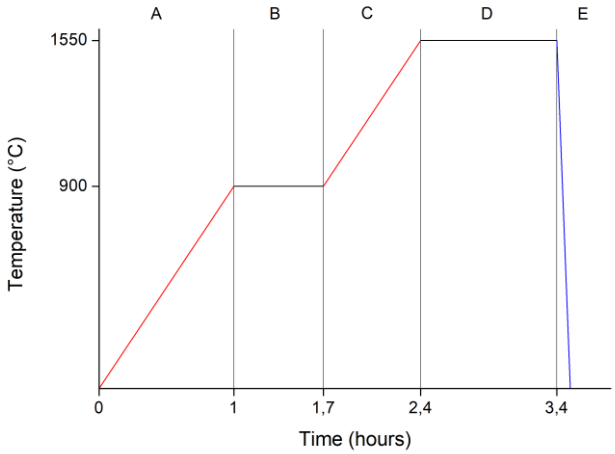

Figure 15 – Thermal cycle used in the production of the amorphous binder.

Figure 16 shows the muffle furnace used in the production of the amorphous binder.

Figure 16 – Muffle furnace used in the production of the amorphous binder.

After quenching, the sieves with the amorphous hydraulic binder were removed from the water and put in a stove to be subjected to a drying step at 100°C for 24 hours.

[1] It is particularly important to maintain a high CO_2 concentration (or high CO_2 partial pressure) in the heating chamber since it limits the oxidation of the SiC crucible used, hence increasing its lifetime.

3.2. Milling and storage of the binder

Following the drying step, the amorphous hydraulic binder was ground to a powder. As mortar tests require a much larger amount of amorphous (about 450g) than needed for paste tests (about 100g), it was necessary to produce several batches of amorphous in the furnace already presented in section 3.1 to start testing in mortars. The greater amount of material needed for the mortar tests also led to a change in the conditions of preparation of the amorphous for each test, namely its grinding mode, since the grinding of the amorphous in a ring mill (Figure 17A), the mill used in previous studies in pastes, is impractical when it is necessary to do a large number of tests on mortars, so the grinding of the amorphous was generally carried in a ball mill, filled with 10 kilograms of balls with 10 mm of diameter, 10 kilograms of balls with 20 mm of diameter and 10 kilograms of balls with 30 mm of diameter (Figure 17B) for the mortar tests.

The ball mill (internal diameter – 270 mm; height – 230 mm) has a much higher grinding capacity than the ring mill (internal diameter – 125 mm; height – 40 mm), allowing to grind about 2 to 3 kg in a much easier way, and also allows for a better homogenization of the amorphous used in each test.

The grinding of such high quantities made it necessary to store the ground amorphous that was not used in the production of mortars or pastes in the moments after grinding. Thus, after the amorphous grinding and the production of mortars or pastes, the ground amorphous was stored in vacuum-sealed bags and kept there until new tests were performed.

Chapter 4 investigates the influence of the type of mill used, the fineness of the amorphous and the storage time in its reactivity and, therefore in its mechanical performance.

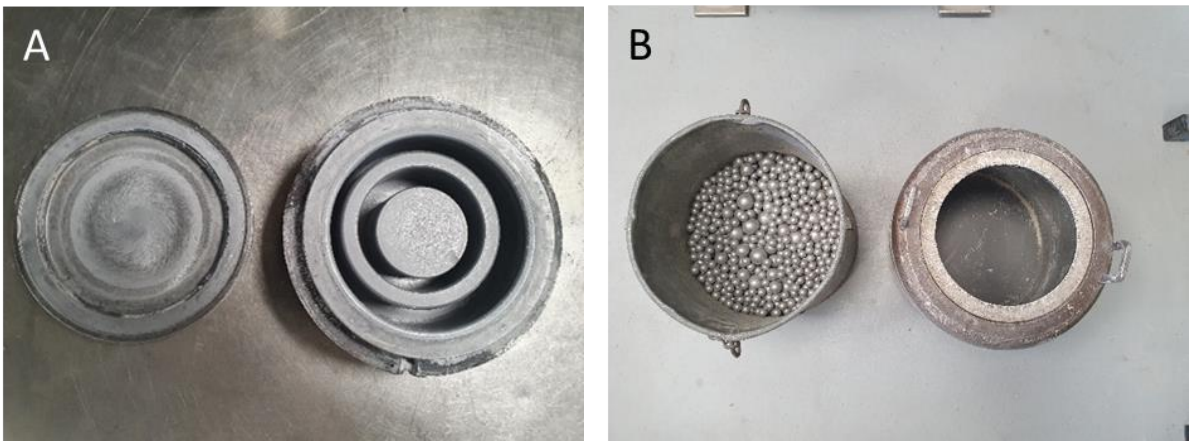

Figure 17 – A. Ring mill (left) and B. ball mill (right).

3.3. Paste preparation

The pastes were prepared by mixing the ground binder with an aqueous alkaline solution using a bench-top mixer for 90 seconds, to ensure a good homogenization of the paste. Different water/cement weight ratio (W/C) were used during this work: 0.25, 0.263 and 0.27. To prepare the different alkaline activator solutions, NaOH from VWR, Na_2SiO_3 from Chem-Lab, Na_2SO_4 from Panreac and $CaSO_4$ from Merck were used. The following types of alkaline activators mixtures were used: NaOH + Na_2SiO_3, NaOH + Na_2SO_4, NaOH + $CaSO_4$, NaOH + Na_2SiO_3 + Na_2SO_4 and NaOH + Na_2SiO_3 + $CaSO_4$. The results and discussion on the effect of the type of activator used is presented in chapter 65.

In order to prepare samples for the mechanical tests, the pastes were poured into inox steel moulds with dimensions of 20 × 20 × 40 mm^3 and cured at 20^{o}C in a moisture-controlled environment with a relative humidity above 95%. The prisms were demoulded at 2 or 7 days and left to cure in the same environment until the age at which they were mechanically tested.

Figure 18 – Mould used in the production of paste samples.

3.4. Mortar preparation

The mortars were prepared according to EN 196–1 [54], by mixing 450 g of the amorphous hydraulic binder in powder form with an aqueous alkaline solution of Na_2SiO_3 and NaOH at different W/C ratios, such as 0.38, 0.365, 0.35 and 0.335, and by adding 1350 g of AFNOR sand. The mortar mix was then blended using a Tonimix mixer, from ToniTechnik, for 120 seconds to ensure a good homogenization of the mortar. Then, the samples were poured into inox steel moulds with dimensions of 40 × 40 × 160 mm^3 and cured at 20^{o}C in a moisture-controlled environment with a relative humidity above 95%. The prisms were demoulded at 7 days and left to cure in the same environment until the age at which they were mechanically tested.

Figure 19 – Blender and mould used in the preparation of mortar samples.

3.5. X-ray Diffraction with Rietveld Analysis (XRD – Rietveld)

X-ray diffraction is a non-destructive, fast and of easy sample preparation technique that has a wide number of applications, i.e., is used to qualitatively identify the phases present in a sample, to quantify the concentrations of each phase present in a multiphase sample, to determine unit cell metrics and to determine crystallite orientation in polycrystalline materials [55]. The crystalline phase identification is determined by, firstly, obtaining the X-ray diffraction pattern and measuring the d-spacings to obtain the integrated intensities, so that that data can be compared with known standards patterns in international databases [56] [57]. The quantification of each crystalline phase present using the Rietveld analysis is a very powerful technique in the study of the hydration of cementitious materials because it allows to follow their phase development by determining the amounts of the different phases present in each system as a function of the hydration age [49] [58].

The Rietveld analysis, as proposed by Hugo M. Rietveld, is broadly accepted due to its whole-pattern fitting approach instead of single-peak analysis [59]. The Rietveld method consists in iteratively comparing the experimental pattern with a pattern simulated based on the supposed amounts, crystal parameters, and equipment parameters of a mixture of well-known phases. The Rietveld analysis always returns the sum of the phases present normalised to 100%, which requires that all the phases present must be inserted into the analysis and their crystal structures known. In the case of existence of amorphous or unknown phases, the amounts of the crystalline phases will be overestimated by Rietveld analysis. This overestimation can be resolved by adding a known amount of a reference standard. The amount of each phase can then be corrected by dividing the values of each phase by the ratio of the measured to true amount of standard added. The difference between the total of the corrected phase amounts and 100% gives the amount of amorphous or unknown phases [58].

In this dissertation, the XRD diffractograms were acquired in a X'Pert Pro, from PANalytical, diffractometer using monochromatic $CuK_{\alpha 1}$ radiation (λ = 1.54059 Å) and working in reflection geometry

(θ/2θ). The optics configuration consisted in a fixed incident anti-scatter slit (1°), a fixed divergence slit (1/2°), a fixed diffracted anti-scatter slit (1/2°) and an X'Celerator detector, working in scanning mode with maximum active length. For each sample, data was collected from 5 to 70° (2θ). The samples were rotated during data collection at 16 rpm and the X-ray tube worked at 45 kV and 40 mA. Rietveld analysis was performed using the PANalytical software Highscore Plus. To each sample, 20% in weight of an internal standard of corundum (99.9% α-Al_2O_3 from Alfa Aesar) was added, with the purpose of better identify and quantifying the amorphous content of the samples.

3.6. Fourier Transform Infrared Spectroscopy (FTIR)

Fourier Transform Infrared spectroscopy is a type of infrared spectroscopy that is used to generate an infrared spectrum of absorption, emission, photoconductivity or Raman scattering of a solid, liquid or gas [60].

The principles of infrared spectroscopy are based on the molecules vibrations and bonds stretching and bending when infrared radiation is absorbed by them. An infrared spectrum is created by passing infrared radiation through a sample and determining what fraction of the incident radiation is absorbed at a particular energy. The energy at which any peak in an absorption spectrum appears corresponds to the frequency of a vibration of a part of a sample molecule. However, for an IR detectable transition, the molecules of the sample must undergo dipole moment change during vibration [61].

Currently, two different methods can be used to acquire an IR spectrum namely, transmission and reflectance. The present thesis resorted to a reflectance method, specifically the attenuated total reflectance (ATR), which utilizes the phenomenon of total internal reflection. This phenomenon consists on the fact that at a particular angle of incidence, when an infrared beam travels from a medium of high refractive index (crystal) to a medium of low refractive index (sample), almost all of the light waves are reflected back. In this condition, some amount of the light energy extends beyond the crystal in the form of waves, called evanescent waves. When the sample is applied on the crystal some amount of the infrared radiation penetrating beyond the crystal is absorbed by the sample. This absorbance is translated into the infrared spectrum of the sample [62].

In this work, the FTIR-ATR spectra were acquired using a bench-top Bruker spectrometer, model Alpha, operating with an ATR module. The spectra were gathered in the range from 400 to 4000 cm^{-1}, with 24 accumulations and 4 cm^{-1} resolution.

3.7. Isothermal Calorimetry

Isothermal calorimetry is a widely used technique in the study of the cement's reactivity and the mechanisms that take place during its hydration, since most of the reactions occurring during hydration generate heat, these exothermic reactions can be recorded and quantified by an isothermal calorimeter [63].

All calorimetry experiments were performed with a TAM Air isothermal calorimeter using glass ampoules, at 20°C and using water as a reference. The heat of hydration data was collected for 7 days.

3.8. Thermogravimetric Analysis (TGA)

Thermogravimetric analysis is a useful technique that measures the mass of a sample over time during specific temperature steps, allowing for the determination of the amount of free water, between room temperature and 105°C, and the amount of bound water, between 105°C and 500°C in a hydrated low calcium amorphous binder [64].

The TGA measurements were performed in an ELTRA multichannel TGA device running at constant heating rates between fixed temperatures (105, 250, 500 and 950°C) maintained until reaching a constant mass. From room temperature to 105°C it was applied a heating rate of 4°C/min, from 105°C to 250°C a heating rate of 10°C/min, in the last two steps, from 250°C to 500°C and between 500°C and 950°C, the applied heating rate was 15°C/min.

3.9. Compressive Strength Test

For the determination of the compressive strength of the pastes and mortars produced with the low calcium amorphous binder, compressive strength tests were performed, according to the European standard EN 196–1, in an Ibertest Autotest 400/10 equipment with a force rate of 2.4 kN/s in paste prisms with 20 × 20 × 40 mm^3 and mortar prisms with 40 × 40 × 160 mm^3.

3.10. Blaine surface area

Surface area is a property commonly used that provides information about the fineness on the cement. The surface area depends on size distribution of cement particles (smaller particles of cement, larger surface area) [65]. To determine the surface area, the method used was the Blaine surface area. This method does not provide an absolute value for the surface area since it does not consider the fine fraction successfully. However, it does deliver an indicative value for each sample that can be compared against each other [65].

The Blaine surface area method is an air permeability method that determines the fineness of cement as its specific surface area by counting the time it takes a specific amount of air to pass through a compact layer of cement [66]. The surface area is calculated through Equation 6, where S is the surface area in (cm^2/g), K is the apparatus constant, e is the sample's porosity, t is the time measured in seconds (s), ρ is the binder density in (g/cm^3) and η is the air viscosity at ambient temperature in (Pa.s).

$$S = \frac{K}{\rho} \times \frac{\sqrt{e^3}}{(1-e)} \times \frac{\sqrt{t}}{\sqrt{10 \times \eta}} \quad (6)$$

Blaine surface area tests were performed according to norm NP EN 196–6 [66], at 21°C, in an apparatus with a volume cell of 1.7507 cm^3 and apparatus constant, *K*, of 23.1162.

3.11. Workability Test

The workability of a mortar is one of its most important properties [67]. Workability is the combination of several properties such as consistency, plasticity and cohesion. Since cohesion and plasticity are difficult to measure, consistency is commonly used to measure workability. The workability of a mortar is highly dependent on its W/C ratio, which also influences their mechanical performance, consequently, their workability is a key parameter to optimize the W/C ratio in alkali-activated mortars [68].

To determine the workability of a mortar, each mortar was prepared as described in section 3.4 and the workability tests were obtained through the flow table test according to European standard EN 1015–3 [69]. This norm states that the mortar should be introduced in the mould in two layers. Each layer is compacted with 10 short hits to guarantee a uniform filling of the mould. Then, the excess of mortar is removed, and the mould is taken off. The mortar is then spread by shaking the flow table 15 times at a constant rate, around 1 time per second. The workability value is then calculated from the average of the diameters of the spread mortar in the disc, measured in two perpendicular directions.

4. Effects of fineness, the mill used and storage time in the reactivity of the binder

This chapter aims to provide valuable information about how the hydraulic reactivity of the amorphous binder is influenced by the fineness of the binder's particles and the type of mill used for grinding. Furthermore, it contributes to draw some first conclusions on the effect that the binder's storage time has on its hydraulic reactivity.

The need to understand the effects that different grinding processes and the storage time have in the reactivity of the amorphous arose when the mechanical performance of pastes decreased when the grinding started to be operated at a larger scale in the ball mill, instead of the ring mill. At that point, three different scenarios could provide explanations to the decrease in mechanical performance:

- The two different milling processes cause different fineness of the amorphous binder, which is a property that has a significant effect on the reactivity of the binder.
- The particle surface charges, which decrease in the case of the ball mill, since this mill provides a much less intense grinding than the ring mill, could translate into a lower reactivity.
- The storage duration, since as time progresses, calcite can form on the particles surface of the milled binder, causing a loss in the hydraulic reactivity.

In this chapter, these three scenarios will be discussed.

4.1. Experimental procedure

In order to fulfil the objectives, the amorphous binder was ground in two different mills, a ring mill and a ball mill, and then the ground binder was hydrated with an aqueous alkaline solution to produce the pastes and mortars. For the study on the storage time, the ground binder was stored in vacuum for different time periods, 1 and 7 days, until pastes were produced.

From previous studies on the same binder, the best mechanical performances were achieved when pastes were prepared with an aqueous alkaline solution of Na_2SiO_3 and NaOH with a 2%wt. Na_2O concentration, using a water/cement ratio of 0.25 [12]. Therefore, in this chapter, the studies on: fineness, type of mill used, and the storage time, were performed on pastes prepared using this same hydration procedure.

The mortars were prepared as described in section 3.4, mixing the ground amorphous with an aqueous alkaline solution of Na_2SiO_3 and NaOH with a 2.92%wt. Na_2O concentration using a water/cement ratio of 0.365, in order to maintain the same Na/H_2O concentration used in pastes.

The effects of different fineness of the ground amorphous was studied in paste samples from four different amorphous batches (A, B, C and D), while the tests on mortars were run on one single batch

(A), in single tests due to laboratory limitations. All the amorphous were produced using the same production procedure, as described in section 3.1.

Binder from batch A was tested in three different scenarios of milling processes, a first one where the binder was ground for 145 minutes in a ball mill (lower fineness) and stored for 7 days in a vacuum-sealed bag before preparation of the paste, a second one where the binder was ground for 3 minutes in a ring mill, with no storage time until the preparation of the paste and a third where the binder was initially ground in a ball mill for 145 minutes and stored for 7 days in a vacuum-sealed bag and then ground in a ring mill for 30 seconds (higher fineness), with no storage time until the preparation of the paste.

Binders from batches B, C and D were tested in two different scenarios of milling processes, a first one where the binder was ground for 1 minute in a ring mill and a second one where the binder was ground for 3 minutes in a ring mill, with no storage time until the preparation of the pastes.

The milling conditions and the adopted nomenclature for each paste and mortar sample in the fineness study is described in Table 2.

Table 2 – Milling conditions and adopted nomenclature for each sample of paste and mortar in the fineness study.

Type	Binder	Mill used	Milling time (min)	Sample name
Pastes	A	Ball mill	145	A_145min_Ball
		Ring mill	3	A_3min_Ring
		Ball mill + Ring mill	145 + 0.5	A_145+0.5min_Ball+Ring
	B	Ring mill	1	B_1min_Ring
		Ring mill	3	B_3min_Ring
	C	Ring mill	1	C_1min_Ring
		Ring mill	3	C_3min_Ring
	D	Ring mill	1	D_1min_Ring
		Ring mill	3	D_3min_Ring
Mortars	A	Ball mill	145	Mor_A_145min_Ball
		Ball mill + Ring mill	145 + 0.5	Mor_A_145+0.5min_Ball+Ring

The effect that the mill used has on the reactivity of the amorphous was studied in pastes from amorphous C and D and mortar samples from amorphous C.

In order to be able to draw conclusions about the effect that the type of mill used has on the amorphous reactivity, it was required to grind the amorphous in the ball mill to a fineness similar to that usually obtained in a ring mill grinding for 1 minute, where we obtain a fineness commonly used in the traditional cement industry.

The milling conditions and the adopted nomenclature for each paste and mortar sample in the mill study are shown in Table 3.

Table 3 – Milling conditions and adopted nomenclature for each sample of paste and mortar in the mill study.

Type	Binder	Mill used	Milling time (min)	Sample name
Pastes	C	Ring mill	1	C_1min_Ring
		Ball mill	180	C_180min_Ball
	D	Ring mill	1	D_1min_Ring
		Ball mill	220	D_220min_Ball
Mortars	C	Ring mill	1	Mor_C_1min_Ring
		Ball mill	180	Mor_C_180min_Ball

In order to evaluate the effect that the storage duration has on the reactivity of the amorphous binder, pastes were prepared using binder from batch A ground during 3 minutes in a ring mill (A_3min_Ring) and stored in vacuum-sealed bags for different periods of time (<1 day and 7 days).

The milling conditions and the adopted nomenclature for each paste sample in the storage time study are defined in Table 4.

Table 4 – Milling conditions and adopted nomenclature for each sample of paste in the storage time study.

Type	Binder	Mill used	Milling time (min)	Storage time (days)	Sample name
Pastes	A	Ring mill	3	<1	A_3min_Ring_1dayST
		Ring mill	3	7	A_3min_Ring_7daysST

4.2. Results

4.2.1. Influence of the fineness

4.2.1.1. X-ray Diffraction with Rietveld Analysis (XRD-Rietveld)

Rietveld analysis allowed the quantification of the phases present in the analysed samples, namely Pseudo-wollastonite, reference code 96-900-2180, Tobermorite 9Å, reference code ICSD 87689, Calcite, reference code 96-900-0967 and Aluminium Oxide, used as internal pattern for the quantification of the amorphous content, reference code 96-900-8082. XRD measurements were performed as described in section 3.5.

Table 5 presents the Rietveld analysis results, namely the development of the phases proportion of binders B, C and D with different fineness, at different hydration ages. Pastes prepared with binder A could not be tested due to Covid-19 lockdown implications.

As expected, Table 5 shows that, as hydration develops, the Pseudo-Wollastonite and Amorphous content diminishes and the amount of hydration products, such as the Tobermorite phase, increases. It is also possible to see, more evidently in some samples, the development of a Calcite

phase, a product of the reaction of atmospheric CO_2 and the CaO of the sample. A note worth mentioning is that, in addition to the formation of crystalline C–S–H, in the form of Tobermorite, amorphous C–S–H is also formed, which is accounted for in the amorphous phase of the samples.

The higher degree of heterogeneity of binders C and D in the anhydrous state, due to their higher amount of crystalline structures, led to some discrepant values in the quantification of the Amorphous and Pseudo-Wollastonite phases. Nonetheless, from the results, it can be concluded that, generally the samples with higher fineness present slightly higher Tobermorite content and less Calcite content than the samples with lower fineness.

Table 5 – Rietveld analysis quantification of paste samples from binders B, C and D with different fineness.

		Rietveld analysis (% Phase quantification)			
Sample	**Time (days)**	**Amorphous**	**Pseudo-Wollastonite**	**Tobermorite**	**Calcite**
B	**Anhydrous**	**85,5**	**14,5**	**–**	**–**
B_1min_Ring	7	84,9	10,6	4,5	–
	28	83,1	10,6	6,3	–
	90	82,7	10,0	7,3	–
B_3min_Ring	7	84,9	10,5	4,6	–
	28	83,2	10,4	6,4	–
	90	82,6	9,4	8,0	–
C	**Anhydrous**	**76,8**	**23,2**	**–**	**–**
C_1min_Ring	2	82,4	16,3	1,3	–
	7	83,1	13,2	2,6	1,1
	28	77,6	14,9	5,4	2,1
C_3min_Ring	2	85,2	12,9	1,9	–
	7	85,3	11,8	2,9	–
	28	81,0	14,0	5,0	–
D	**Anhydrous**	**82,5**	**17,5**	**–**	**–**
D_1min_Ring	2	74,0	25,1	0,9	–
	7	72,3	24,9	2,2	0,6
	28	71,3	24,9	2,7	1,1
D_3min_Ring	2	77,2	21,5	1,3	–
	7	76,0	22,1	1,9	–
	28	72,8	24,0	2,7	0,5

4.2.1.2. Blaine Surface Area

In order to evaluate the effect that fineness has on the reactivity of the amorphous, it was necessary to characterize the fineness of each sample after grinding. To determine the fineness of each sample, the Blaine surface area method was used. The experimental procedure is described in section 3.10.

The results of Blaine surface area are presented in Table 6. From the results, it is possible to notice that the volume of amorphous milled each time and the grinding duration have a considerable impact on the fineness of the ground binder.

Table 6 – Blaine surface area values for each amorphous sample tested in the fineness study.

Binder	Sample name	Quantity milled each cycle (g)	Surface area (cm^2/g)
A	A_145min_Ball	2500	3874
	A_3min_Ring	70/80	4097
	A_145+0.5min_Ball+Ring	2500 + 70/80	4360
B	B_1min_Ring	50	Not measured
	B_3min_Ring	50	Not measured
C	C_1min_Ring	50	4120
	C_3min_Ring	50	5973
D	D_1min_Ring	50	4054
	D_3min_Ring	50	6517

For a constant grinding duration in the ring mill, the higher the quantity of binder placed in the mill, the smaller the particle fineness obtained, as can be seen by comparing the surface areas of *A_3min_Ring* with *C_3min_Ring* and *D_3min_Ring*. Also, for a constant grinding duration in the ring mill and the same amount placed in the mill, the difference in fineness seen in samples *C_3min_Ring* and *D_3min_Ring* may be due to the higher amount of crystalline phase present in amorphous C when compared to amorphous D, as reported in section 4.2.1.1, which makes the binder C slightly harder to grind.

On the other hand, for the same quantity placed in the mill, the longer the grinding duration, the greater is the fineness of the amorphous, as seen between *C_1min_Ring* and *C_3min_Ring*, for example.

The Blaine surface area was not measured for the samples from binder B due to lack of sufficient quantity for the test, however, it is important to note that *B_3min_Ring* had a greater fineness than *B_1min_Ring*, for the beforementioned reason.

Comparing the samples from binder A, it is possible to see that the sample ground in the ring mill for 3 minutes, *A_3min_Ring*, had greater fineness than the sample ground only on the ball mill for 145 minutes, *A_145min_Ball*.

4.2.1.3. Isothermal Calorimetry

Isothermal calorimetry is a test that provides information on the amount of heat released by a sample through time. It can be used to track the degree of hydration of the amorphous, given that the release of heat is an indication of the formation of hydration products, primarily calcium silicate hydrates that are responsible for the development of compressive strength. The experimental procedure is described in section 3.7.

Figure 20 displays the evolution of normalized heat flow and the normalized cumulative heat curves in function of time for each sample of binder A with different fineness, where it is possible to see that the greater the fineness, the sooner the peak of hydration is achieved and higher the amount of heat released after 7 days, when comparing samples *A_145min_Ball* and *A_3min_Ring.*

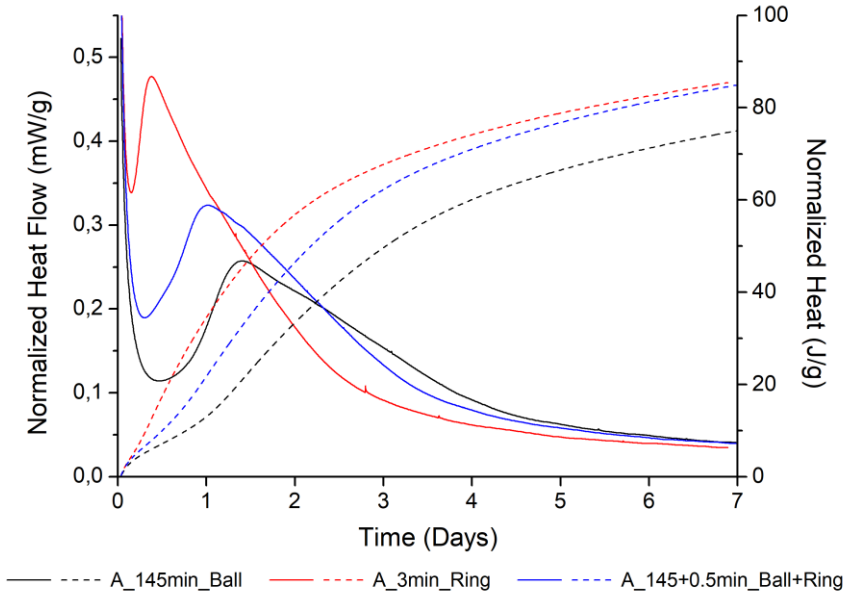

Figure 20 – Normalized heat flow and normalized cumulative heat curves in function of time of hydration for samples of binder A with different fineness.

Although sample *A_145+0.5min_Ball+Ring* presents slightly higher fineness, its peak of hydration is reached later and releases less heat after 7 days than *A_3min_Ring* due to the fact that the amorphous of sample *A_145+0.5min_Ball+Ring* after being ground for 145 minutes in the ball mill was stored for 7 days in a vacuum-sealed bag before being ground for 30 seconds in the ring mill, which allowed for some carbonation of the surface of the ground amorphous, decreasing the early reaction kinetics. Nonetheless, milling for 30 seconds in the ring mill removed some of the carbonated surface which helped the binder to improve the reaction kinetics compared to sample *A_145min_Ball* that achieved the peak of hydration even later and released less heat.

The evolution of normalized heat flow and the normalized cumulative heat curves in function of time for each sample of binder B with higher fineness (*B_3min_Ring*) and lower fineness (*B_1min_Ring*) is presented in Figure 21, demonstrating another example of how fineness affects the hydraulic reactivity of the binder. The increase in surface area of the binder represents an increase of reactions sites, leading to a higher formation of hydration products, resulting in an earlier peak of hydration and a higher amount of heat released after 7 days.

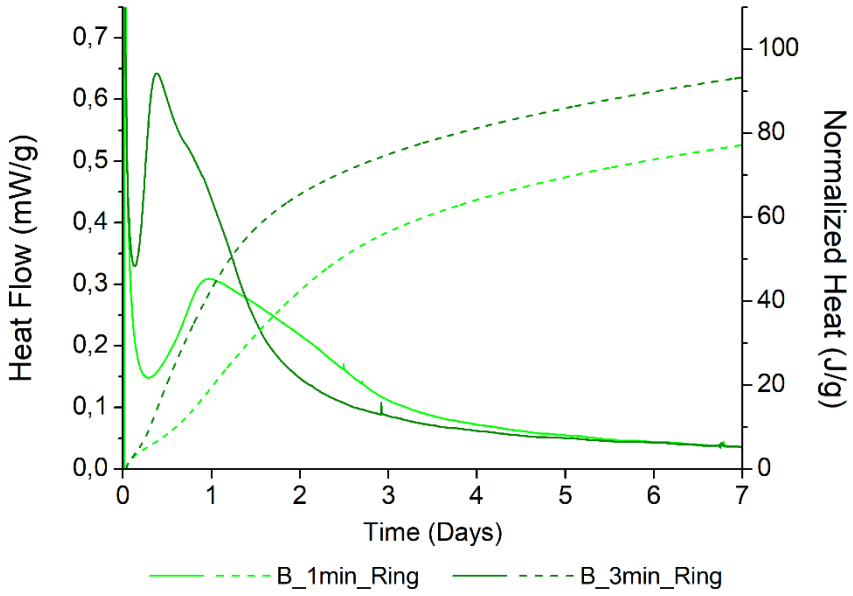

Figure 21 – Normalized heat flow and normalized cumulative heat curves in function of time of hydration for samples of binder B with different fineness.

To put it briefly, for samples with the same storage time, ground in the same mill, but for different time periods (different fineness), the peak of hydration is reached much sooner for the samples with greater fineness, bursting a higher heat flow at that moment and releasing higher amounts of heat after 7 days, indicating that the hydraulic reactivity of the amorphous is significantly improved with increased fineness.

4.2.1.4. Compressive Strength Tests

Figure 22 shows the development of compressive strength as a function of time for each paste sample produced with different binders with the same milling procedure, 3 minutes in the ring mill. The compressive strength tests were performed according to the experimental procedure reported in section 3.9.

From Figure 22, it is possible to see that, for 7 days of hydration, pastes prepared with binders C and D developed lower compressive resistances, which can be explained by the higher crystalline content of these binders, namely the pseudo-wollastonite content, as seen in section 4.2.1.1, that reduces the hydraulic reactivity of the binder, delaying its compressive strength development. At 28 days, the paste prepared with binder D showed a significant improvement of compressive strength,

reaching a similar value to the paste prepared with binder B, that has lower crystalline content, while paste prepared with binder C did not show such remarkable development, indicating that the higher crystalline content in its anhydrous state still impairs the mechanical performance at later ages.

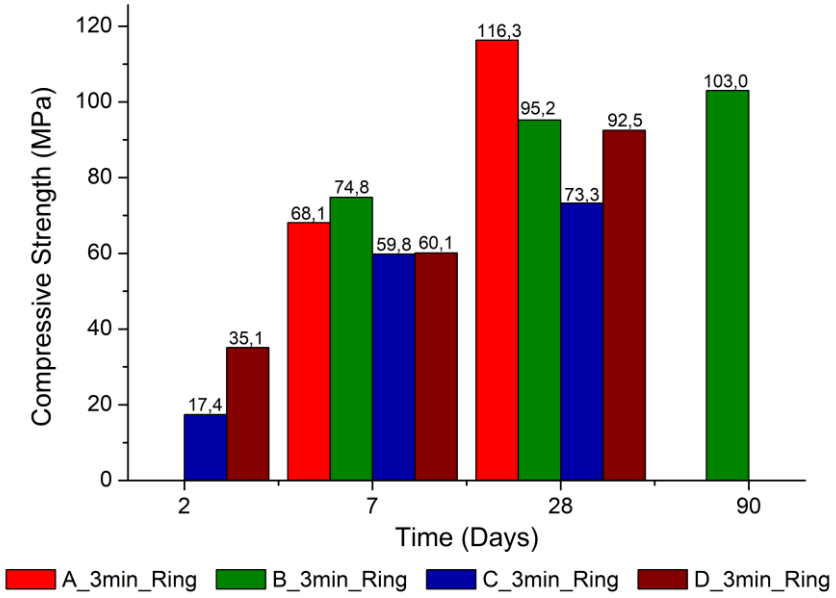

Figure 22 – Compressive strength evolution in function of time of hydration for paste samples of different binders.

Figures 23 to 26 display the development of compressive strength as a function of time for each paste sample produced with binders A to D, respectively, with different fineness. Figure 27 exhibits the progression of compressive strength with hydration time for mortar samples of binder A with different fineness.

In Figures 23 to 26 it is clear that fineness has a strong impact on early age reactivity, at 2 and 7 days, unveiling that samples with a greater fineness have the capacity to develop much higher early age compressive strengths, as seen in the calorimetry results in section 4.2.1.3, except for the case of samples produced with binder A, Figure 23, that shows that the sample with higher fineness, *A_145+0.5min_Ball+Ring*, developed lower compressive strength than a sample with lower fineness, *A_3min_Ring*, due to the formation of some carbonation of the surface of the ground amorphous, which hindered early reaction kinetics.

At later ages, 28 and 90 days, that effect starts to diminish, more evidently in pastes produced with binders A and B, Figures 23 and 24, where the compressive strength do not seem to be affected by the difference in fineness of the binders. However, pastes produced with binders C and D, Figures 25 and 26, present higher compressive strength in the case of higher fineness, at all ages, indicating that lower fineness exacerbates the loss of reactivity caused by the greater crystalline content of these binders.

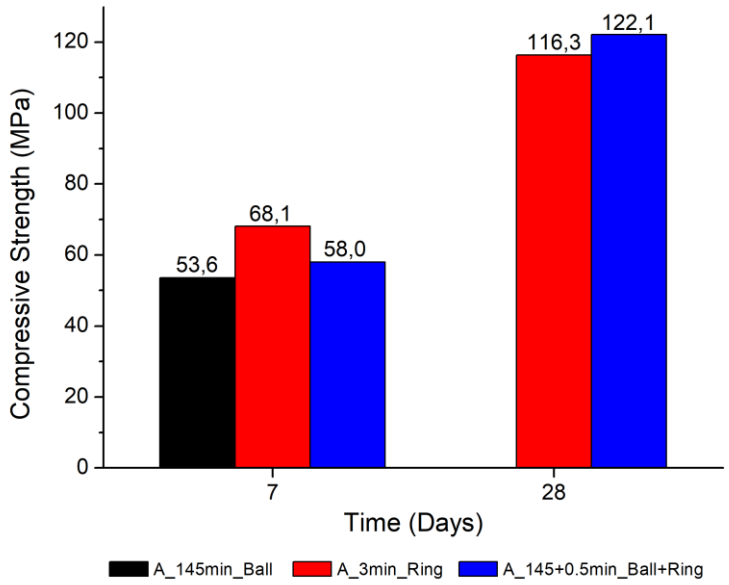

Figure 23 – Compressive strength evolution in function of time of hydration for paste samples of binder A with different fineness.

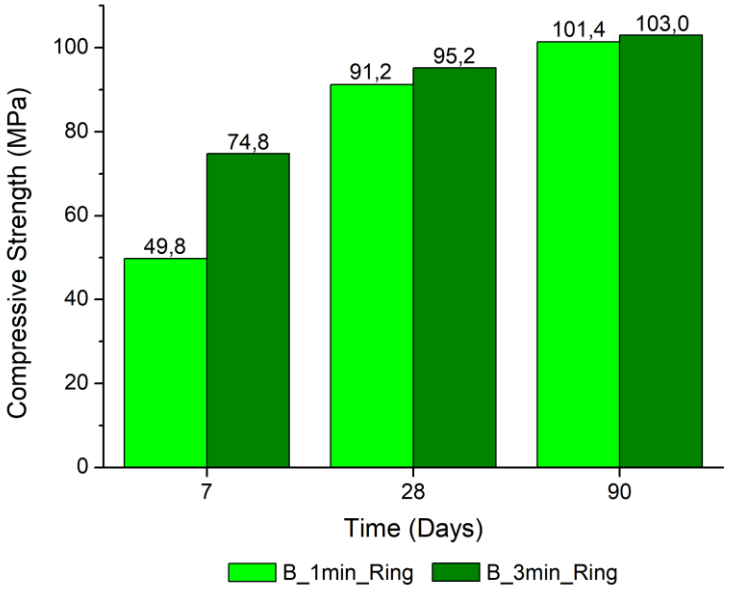

Figure 24 – Compressive strength evolution in function of time of hydration for paste samples of binder B with different fineness.

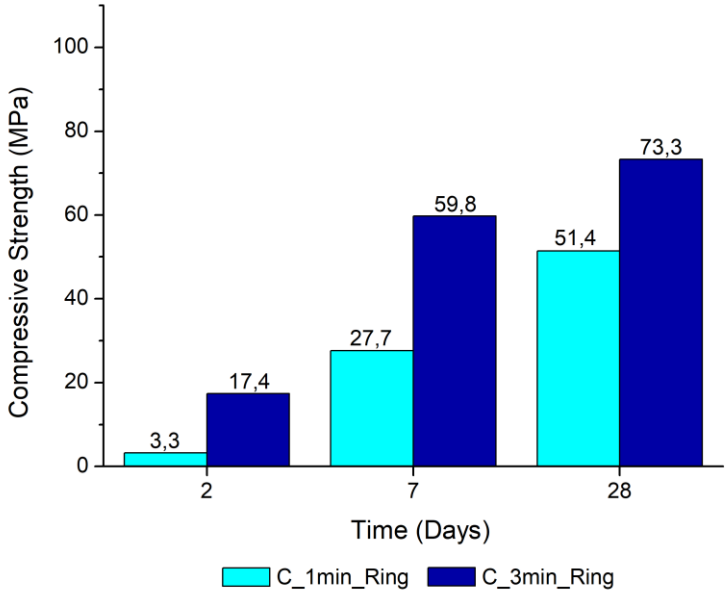

Figure 25 – Compressive strength evolution in function of time of hydration for paste samples of binder C with different fineness.

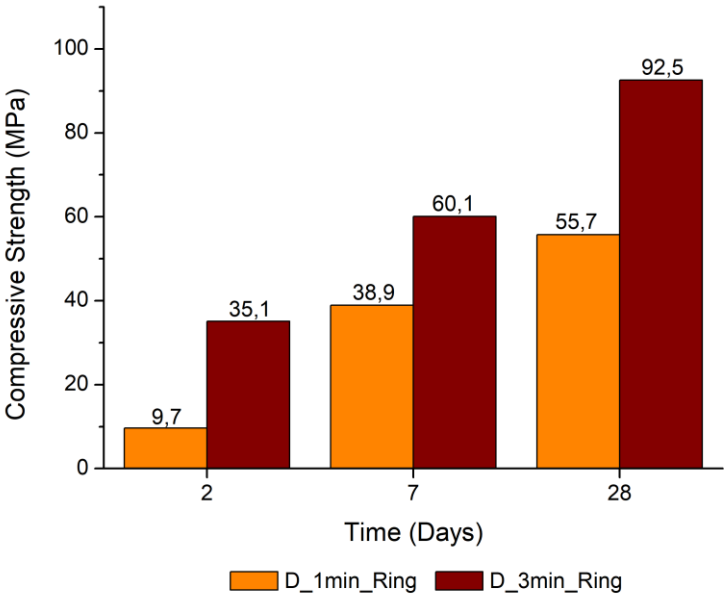

Figure 26 – Compressive strength evolution in function of time of hydration for paste samples of binder D with different fineness.

Figure 27 illustrates that the compressive strength in mortars with different fineness seems to develop at the same rate as in pastes, as the samples with greater fineness reveal a noticeably higher reactivity at early ages, that slowly fades away as time progresses.

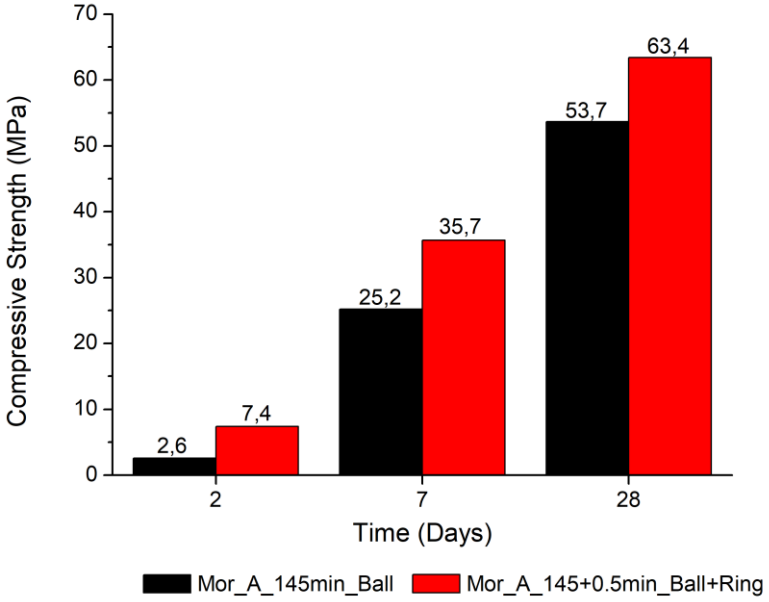

Figure 27 – Compressive strength evolution in function of time of hydration for mortar samples of binder A with different fineness.

4.2.1.5. Thermogravimetric Analysis (TGA)

Figures 28 to 30 display the evolution of the amount of bound water through time of hydration for the pastes prepared with binders B, C and D. Thermogravimetric measurements were conducted as described in section 3.8.

The pastes prepared with binder powders with higher fineness, ground for 3 minutes in the ring mill, have higher amounts of bound water at all ages, when compared with the respective paste prepared with binder with lower fineness (ground for 1 minute), as it is shown in Figures 28 to 30. This result is in agreement with the results of the compressive strength tests, as the amount of bound water is an indicator of the amount of hydration products formed, namely C–S–H, that is responsible for the compressive strength development [52].

Moreover, the rate of development of the amount of bound water is almost parallel between the pastes prepared with the same binder but with different fineness, indicating that the difference in fineness does not have much influence in the development of bound water, and consequently C–S–H, through time, only in the amount of bound water at very early ages, giving them a huge boost in initial reactivity. This boost in initial reactivity is due to the higher number of nucleation sites, resulting from the greater fineness, which increase the surface area of the binder particles, reducing the energy barrier for dissolution of the binder species and promoting the precipitation of hydration products faster [70].

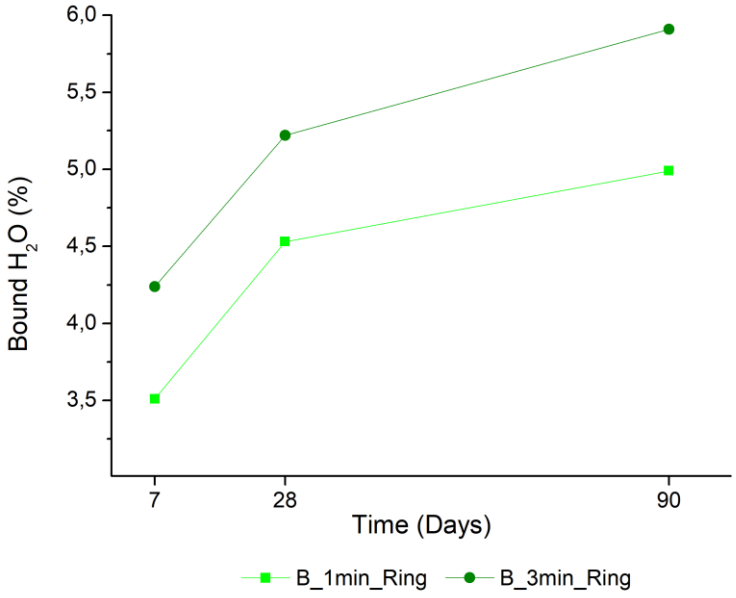

Figure 28 – Amount of bound water through time of hydration in pastes of binder B with different fineness.

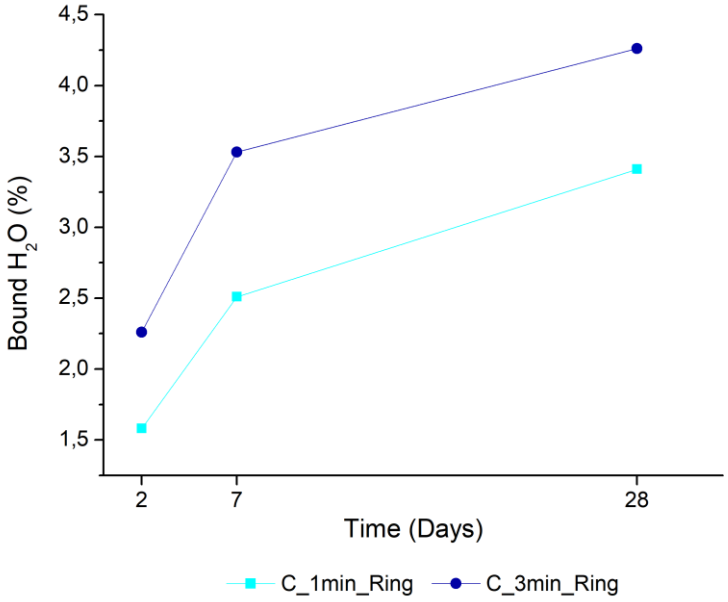

Figure 29 – Amount of bound water through time of hydration in pastes of binder C with different fineness.

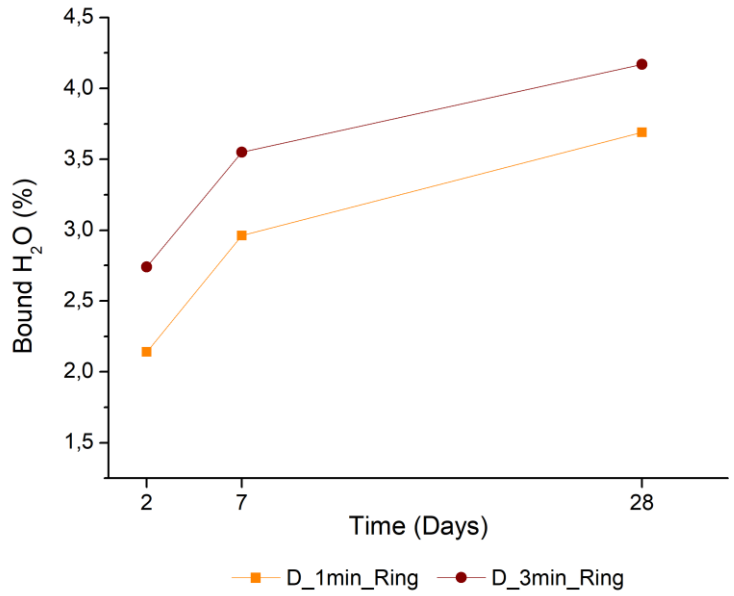

Figure 30 – Amount of bound water through time of hydration in pastes of binder D with different fineness.

Figure 31 shows the evolution of the amount of bound water through time of hydration for the mortar prepared with binder A.

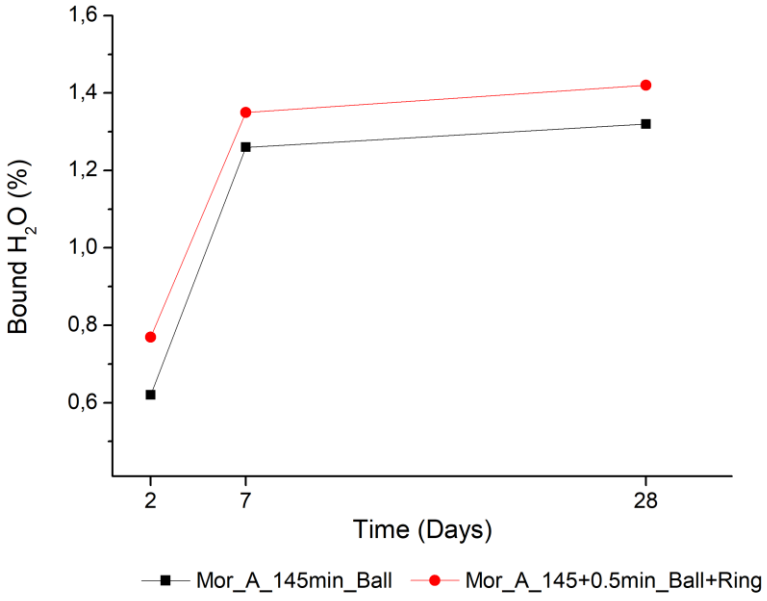

Figure 31 – Amount of bound water through time of hydration in mortars of binder A with different fineness.

The development of bound water through time in mortar follows the same trend as the paste samples, where the sample with greater fineness present similar rate of growth as the sample with lower fineness. Furthermore, and as in paste samples, the sample with greater fineness presents a higher amount of bound water at all ages, due to its higher surface area, and subsequently, higher hydraulic reactivity.

4.2.1.6. Fourier Transform Infrared Spectroscopy (FTIR)

In order to follow the evolution of hydration in the samples, the anhydrous binders B, C and D and their hydrated samples were studied through FTIR spectroscopy, where it is possible to identify different deviations in the bands and variation in the peaks along the spectra as the time of hydration goes on. The different bands can be identified by the letters (a) to (i). All samples were analysed following the experimental procedure described in section 3.6.

Figure 32 displays the FTIR spectra of anhydrous binder B and its hydrated pastes with different fineness at 7, 28 and 90 days of hydration. The key changes in both spectra are as follows:

- **(a)** – (~ 430–530 cm^{-1}) – due to the bending vibrations of (Si)O-Si-O(Si) bonds in pseudowollastonite. With hydration, this band contracts due to deformation of SiO_4 tetrahedra, in the same plane as the Si-O bond, in tobermorite-type C–S–H structures [71], [72].
- **(b)** – (~ 560 cm^{-1}) – due to the bending vibrations of $^{-}$O-Si-O^{-} in pseudowollastonite [71].
- **(c)** – (~ 670 cm^{-1}) – associated to the deformation of Si-O-Si bond in tobermorite-type C–S–H structures [72], [73].
- **(d)** – (~ 720 cm^{-1}) – band characteristic of 3-membered rings in the pseudowollastonite spectra that can be associated with the stretching vibrations causing ring deformations during vibrations [71].
- **(e)** – (~ 850–880 cm^{-1}) – corresponding to Q^0 silicon species. As hydration goes on, the band narrows, indicating that Q^0 species are reacting with available calcium and water producing C–S–H . Q^1 (900 cm^{-1}) and Q^2 (950 cm^{-1}) silicon species should also be seen in the spectra, however they appear overlapped due to the more intense bands of pseudowollastonite, band (f) [74], [75].
- **(f)** – (~ 920, 940 and 980 cm^{-1}) – associated to stretching non-bridging vibrations of Si-O of pseudowollastonite. During hydration, this band diminishes intensity due to consumption of pseudowollastonite to form a more ordered structure, like C–S–H [71], [72], [76].
- **(g)** – (~1060–1090 cm^{-1}) – related to Si-O stretching bridging vibrations of Si-O(Si) of pseudowollastonite. The bands deformation to lower wavenumbers indicates the formation of a more ordered Q^2 structure [71], [72], [77].
- **(h)** – (~870 and 1350–1550 cm^{-1}) – linked to asymmetric stretching of CO_3^{2-}. As time goes by, this band is revealed due to formation of carbonate, indicating the presence of calcite [78], [79].
- **(i)** – (~ 2800–3550 cm^{-1}) – related to stretching vibrations of O-H groups in H_2O molecules. As hydration develops, this band gets more intense indicating a greater amount of bound water present in C–S–H molecules [80].

At 7 days, both pastes produced with binder B, *B_1min_Ring* and *B_3min_Ring,* were not dehydrated, which resulted in larger bands from the higher contribution of H_2O molecules.

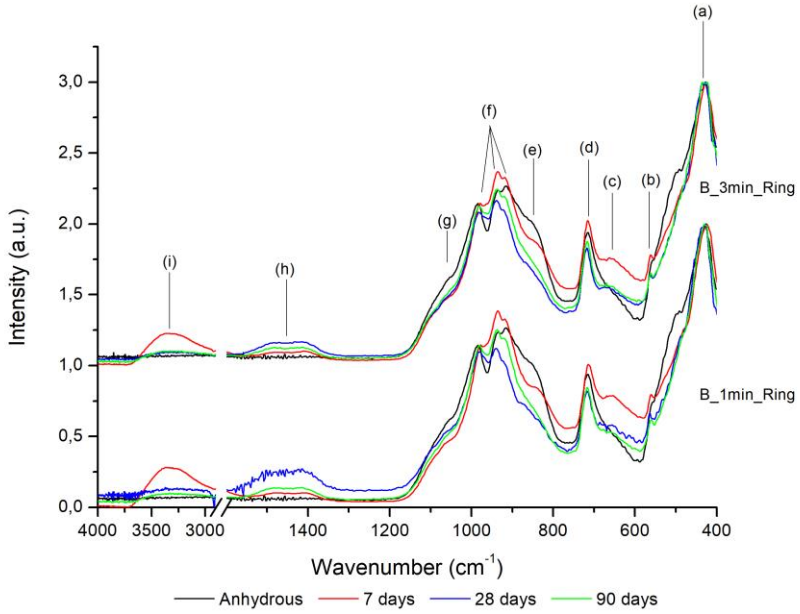

Figure 32 – FTIR spectra of anhydrous binder B and its hydrated samples with different fineness at 7, 28 and 90 days.

When compared to pastes produced with binder B (Figure 32), pastes obtained with binder C and D (Figures 33 and 34, respectively) show larger bands (d), a revealing sign that binder C and D present higher amounts of pseudowollastonite, also seen in XRD results in section 4.2.1.1. Bands (e) is much less intense, indicating lower amounts of Q^0 silicon species available at early ages of hydration, which caused a decrease in reactivity at those ages, resulting in inferior amounts of C–S–H, also revealed by lower bands (c) and (i), and consequently, significantly lower compressive strengths, as seen in section 4.2.1.4. More intense bands (g) in both binders C and D reveal that the higher amounts of pseudowollastonite is primarily in Q^2 species, as expected from the description in Figure 10. Bands (h) are larger, indicative of higher amounts of carbonation of these samples.

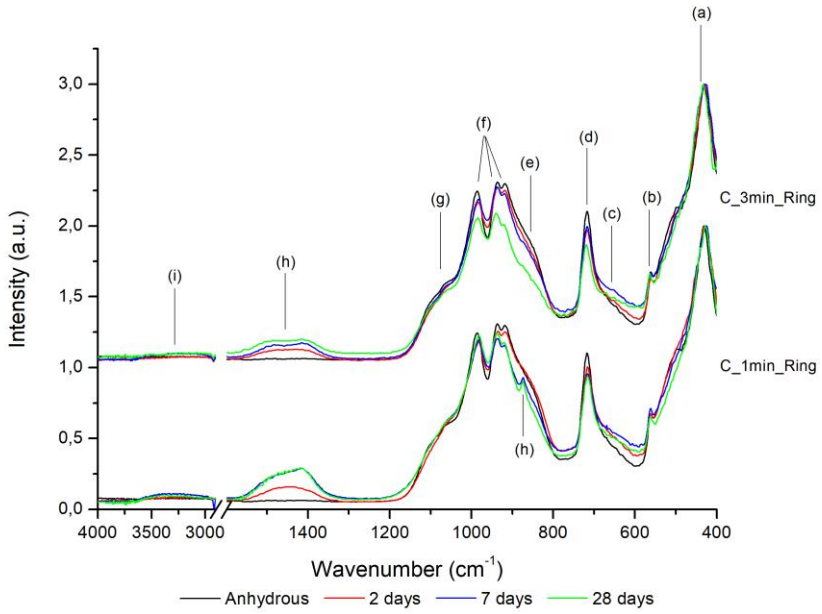

Figure 33 – FTIR spectra of anhydrous binder C and its hydrated samples with different fineness at 2, 7 and 28 days.

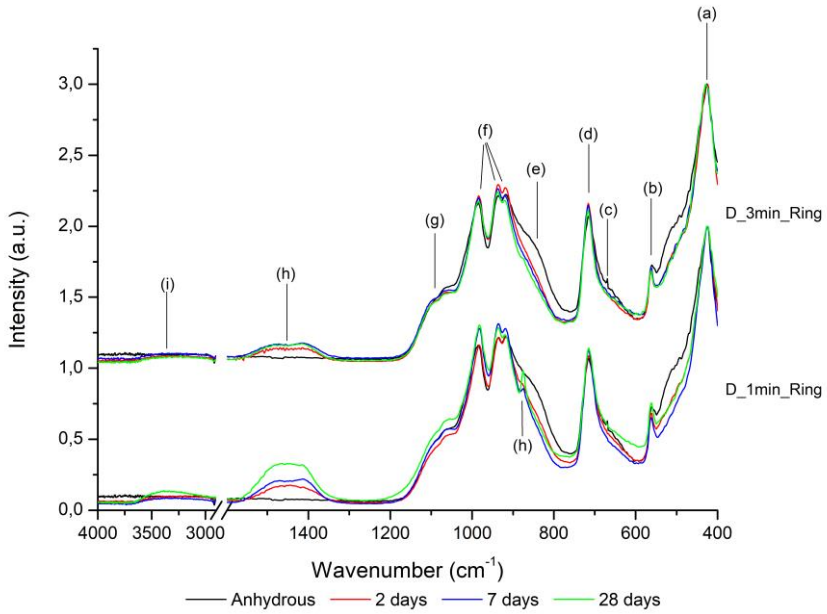

Figure 34 – FTIR spectra of anhydrous binder D and its hydrated samples with different fineness at 2, 7 and 28 days.

4.2.2. Influence of the type of mill

4.2.2.1. X-Ray Diffraction and Rietveld Analysis (XRD)

Table 7 shows the development of phase quantification through Rietveld analysis of XRD measurements of pastes prepared with binder C and D with similar fineness from different mills, in the anhydrous state and at different hydration ages. All XRD measurements were performed as described in section 3.5.

Samples of binder D show comparable results to the samples of binder C, as Tobermorite and Calcite phases develop almost equally between both samples of similar fineness. However, the Amorphous and Pseudo-Wollastonite values of both samples of binder D reveal much higher disparity, indicating that sample *D_1min_Ring* could contain a higher crystalline content than *D_220min_Ball*, from possible differences in crystallinity in the binder doses for each grinding.

Table 7 – Rietveld analysis quantification of paste samples from binders C and D with similar fineness.

		Rietveld analysis (% Phase quantification)			
Sample	**Time (days)**	**Amorphous**	**Pseudo-Wollastonite**	**Tobermorite**	**Calcite**
C	**Anhydrous**	**76,8**	**23,2**	**–**	**–**
C_1min_Ring	2	82,4	16,3	1,3	–
	7	83,1	13,2	2,6	1,1
	28	77,6	14,9	5,4	2,1
C_180min_Ball	2	82,2	16,4	1,3	0,2
	7	81,8	15,0	1,9	0,7
	28	78,8	14,5	4,2	2,5
D	**Anhydrous**	**82,5**	**17,5**	**–**	**–**
D_1min_Ring	2	74,0	25,1	0,9	–
	7	72,3	24,9	2,2	0,6
	28	71,3	24,9	2,7	1,1
D_220min_Ball	2	81,1	17,5	1,3	0,1
	7	80,1	16,5	1,9	1,0
	28	76,9	19,0	3,0	1,1

4.2.2.2. Blaine Surface Area

To study the effect that the type of mill has on the reactivity of the amorphous binder, it was necessary to evaluate the behaviour of the binder after hydration, when milled using two different mills at similar fineness values. The experimental procedure is described in section 3.10.

The fineness of binder C, after grinding, was measured through the Blaine surface method until similar values between both mills was achieved. It was found that, to achieve a similar Blaine value of around 4000 cm^2/g, it was necessary to mill the binder C for 1 minute in the ring mill and for 180 minutes in the ball mill. Consequently, for the grinding of binder D, in the ring mill, the binder was ground for 1 minute, and then verified if the Blaine value was around 4000 cm^2/g, which was confirmed, and in the ball mill, the binder was ground for 180 minutes, and then verified if the Blaine value was around 4000 cm^2/g, which at that time was yet to be confirmed (3939 cm^2/g), thus, further measurements were made until the Blaine value approached the Blaine value of binder C. Due to the uncertainty associated with the Blaine method and the sample taking from inside the ball mill, the Blaine value of binder D after milling in ball mill for 220 minutes, 4351 cm^2/g, is slightly different from the Blaine value of binder C after milling in a ball mill for 180 minutes, 4085 cm^2/g, nonetheless comparisons can be drawn between the two binders.

Table 8 presents the final values of Blaine surface area for each sample analysed. Figure 35 shows the measured values of Blaine surface area at different time steps for binders C and D in the ball mill and for binder C in the ring mill. From the plot values, a trend line was traced relating mill time with Blaine value, that can be used for an approximate determination of the grinding time needed to achieve a certain Blaine surface value in future grindings.

Table 8 – Blaine surface area values for each amorphous sample tested in the mill study.

Binder	Sample name	Quantity milled each cycle (g)	Surface area (cm^2/g)
C	C_1min_Ring	50	4120
	C_180min_Ball	2000	4085
D	D_1min_Ring	50	4054
	D_220min_Ball	2000	4351
C	Mor_C_1min_Ring	50	4120
	Mor_C_180min_Ball	2000	4085

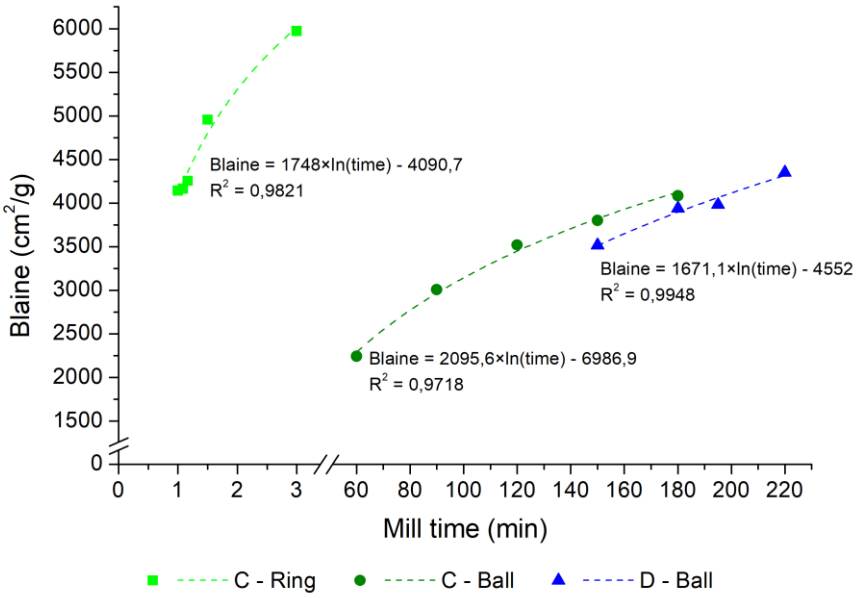

Figure 35 – Blaine surface area obtained as a function of mill time for the grinding of the amorphous binders in ball mill and ring mill.

4.2.2.3. Compressive Strength Tests

The compressive strength test is essential to study the influence of the type of mill used for the grinding on the reactivity of the amorphous, giving a straightforward and simple result from which it is possible to draw conclusions on the state of hydration at different ages when comparing the results from each sample.

To study the effect of the type of mill, pastes and mortars were prepared and studied at 2, 7 and 28 days. The compressive strength tests were performed according to the experimental procedure reported in section 3.9.

Figures 36 and 37 show the results for the compressive strength tests in function of time of hydration for the paste samples with similar fineness of binder C and D, respectively.

Both binders show slight differences in compressive strengths, with the binders milled in the ball mill showing slightly higher resistances at almost all ages and differing about 11% at 28 days from the binders milled in the ring mill. Nonetheless, these differences are acceptable, occurring from possible minor defects in the paste samples and the test variability and indicate that the type of mill used and the different particle surface charges coming from the different mills do not have a significant effect on the binder's hydraulic reactivity.

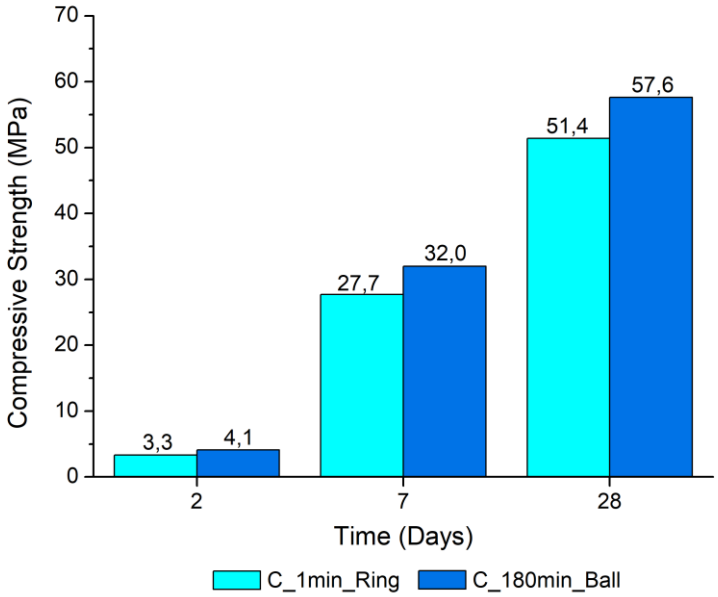

Figure 36 – Compressive strength evolution in function of time of hydration for paste samples of binder C with similar fineness from different mills.

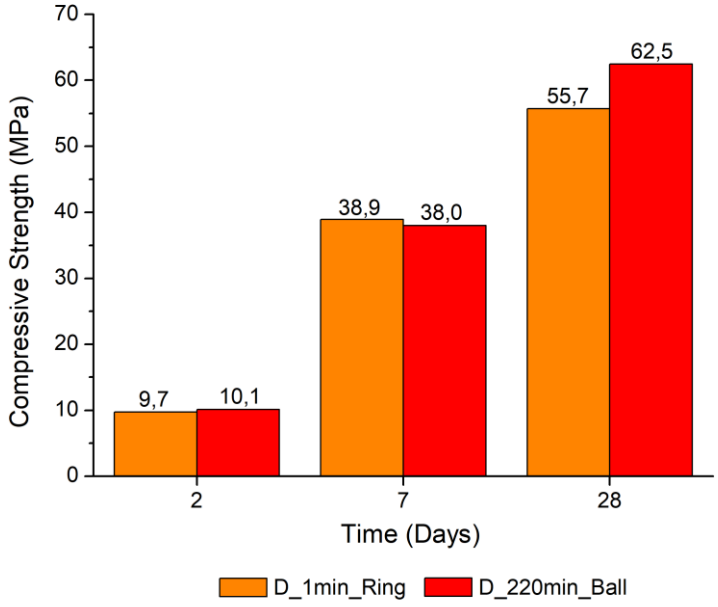

Figure 37 – Compressive strength evolution in function of time of hydration for paste samples of binder D with similar fineness from different mills.

The results for the compressive strength tests in function of time of hydration for the mortar samples with similar fineness of binder C are revealed in Figure 38, where it is possible to see that the compressive strengths developed significantly different from those of the pastes prepared with binder C, Figure 36. In mortars, the binder milled in the ring mill showed better mechanical performance than the binder milled in the ball mill, at all ages mainly at 7 days differing about 40% from the compressive

strength of the mortar prepared with the binder milled in the ball mill. However, at 28 days, the difference narrowed to about 18%.

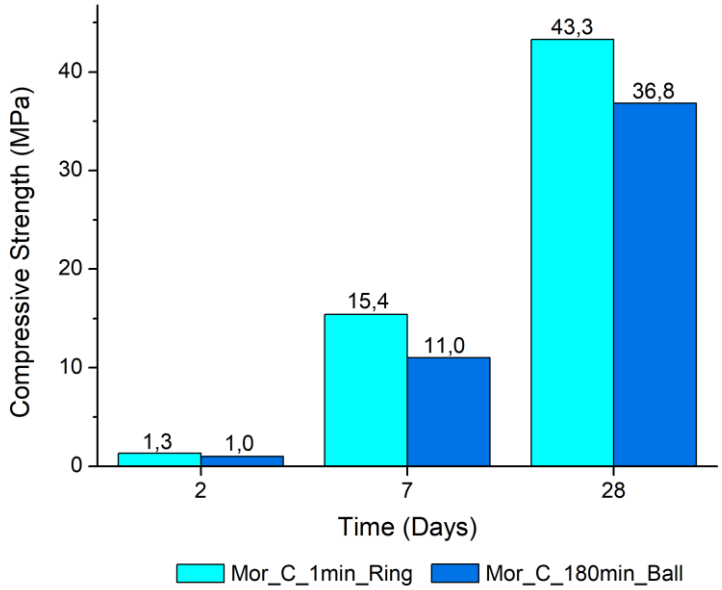

Figure 38 – Compressive strength evolution in function of time of hydration for mortar samples of binder C with similar fineness from different mills.

4.2.2.4. Thermogravimetric Analysis (TGA)

Thermogravimetric analysis tests were performed for every paste and mortar samples tested in the type of mill study and conducted as described in section 3.8. The evolution of the amount of bound water through time of hydration, namely 2, 7 and 28 days, for the paste samples of binders C and D, with similar fineness but ground in different mills is shown in Figures 39 and 40, respectively, where it is quite clear that the evolution of bound water of the samples ground in the ring mill follow a very identical trend to those ground in the ball mill for similar fineness.

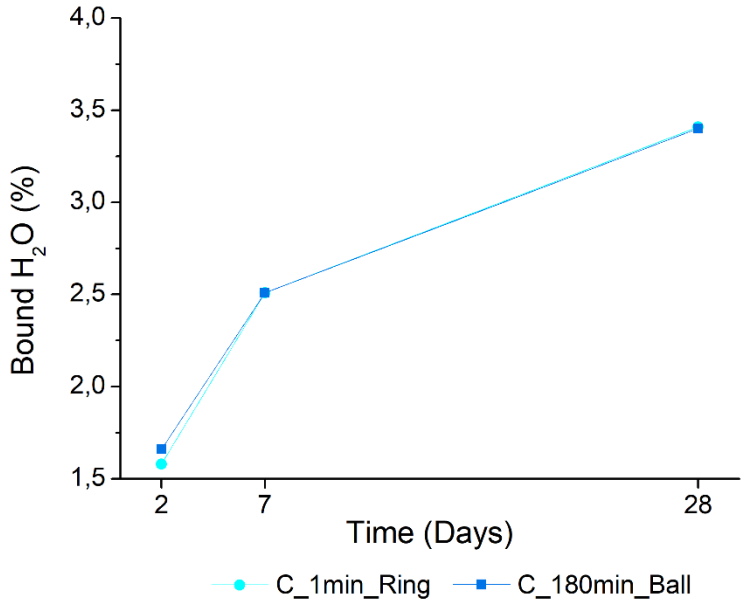

Figure 39 – Amount of bound water over time of hydration in pastes of binder C with similar fineness from different mills.

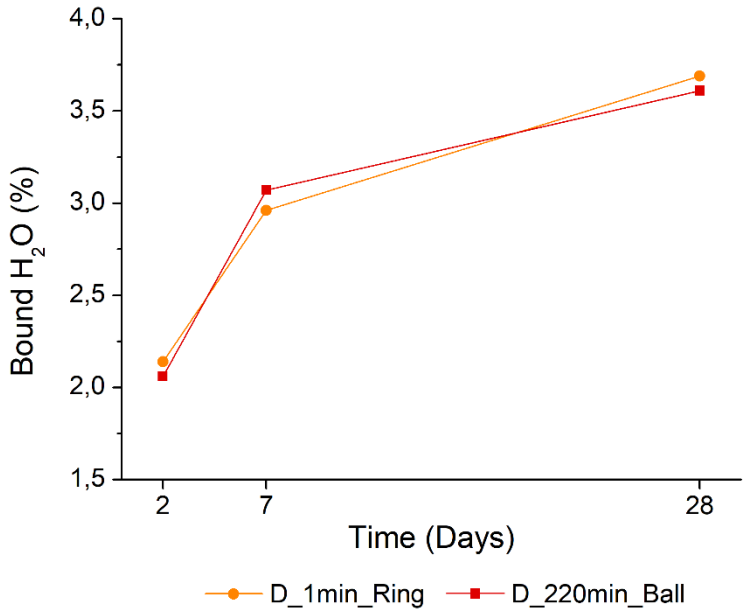

Figure 40 – Amount of bound water over time of hydration in pastes of binder D with similar fineness from different mills.

Figure 41 shows the evolution of amount of bound water through time of hydration for the mortars produced with binders C with similar fineness but ground in different mills, where the amount of bound water presents a greater disparity over time, something also seen in the mortar compressive strength results, however, overall, both samples seem to follow comparable trends, which means that hydration is occurring in a fairly similar way in both mortars.

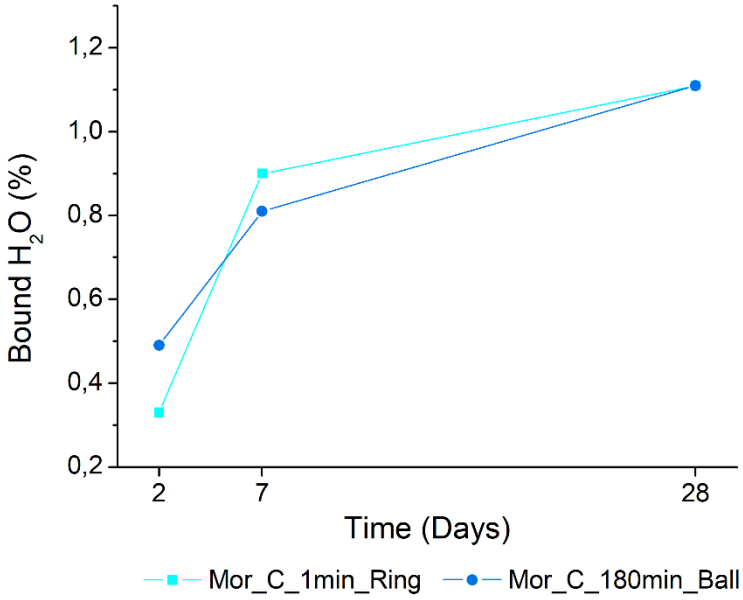

Figure 41 – Amount of bound water over time of hydration in mortar samples of binder C with similar fineness from different mills.

Plotting the compressive strength results with the amount of bound water results for each age not only provides information on how the hydration develops in each sample studied, but also gives insight about how the compressive strength is influenced by the amount of bound water and consequently, the amount of C–S–H.

In pastes, the effect that the amount of bound water has on the compressive strength appears to follow a linear trendline from 2 days until 28 days of hydration, as seen in Figure 42 displaying the results of compressive strength as a function of the amount of bound water for pastes of binder C and D with similar fineness from different mills.

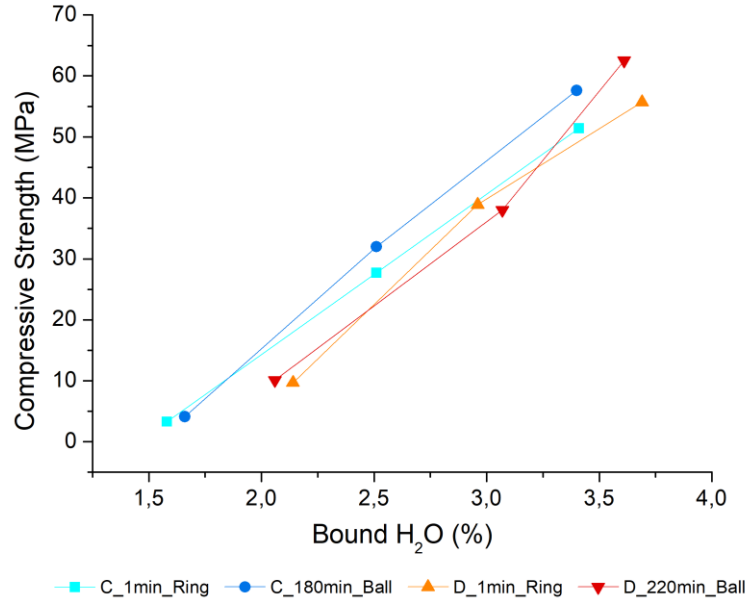

Figure 42 – Compressive strength in function of amount of bound water in pastes of binder C and D with similar fineness from different mills.

In mortars, as seen in Figure 43, the effect that the amount of bound water has on the compressive strength appears to be less significant until 7 days of hydration, or at around 1%wt. of bound water in the mortar, and much more significant after that moment, due to the slower reactivity displayed by the mortars.

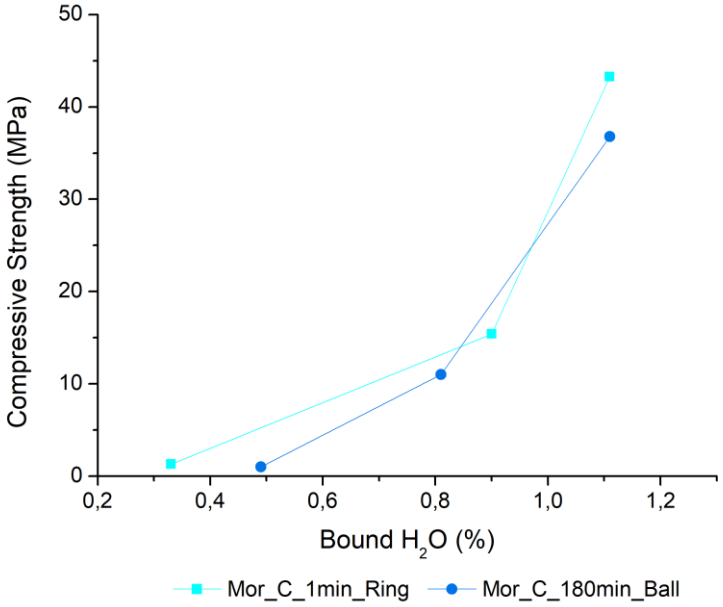

Figure 43 – Compressive strength in function of amount of bound water in mortars of binder C with similar fineness from different mills.

4.2.2.5. Fourier Transform Infrared Spectroscopy (FTIR)

Figure 44 shows the FTIR spectra for the anhydrous binder C and its hydrated pastes with similar fineness from different mills at 2, 7 and 28 days. All samples were analysed following the experimental procedure described in section 3.6.

As expected, both samples present very identical spectra. The most noticeable, though minimal, changes between the two samples can be seen in band (e) showing in sample *C_180min_Ball* a slight higher narrowing of this band, indicating larger consumption of Q^0 species, in band (g) showing a larger deformation of this band in samples from *C_180min_Ball*, related to higher formation of more ordered Q^2 structures in those samples and in band (h), samples from *C_1min_Ring* show less intense bands, indicative of lower levels of carbonation in these samples, confirming the XRD results, section 4.2.2.1 [81].

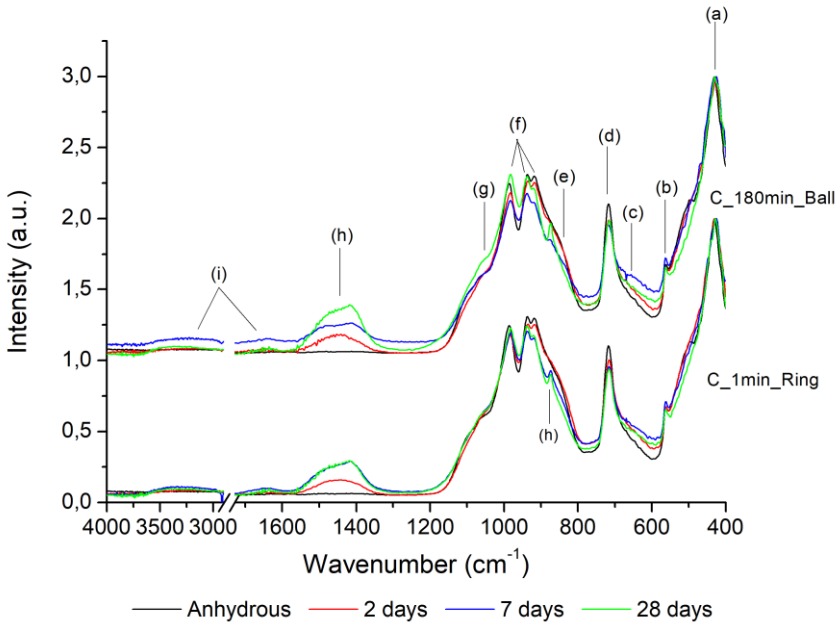

Figure 44 – FTIR spectra of anhydrous binder C and its hydrated samples with similar fineness from different mills at 2, 7 and 28 days.

Figure 45 displays the FTIR spectra for the anhydrous binder D and its hydrated pastes with similar fineness from different mills at 2, 7 and 28 days. In this case, sample *D_1min_Ring* presents slightly higher levels of ordered Q^2 structure and C–S–H, as seen by the greater deformation of bands (g) and (c). Sample *D_1min_Ring* also shows a higher carbonation level, as seen by the bands (h).

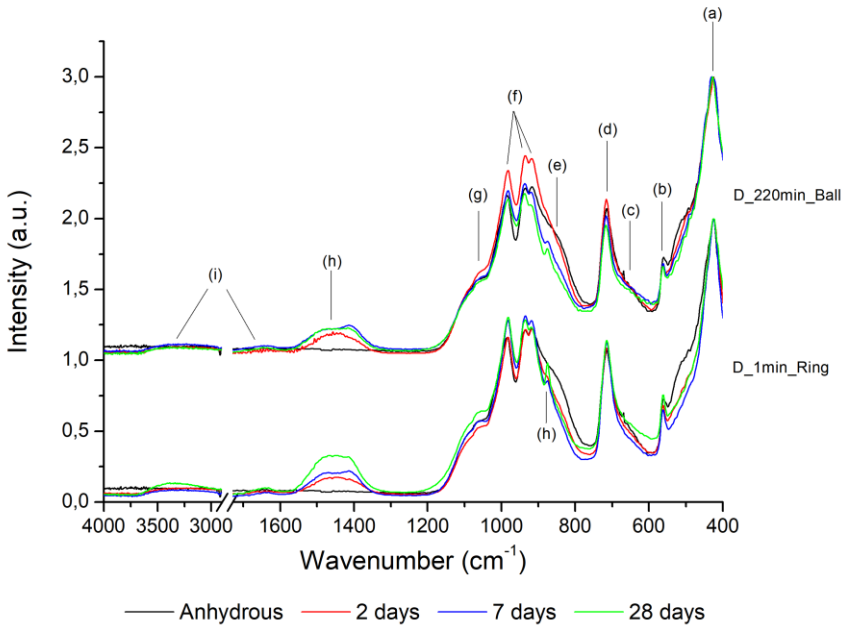

Figure 45 – FTIR spectra of anhydrous binder D and its hydrated samples with similar fineness from different mills at 2, 7 and 28 days.

4.2.2.6. Hardgrove Grinding Test

A first Hardgrove grinding test was conducted to determine the Hargrove grindability index and the Bond work index, to evaluate the grindability of the amorphous binder, a technologically important property, to assess whether the technology of grinding used in the cement industry is sufficient to provide satisfactory grinding or whether it is necessary to design new grinding techniques, and from an economic point of view, to assess whether very high grinding costs are expected to harm the financial success of the project.

The results of the Hardgrove grinding test are presented in Table 9.

Table 9 – Hardgrove grindability index and Bond work index of the amorphous binder.

HGI	Wi (kWh/ton)
47.4	18.6

4.2.3. Influence of storage time

4.2.3.1. X-Ray Diffraction and Rietveld Analysis (XRD)

The quantification of phase development through Rietveld analysis of XRD measurements of samples from binder A with different storage times, in the anhydrous state and at different hydration ages is shown in Table 10. All XRD measurements were performed as described in section 3.5.

Since sample *A_3min_Ring_1dayST* was only tested at 28 days, due to Covid-19 lockdown implications, it is also presented the phase development of a sample from binder B with 1 day of storage time to have more points for comparison.

From the analysis of the results of Table 10, the storage time of 7 days appears to not have much influence in the phase development of *A_3min_Ring_7daysST*, presenting a successive increase in the amount of tobermorite, which is very similar to the development of phases seen in the sample *B_3min_Ring_1dayST* and sample *A_3min_Ring_1dayST* at 28 days.

Table 10 – Rietveld analysis quantification of paste samples from binders A and B with different storage times.

		Rietveld analysis (% Phase quantification)			
Sample	**Time (days)**	**Amorphous**	**Pseudo-Wollastonite**	**Tobermorite**	**Calcite**
A	**Anhydrous**	**90,4**	**9,7**	**–**	**–**
A_3min_Ring_1dayST	7	Not measured			
	28	86,0	7,3	6,7	–
	90	Not measured			
A_3min_Ring_7daysST	7	89,0	6,2	4,8	–
	28	87,9	5,9	6,2	–
	90	87,1	5,3	7,6	–
B	**Anhydrous**	**85,5**	**14,5**	**–**	**–**
B_3min_Ring_1dayST	7	84,9	10,5	4,6	–
	28	83,2	10,4	6,4	–
	90	82,6	9,4	8,0	–

4.2.3.2. Isothermal Calorimetry

Figure 46 shows the evolution of normalized heat flow and the normalized cumulative heat curves in function of time of hydration for the samples of binder A with different storage times, 1 and 7 days respectively. The experimental procedure is described in section 3.7.

Although the heat flow curve illustrates that *A_3min_Ring_7daysST* hits the peak of hydration considerably later (~ 22 hours) than *A_3min_Ring_1dayST* (~ 9 hours), the total amount of heat released after 7 days is very similar between the two samples, with the sample with 7 days of storage time releasing 91,3 J/g of heat and the sample prepared with freshly ground binder releasing 85,4 J/g of heat. Thus, a storage time of up to 7 days after grinding does not seem to have a significant impact in the overall reactivity of the amorphous binder and the amount of hydration products formed after 7 days, delaying only the early kinetics of the reaction and formation of hydration products.

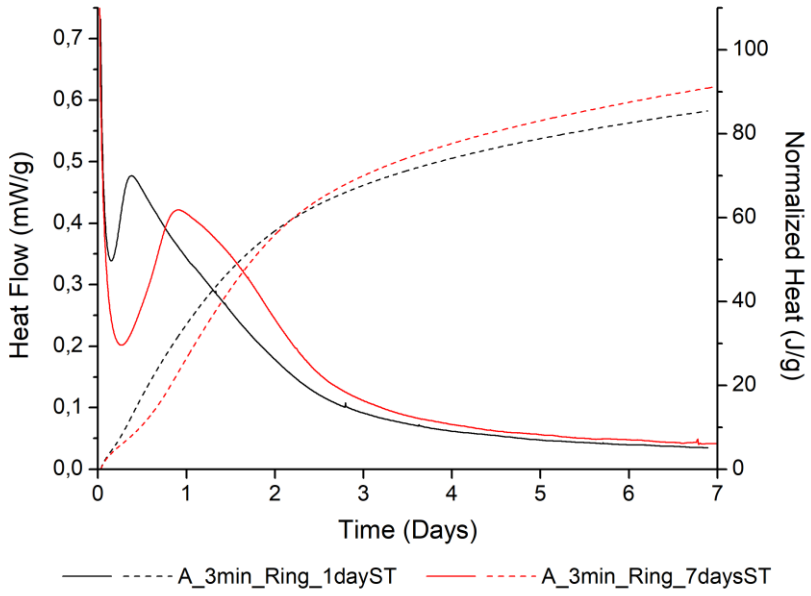

Figure 46 – Normalized heat flow and normalized cumulative heat curves in function of time of hydration for samples of binder A with different storage times.

4.2.3.3. Compressive Strength Tests

Figure 47 displays the evolution of compressive strength over the time of hydration for the paste samples of binder A with different storage times, 1 and 7 days respectively, after milling. A sample of binder B with 1 day of storage time is also shown in the figure to give a reference point for the compressive strength at 90 days. The compressive strength tests were performed according to the experimental procedure reported in section 3.9.

From the calorimetry results, section 4.2.3.2, it was concluded that the amount of hydration products formed after 7 days between both samples of binder A was similar, which is verified by the compressive strength results in Figure 47, showing almost equal compressive strengths at 7 days. Even when compared with the compressive strength of *B_3min_Ring_1dayST*, the result of *A_3min_Ring_7daysST* is very similar.

At 28 days, *A_3min_Ring_7daysST* did not show a development in compressive strength, whereas *A_3min_Ring_1dayST* and *B_3min_Ring_1dayST* increased to 116,3 MPa and 95,2 MPa, respectively. This lack of improvement may be related to an imperfect test piece, which corrupted the real performance of the sample at 28 days. This statement is also supported by the compressive strength result of *A_3min_Ring_7daysST* at 90 days that showed a great increase in performance, achieving 118,7 MPa, even more than the sample *B_3min_Ring_1dayST* that reached 103,0 MPa at 90 days. The compressive strength of *A_3min_Ring_1dayST* at 90 days was not tested, but based on other tests of this amorphous binders performed under the same conditions, it is expected that at 90 days, the compressive strength of this sample would be around 120 MPa, which represents the maximum compressive strength achieved so far for this type of binder in tests performed under the described conditions.

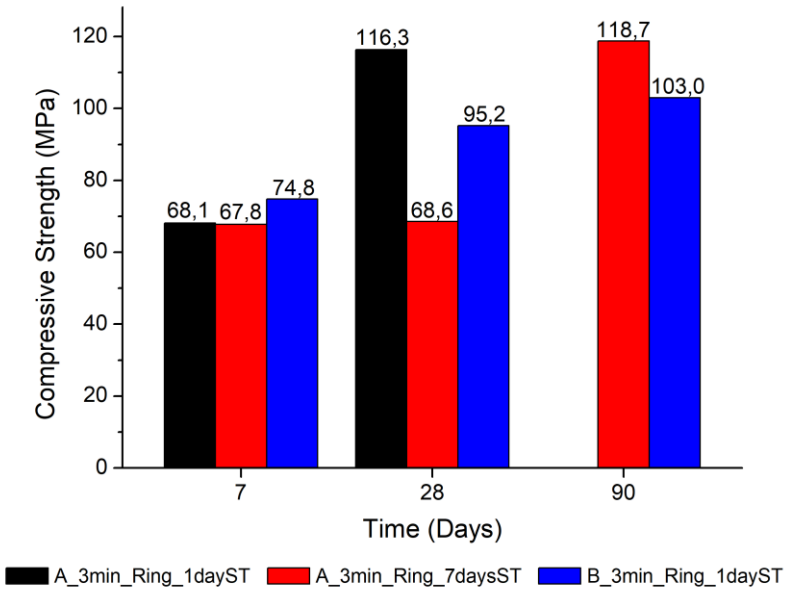

Figure 47 – Compressive strength evolution in function of time of hydration for samples of binder A and B with different storage times after milling.

4.2.3.4. Thermogravimetric Analysis (TGA)

In Figure 48 it is represented the evolution of the amount of bound water over the time of hydration for the paste samples with different storage times after milling from binder A and a paste of binder B with 1 day of storage time for a reference point at 90 days. The thermogravimetric measurements were conducted as described in section 3.8.

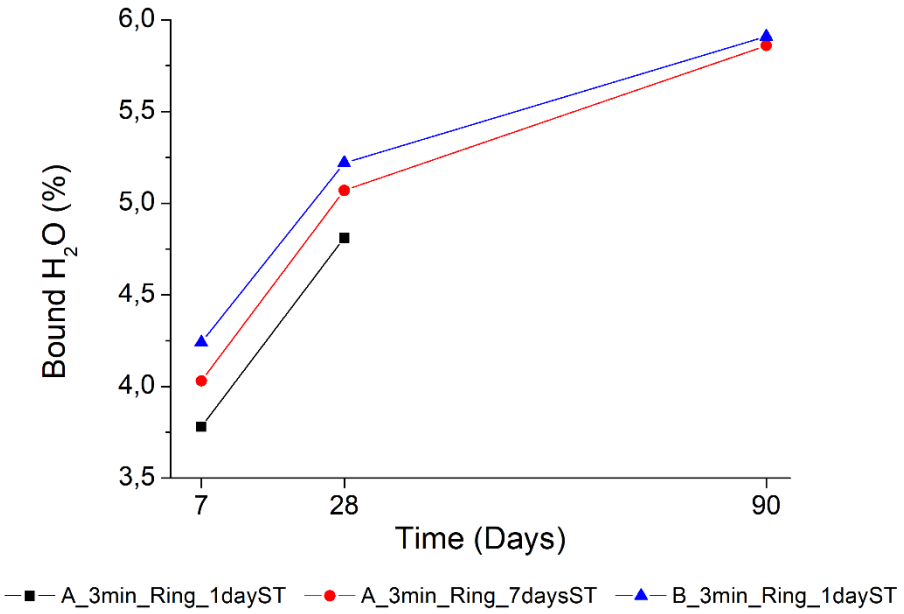

Figure 48 – Amount of bound water over time of hydration in pastes of binder A and B with different storage times after milling.

From Figure 48 it is evident that the sample with 7 days of storage time shows an almost equal rate of development of amount of bound water over all ages as the other samples with only 1 day of storage time, confirming that reactivity across all three samples is very identical and that a storage time of 7 days does not affect the performance of this binder significantly.

Moreover, from 7 to 28 days, *A_3min_Ring_7daysST* exhibits a substantial increase in the amount of bound water, which should translate into an increase in compressive strength at 28 days, which was not the case, as seen in section 4.2.3.3, confirming that the result of compressive strength at 28 days of this sample can be explained by a defective test sample.

4.2.3.5. Fourier Transform Infrared Spectroscopy (FTIR)

In Figure 49, the FTIR spectra for the anhydrous binder A and its hydrated pastes with 7 days of storage at 7, 28 and 90 days of hydration are exhibited. All samples were analysed following the experimental procedure described in section 3.6.

Due to the lack of FTIR data for the hydrated samples of binder A with 1 day of storage time, it is also displayed the FTIR spectra for the anhydrous binder B and its hydrated pastes with 1 day of storage at 7, 28 and 90 days of hydration. At 7 days, both samples from *A_3min_Ring_7daysST* and *B_3min_Ring_1daySST* were not dehydrated, which resulted in more intense bands due to the higher contribution of H_2O molecules vibration signal.

The FTIR spectra of both binders show an identical development over the time of hydration, as expected due to their similar compressive strength and amount of bound water results. In both binders, as hydration progresses and C–S–H is formed, the amount of Q^0 species, band (e), diminishes significantly. Band (g) also deform, as a more ordered Q^2 structure is formed, more significantly in *A_3min_Ring_7daysST*.

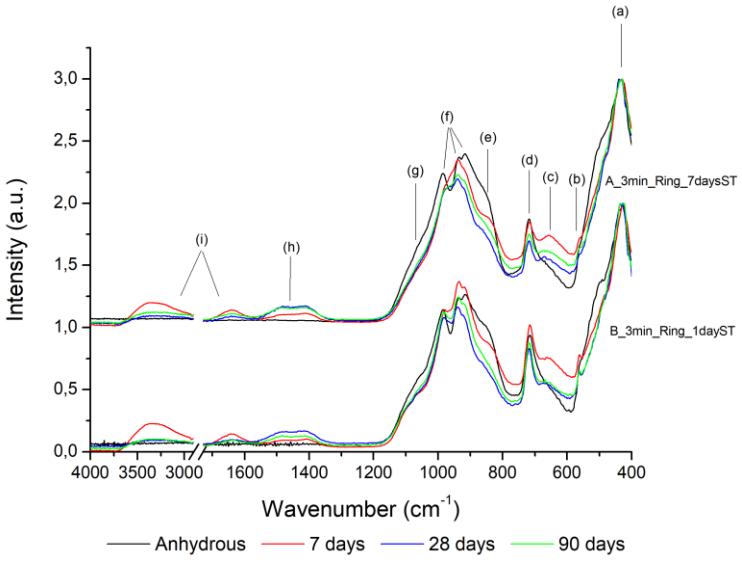

Figure 49 – FTIR spectra of anhydrous binders A and B and its hydrated samples with different storage times at 7, 28 and 90 days.

4.3. Discussion

This section presents the discussion of the results obtained in the fineness study, the mill study and the storage time study.

The calorimetry results showed that as fineness increases, the reaction kinetics of the binder with water also increases, more evidently in samples of binder B, Figure 21, where the amount of heat released after 7 days was higher and the maximum of the main hydration peak was achieved much earlier in sample *B_3min_Ring*, with higher fineness. The increased reaction kinetics of samples with higher fineness is due to the larger surface area of its particles and to its estimated reduced pore volume between the particles, resulting in a larger and easier development of bonds between C–S–H structures that allows for a faster hardening of cement and better mechanical performance.

Samples of binder A did not show such a clear relation between fineness and reaction kinetics, since the sample with higher fineness did not release the most amount of heat after 7 days nor achieved the peak of hydration earlier, Figure 20. This result is explained by the fact that the three samples of binder A differ on more than just fineness. They also differ on the storage time after grinding and the type of mill used. Such properties could be affecting the results, so, it was necessary to assess the effect that such properties have on the reactivity of the amorphous binder.

The compressive strength results verify the aforementioned calorimetry results of pastes prepared with binder B, displaying an interesting relation between both tests, Table 11, where a higher amount of heat released after 7 days corresponds to a greater compressive strength at 7 days. This relation, presented in section 5.3 with all data points of paste samples prepared with alkaline activation of Na_2SiO_3 in this thesis, proves that the release of heat during hydration is related to the formation of a C–S–H in this binder, which is also seen in OPC studies [82].

Table 11 – Calorimetry and compressive strength results of samples of binders A and B in the fineness study.

			Compressive strength (MPa)		
Sample	**Peak (hours)**	**Total heat released (J/g)**	7 days	28 days	90 days
A_145min_Ball	33,8	75,0	53,6		
A_3min_Ring	9,1	85,4	68,1	116,3	
A_145+0.5min_Ball+Ring	24,4	84,9	58,0	122,1	
B_1min_Ring	23,4	77,1	49,8	91,2	101,4
B_3min_Ring	9,1	93,3	74,8	95,2	103,0

While samples from binders A and B show an almost complete mitigation of the effect of fineness for later ages (28 and 90 days), samples from binders C and D, Figures 25 and 26 respectively, continue to display clear differences in mechanical performance at 28 days between the samples with different fineness, mainly due to the higher pseudo-wollastonite content of binders C and D, proven by Rietveld

analysis in section 4.2.1.1, which seem to weaken the hydraulic activity of the binder, delaying the compressive strength development in pastes prepared with lower fineness.

In Figure 27, compressive strength results of mortar samples prepared with binders characterized by different fineness, revealed differences in mechanical performance at all ages, nonetheless, as time progresses, the difference is diminished, reaching about 15% at 28 days. This variation may not only be explained by the increased fineness of sample *Mor_A_145+0.5min_Ball+Ring*, but also the fact that sample *Mor_A_145min_Ball* was prepared with a binder milled a week before the mortar preparation, allowing for the possible formation of some carbonation on the surface that could have slowed the reaction kinetics of this sample.

Figure 50 displays the results of compressive strength as a function of Blaine values for paste samples of binders C and D at 2, 7 and 28 days, showing the strong influence that fineness has on the compressive strength at each age. The higher the Blaine value, the higher the fineness and the smaller the particles of the binder, consequently, there is a larger surface area available to hydraulically react, accelerating the reaction kinetics and the development of compressive strength performances [65]. These results allowed to draw a linear trend line for each age, which can be used to predict, fairly reasonably, the compressive strength of a paste according to its Blaine value.

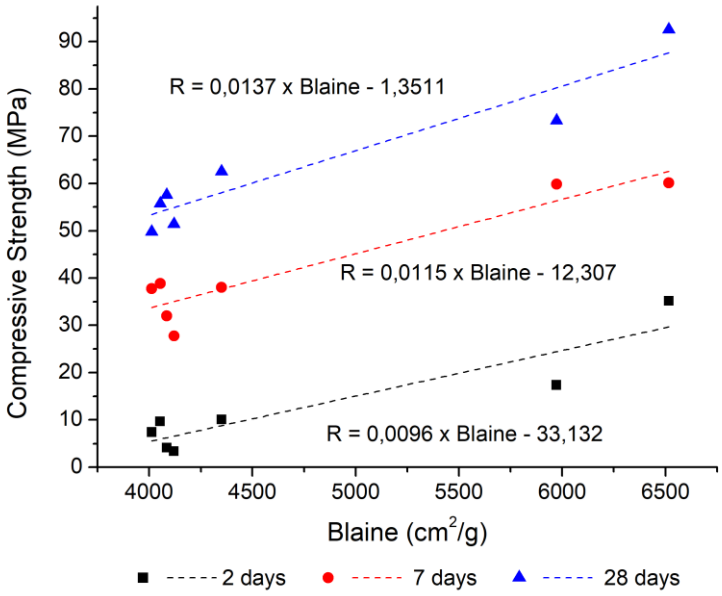

Figure 50 – Compressive strength in function of Blaine values for paste samples of binders C and D.

It is worth mentioning that, although the samples with higher fineness (milled for 3 minutes in the ring mill) develop greater mechanical performance, the workability of their prepared pastes is much worse, when compared to the pastes prepared with samples with lower fineness (milled for 1 minute in the ring mill). The worse workability of their pastes is associated with the fact that the binder's surface area available to react with water is much higher in the samples with greater fineness, which leads to higher degree of reaction with water, and consequently, higher formation of C–S–H at the expense of plasticity.

The results of thermogravimetric analysis (section 4.2.1.5) also reveal different amounts of bound water between the samples with different fineness, showing, for all ages, higher amounts of bound water for the samples with higher fineness, indicating a larger formation of hydration products, namely C–S–H in these samples. These results agree with compressive strength tests, given that samples with higher fineness present a larger formation of C–S–H, which then results in higher compressive strength. The only exception being sample B, which for similar values of compressive strength obtained at 28 and 90 days of hydration for the pastes prepared with different fineness, registered a trend similar with the other samples, regarding the evolution of the amount of bound water, with the finer sample containing larger amount of bound water.

The difference in C–S–H formation between the samples with different fineness should also be seen in Rietveld analysis of XRD measurements, where the quantification of Tobermorite phase should display what is also seen in the evolution of the amount of bound water, a clear distinction of the amount of C–S–H formed between the sample with higher fineness and the samples with lower fineness, however, this is not the case, as seen in Table 5, the Tobermorite values are very similar between the samples with different fineness. This result can be related to the fact that only a small fraction of the C–S–H formed in this binder is crystalline (< 20 %) and in the form of nanocrystals, hindering XRD measurements of C–S–H phase, leading to possible errors in its phase quantification.

The Rietveld analysis also reveals that, as hydration develops, the Pseudo-Wollastonite content decreases, as it was observed by Paradiso *et al*. [52], indicating its consumption, which is also verified by FTIR results Figures 32, 33 and 34, where the bands related to Pseudo-Wollastonite deform and contract as hydration time advances. Moreover, the consumption of this phase could be related with the formation of $CaCO_3$, since it is known that Wollastonite and its polymorphs are prone to carbonate instead of hydrating [83].

The compressive strength tests in the mill study, section 4.2.2.3, showed that paste samples with similar fineness ground in different mills have relatively identical mechanical performances, as it can be seen in Figures 36 and 37. The difference in compressive strength between the samples of binder C decreased as time progressed, from around 19% at 2 days to around 11% at 28 days. For binder D, the difference in compressive strength stood around 4% at 2 and 7 days, and around 11% at 28 days. These small differences at 28 days can be explained from the preparation of the samples and the test variability. In mortars, Figure 38, samples with similar fineness from different mills presented larger discrepancies in the results, with sample *Mor_C_180min_Ball* differing around 18% from the compressive strength result obtained for *Mor_C_1min_Ring*. These differences in the compressive strength values in the mortar samples can come from possible defects in some mortar prims or be related to the results dispersion given that samples were only tested once. Despite the slightly larger discrepancies in the mortar results, it can be concluded that the type of mill used for the grinding does not have a significant effect on the reactivity.

Thermogravimetric results revealed that paste samples with similar fineness from different mills presented identical amounts of bound water, diverging at most around 5%. From the plots of compressive strength in function of amount of bound water, Figure 42, showed almost linear trendlines

for samples with similar fineness, meaning that the amount of hydration products formed, mainly C–S–H, between the samples is very similar, at all ages, therefore hydration appears to develop at the same rate in both samples, either in binder C or in binder D, and that for similar amounts of bound water, each sample developed similar compressive strength, a sign that the microstructure built during hydration is similar in each sample, indicating, once again, that the mill used for the grinding has little effect on amorphous reactivity.

XRD results, Table 7, are in accordance with the results of TGA, revealing amounts of C–S–H, namely Tobermorite, which are identical among samples with similar fineness, at all ages. The FTIR results are in line with the Rietveld results, showing a progressive increase in C–S–H and Calcite in the sample. However, the FTIR results also show a progressive decrease in the amount of Pseudo-Wollastonite in the sample, something that is not always verified by Rietveld analysis, largely because of the greater crystalline amount of binders C and D, which made it difficult to make representative and homogeneous takings of the whole sample, promoting the existence of greater discrepancies in the crystalline content in sample preparation and also in XRD measurements.

To better prepare for the transition to large-scale amorphous production at a pilot production facility, the Hardgrove grinding test was conducted to evaluate the grindability of the amorphous binder. The Hardgrove grindability index determined was HGI = 47.4, while the Bond work index was Wi = 18.6 kWh/ton, and compared with the Bond work indices of traditional OPC clinkers, which are among the 13 and 16 kWh/ton, the amorphous milling costs are expected to be slightly higher than those of traditional clinkers, however, as the mechanical performances do not appear to be influenced by the type of grinding, it is expected that the current clinker grinding technology used in the cement industry can be used to mill the amorphous without requiring major changes.

In the storage time study, the isothermal calorimetry experiment, Figure 46, revealed that the sample with greater storage time had slower reaction kinetics than the sample prepared with binder freshly ground. The delaying of the kinetics can be associated to the carbonation that occurs on the surface of the amorphous after grinding. This carbonated surface makes the dissolution of calcium and silica species more difficult, slowing down the kinetics of reaction at early ages. Even so, after 7 days, both samples released similar amounts of heat, indicating that the amount of hydration products in both samples should be similar.

Figure 47 shows that the compressive strength results in the storage time study are in agreement with the calorimetry results, given that, at 7 days, the samples with different storage time have almost equal mechanical performance. At 28 days, the sample with the longest storage time, *A_3min_Ring_7daysST* did not develop compressive resistance, so it revealed a large discrepancy in relation to the sample without storage time, *A_3min_Ring_1dayST*, caused by defects in the paste specimen at this age, since at 90 days, sample *A_3min_Ring_7daysST* showed an impressive performance development, reaching a compressive strength similar to other samples without storage time, and TGA measurements at 28 days of paste with 7 days of storage time showed a significant development of amount of bound water. Given these results, it can be concluded that a storage time of up to 7 days does not have a significant effect in the reactivity of the binder.

5. Effects of different activators in the alkaline activation solution

In this chapter, the results of different activators are presented in an attempt to replace, partially or totally, the role of sodium silicate (Na_2SiO_3) in the alkaline activation. In addition, a study of the effect that the successive reduction of the sodium silicate content on alkaline activation has on the mechanical performance of this amorphous binder is also presented.

Until the present moment, the best mechanical performances in pastes of this amorphous binder are achieved through the hydration of its ground powder with an alkaline solution of sodium silicate, sodium hydroxide (NaOH) and water (H_2O). With the current composition, this alkaline solution represents a significant cost that may hinder its hopes of being a real competitor to OPC.

In order to optimize the process, lowering the costs related to alkaline activation, two possible solutions stood out. The first associated to the reduction of the sodium silicate content without decreasing mechanical performance and the second related to the search for an alternative activator to sodium silicate that guarantees an identical compressive strength but that allows for costs reduction. As alternatives, two less expensive activators were tested, sodium sulphate (Na_2SO_4) and calcium sulphate ($CaSO_4$).

Lastly, a study was also conducted regarding the optimization of the W/C ratio in mortars to achieve the best mechanical performance while ensuring a good workability.

5.1. Experimental procedure

In this chapter, three different binders were used, D, E and F. Regarding milling conditions, binders E and F were milled for 3 minutes in the ring mill and binder D was milled in the ball mill for 220 minutes.

The reduction of the Na_2SiO_3 content in the alkaline solution was studied from the usual composition used in chapter 4, an aqueous alkaline solution of Na_2SiO_3 and NaOH, with a 2%wt. Na_2O concentration and a W/C ratio of 0.25, referred to as 100% Na_2SiO_3, followed by successive reductions of 25% until the situation that there is no Na_2SiO_3 in the solution, having only water and NaOH, referred to as 0% Na_2SiO_3, while maintaining the same W/C ratio.

It was also tested if a partial replacement of Na_2SiO_3 for Na_2SO_4 or $CaSO_4$, could provide promising results, and therefore, a viable solution. For the situation of 50% Na_2SiO_3, while keeping the same NaOH concentration and W/C ratio, it was added the correspondent Na_2SO_4 to maintain a 2%wt. Na_2O concentration. For the mixture with CaSO4, the same NaOH + 50% Na_2SiO_3 solution was prepared, adding $CaSO_4$ in the same SO_3 concentration as in the mixture with Na_2SO_4.

Na_2O concentration, W/C ratio, Na_2SiO_3 content and the adopted nomenclature for each paste sample in the Na_2SiO_3 study is described in Table 12.

Table 12 – Na_2O concentration, W/C ratio, Na_2SiO_3 content and the adopted nomenclature for each paste sample in the Na_2SiO_3 study.

Binder	% Na_2O	Activators	W/C	% Na_2SiO_3	Sample name
D	2	NaOH + Na_2SiO_3	0.25	100	D_2%Na_2O_100%Na_2SiO_3
	1.819		0.25	75	D_1.819%Na_2O_75%Na_2SiO_3
	1.638		0.25	50	D_1.638%Na_2O_50%Na_2SiO_3
	1.456		0.25	25	D_1.456%Na_2O_25%Na_2SiO_3
	1.275		0.25	0	D_1.275%Na_2O_0%Na_2SiO_3

Na_2O concentration, W/C ratio, Na_2SiO_3 content and the adopted nomenclature for each paste sample in the Na_2SiO_3 mixtures study is described in Table 13.

Table 13 – Na_2O concentration, W/C ratio, Na_2SiO_3 content and the adopted nomenclature for each paste sample in the Na_2SiO_3 mixtures study.

Binder	% Na_2O	Activators	W/C	% Na_2SiO_3	Sample name
D	2	NaOH + Na_2SiO_3 + Na_2SO_4	0.25	50	D_2%Na_2O_50%Na_2SiO_3+50%Na_2SO_4
	1.638	NaOH + Na_2SiO_3 + $CaSO_4$	0.25	50	D_1.638%Na_2O_50%Na_2SiO_3+50%$CaSO_4$

For the alternative activators study, a total replacement of Na_2SiO_3 in the aqueous alkaline solution of Na_2SiO_3 and NaOH, with a 2%wt. Na_2O concentration and a W/C ratio of 0.25 was tested.

In the Na_2SO_4 study, an aqueous solution prepared with the same concentration and W/C ratio was first tested or with slightly different W/C ratio in order to obtain better plasticity of the pastes, replacing only Na_2SiO_3 with Na_2SO_4. Also, it was studied the effect that a higher concentration of Na_2SO_4 has on the reactivity of the binder while maintaining the same concentration of NaOH and the same W/C ratio.

In the $CaSO_4$ study, two aqueous solutions were tested with the same NaOH concentration and W/C ratio used in the Na_2SO_4 study or with slightly different W/C ratio in order to obtain better plasticity of the pastes, replacing Na_2SO_4 with $CaSO_4$ in the same SO_3 concentration in both solutions.

Na_2O concentration, W/C ratio, Na_2SO_4 concentration and the adopted nomenclature for each paste sample in the Na_2SO_4 study is described in Table 14.

Table 14 – Na_2O concentration, W/C ratio, Na_2SO_4 concentration and the adopted nomenclature for each paste sample tested in the Na_2SO_4 study.

Binder	% Na_2O	Activators	W/C	%wt. Na_2SO_4	Sample name
D	2	NaOH + Na_2SO_4	0.25	1.66	D_2%Na_2O_1.66%wt.Na_2SO_4
E	2		0.263	1.66	E_2%Na_2O_1.66%wt.Na_2SO_4

F	2		0.27	1.66	F_2%Na_2O_1.66%wt.Na_2SO_4
D	3.275		0.25	4.58	D_3.275%Na_2O_4.58%wt.Na_2SO_4

Na_2O concentration, W/C ratio, $CaSO_4$ concentration and the adopted nomenclature for each paste sample in the $CaSO_4$ study is described in Table 15.

Table 15 – Na_2O concentration, W/C ratio, $CaSO_4$ concentration and the adopted nomenclature for each paste sample in the $CaSO_4$ study.

Binder	% Na_2O	Activators	W/C	%wt. $CaSO_4$	Sample name
D	1.275	NaOH + $CaSO_4$	0.25	1.59	D_1.275%Na_2O_1.59%wt.$CaSO_4$
E	1.275		0.27	1.59	E_1.275%Na_2O_1.59%wt.$CaSO_4$
D	1.275		0.25	4.39	D_1.275%Na_2O_4.39%wt.$CaSO_4$

To optimize of W/C ratio in mortars, four mortar samples were prepared using 4 different aqueous alkaline solutions of NaOH and Na_2SiO_3 where the W/C ratio was changed, while maintaining the same Na/H_2O concentration used in paste samples.

Na_2O concentration, W/C ratio and the adopted nomenclature for each mortar sample in the W/C study is described in Table 16.

Table 16 – Na_2O concentration, W/C ratio and the adopted nomenclature for each mortar sample in the W/C ratio study.

Binder	% Na_2O	Activators	W/C	Sample name
D	3.04	NaOH + Na_2SiO_3	0.38	Mor_D_3.04%Na_2O_W/C = 0.38
	2.92		0.365	Mor_D_2.92%Na_2O_W/C = 0.365
	2.80		0.35	Mor_D_2.80%Na_2O_W/C = 0.35
	2.68		0.335	Mor_D_2.68%Na_2O_W/C = 0.335

5.2. Results

5.2.1. Effect of sodium silicate (Na_2SiO_3) content in the alkaline activation

5.2.1.1. X-ray Diffraction with Rietveld Analysis

In Table 17 it is presented the development of phase quantification through Rietveld analysis of XRD measurements of binder D in the anhydrous state and their hydrated samples prepared with different amounts of Na_2SiO_3 in the alkaline activation solution. XRD measurements were performed as described in section 3.5.

The higher degree of heterogeneity of binder D in the anhydrous state, due to their higher amount of crystalline structures, led to some discrepant values in the quantification of the Amorphous and Pseudo-Wollastonite phases.

All samples showed a continuous formation of C–S–H, both in a crystalline structure and in a more amorphous structure. However, and against what was expected, the total amount of C–S–H formed did not increase with the increase in Na_2SiO_3 added to the alkaline solution, according to the results of the Rietveld analysis. This can be explained by the fact that some samples analysed by XRD were not fairly representative of the sample as a whole and it may be associated with the error of the Rietveld analysis (~1%).

Table 17 – Rietveld analysis quantification of paste samples prepared with different amounts of Na_2SiO_3.

		Rietveld analysis (% Phase quantification)			
Sample	**Time (days)**	**Amorphous**	**Pseudo-Wollast.**	**Tobermorite**	**Calcite**
D	**Anhyd.**	**82,5**	**17,5**	**–**	**–**
D_2%Na_2O_100%Na_2SiO_3	2	81,1	17,5	1,3	0,1
	7	80,1	16,5	1,9	1,0
	28	76,9	19,0	3,0	1,1
D_1.819%Na_2O_75%Na_2SiO_3	2	80,6	17,7	1,6	–
	7	75,5	19,7	4,5	–
	28	77,3	18,6	3,6	0,5
D_1.638%Na_2O_50%Na_2SiO_3	2	81,2	16,8	2,0	–
	7	78,3	18,8	2,4	0,4
	28	75,1	20,3	4,1	0,6
D_1.456%Na_2O_25%Na_2SiO_3	2	79,0	18,8	2,2	–
	7	76,8	19,1	4,1	–
	28	78,4	17,8	3,3	0,5
D_1.275%Na_2O_0%Na_2SiO_3	2	79,8	18,8	1,5	–
	7	76,8	19,0	4,1	0,1
	28	78,7	18,0	2,9	0,3

In Table 18 it is presented the development of phase quantification through Rietveld analysis of XRD measurements of binder D in the anhydrous state and their hydrated samples prepared with NaOH and 50% Na_2SiO_3, and samples activated with NaOH and 50% Na_2SiO_3 mixed with Na_2SO_4 or $CaSO_4$, respectively.

Samples *D_1.638%Na_2O_50%Na_2SiO_3* and *D_2%Na_2O_50%Na_2SiO_3+50%Na_2SO_4* show a similar development of the crystalline C–S–H phase, tobermorite, indicating that the hydration of each of these samples occurred in a similar way, despite presenting different values, among themselves, in the amorphous phase and pseudowollastonite due to the heterogeneity of binder D.

Sample *D_1.638%Na_2O_50%Na_2SiO_3+50%$CaSO_4$* reveals a slower development of C–S–H, displaying lower values of tobermorite at all ages.

Table 18 – Rietveld analysis quantification of paste samples prepared with mixtures of Na_2SO_4 or $CaSO_4$.

		Rietveld analysis (% Phase quantification)			
Sample	**Time (days)**	**Amorphous**	**Pseudo-Wollast.**	**Tobermorite**	**Calcite**
D	**Anhyd.**	**82,5**	**17,5**	**–**	**–**
D_1.638%Na_2O_50%Na_2SiO_3	2	81,2	16,8	2,0	–
	7	78,3	18,8	2,4	0,4
	28	75,1	20,3	4,1	0,6
D_2%Na_2O_50%Na_2SiO_3+ 50%Na_2SO_4	2	78,8	19,2	2,0	
	7	81,4	16,2	2,4	
	28	75,0	20,2	4,0	0,8
D_1.638%Na_2O_50%Na_2SiO_3+ 50%$CaSO_4$	2	79,3	19,1	1,6	
	7	79,2	18,2	2,2	0,3
	28	77,3	19,5	2,7	0,5

5.2.1.2. Isothermal Calorimetry

In Figure 51 it is represented the evolution of normalized heat flow and the normalized cumulative heat curves in function of time of hydration for the samples with different amounts of Na_2SiO_3 in the alkaline activation solution. The experimental procedure is described in section 3.7.

From the results, it is evident that the successive increase of Na_2SiO_3 successively delays the maximum of the main hydration peak, with the sample without Na_2SiO_3, *D_1.275%Na_2O_0%Na_2SiO_3*, reaching the reaction peak after approximately 4 hours, whereas the sample with 100% of the usual amount of Na_2SiO_3, *D_2%Na_2O_100%Na_2SiO_3*, reaches this peak after almost 26 hours.

Although samples with a lower amount of Na_2SiO_3 reach their peak of hydration much earlier, the reaction kinetics of these samples show a sudden and significant drop after the peak, which is not seen in samples with more Na_2SiO_3, namely 50%, 75% and 100% Na_2SiO_3. In these samples with more Na_2SiO_3, the kinetic deceleration of the reaction after the peak is more controlled, causing these samples to release more heat after 7 days. Thus, it is evident that with the successive increase of Na_2SiO_3, the amount of heat released after 7 days also increases successively, with sample *D_1.275%Na_2O_0%Na_2SiO_3* releasing 42,1 J/g while sample with 100% Na_2SiO_3 releases 62,2 J/g.

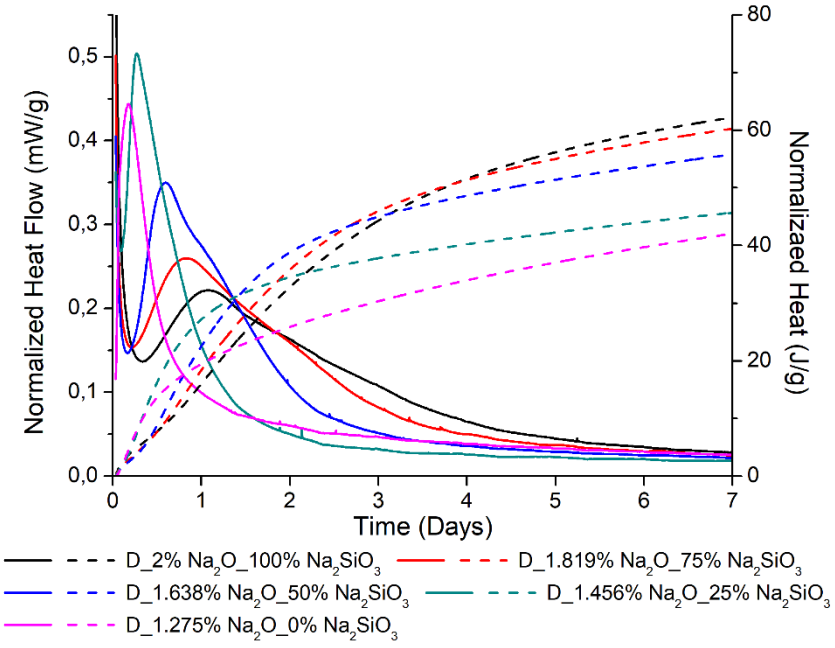

Figure 51 – Normalized heat flow and normalized cumulative heat curves in function of time of hydration for samples with different amounts of Na_2SiO_3.

The key results of the calorimetry experiment are summarized in Table 19, with Hf max, QH2D and QH7D representing the maximum heat flow, the total heat released at 2 days and 7 days of hydration, respectively.

Table 19 – Calorimetry results of samples with different amounts of Na_2SiO_3.

Sample	Hf max (mW/g)	Peak (hours)	QH2D (J/g)	QH7D (J/g)
100% Na_2SiO_3	0,22	25,8	32,8	62,2
75% Na_2SiO_3	0,26	19,9	35,8	60,3
50% Na_2SiO_3	0,35	14,2	38,8	55,8
25% Na_2SiO_3	0,50	6,5	34,5	45,7
0% Na_2SiO_3	0,44	4,2	25,9	42,1

5.2.1.3. Compressive Strength Tests

Figure 52 shows the evolution of compressive strength over the time of hydration for paste samples with different amounts of Na_2SiO_3 in the alkaline activation solution. The compressive strength tests were performed according to the experimental procedure reported in section 3.9.

The results show that as the amount of Na_2SiO_3 increases, so does the compressive strength, except for very early ages, 2 days, where the best mechanical performance is achieved for the sample with 50% Na_2SiO_3, *D_1.638%Na_2O_50%Na_2SiO_3*. A note worth mentioning is that sample with 75% Na_2SiO_3 developed identical, or even better, mechanical performances than sample with 100% Na_2SiO_3, a promising result for the reduction of Na_2SiO_3 in the activation solution.

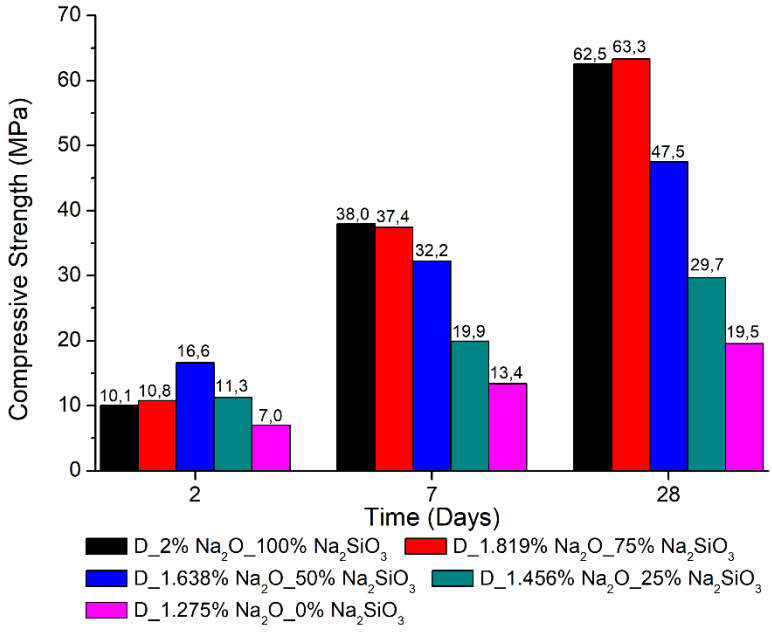

Figure 52 – Compressive strength evolution over time for paste samples with different Na_2SiO_3 content.

From the results in Figure 52, it was clear that the paste prepared with the 50% Na_2SiO_3 solution showed good mechanical performance at young ages, showing only at 28 days significantly lower performance than the pastes prepared with more Na_2SiO_3 content. In an attempt to improve compressive strength at 28 days, Na_2SO_4 was added to the 50% Na_2SiO_3 solution, in order to reach the 2% Na_2O concentration seen in the 100% Na_2SiO_3. In another solution of 50% Na_2SiO_3, $CaSO_4$ was also tested in the same SO_3 concentration as in the Na_2SiO_3 + Na_2SO_4 mixture solution.

Figure 53 displays the evolution of compressive strength over the time of hydration for paste samples prepared with NaOH and 50% Na_2SiO_3 (blue columns), and samples activated with NaOH and 50% Na_2SiO_3 mixed with Na_2SO_4 or $CaSO_4$ (green and orange columns, respectively).

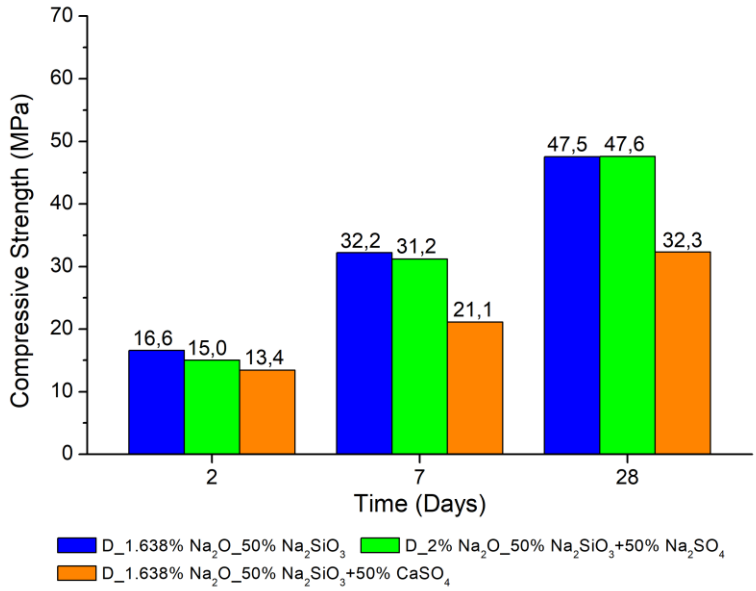

Figure 53 – Compressive strength evolution over time for paste samples with mixtures of activators.

The addition of Na_2SO_4 to the alkaline solution of NaOH and 50% Na_2SiO_3 showed a nearly irrelevant effect in mechanical performance compared to an alkaline activation of only NaOH and 50% Na_2SiO_3, since the compressive strengths were approximately the same. Adding $CaSO_4$ to the alkaline solution of NaOH and 50% Na_2SiO_3 resulted in a loss of reactivity, displaying significantly lower compressive strengths than the sample activated with only NaOH and 50% Na_2SiO_3.

5.2.1.4. Thermogravimetric Analysis (TGA)

Figure 54 shows the evolution of the amount of bound water over the time of hydration for paste samples prepared with different amounts of Na_2SiO_3 in the alkaline activation solution. Thermogravimetric measurements were conducted as described in section 3.8.

The results consistently show that for larger amounts of Na_2SiO_3, more bound water is found in the samples, except for the results at 2 days. Samples prepared with 50% and 75% Na_2SiO_3 show amounts of bound water similar to those of sample prepared with 100% Na_2SiO_3, demonstrating that hydration occurs similarly between these samples, producing similar amounts of hydration products. On the other hand, samples with 0% and 25% Na_2SiO_3 present much lower amounts of bound water.

Thus, it can be concluded that increasing the amount of Na_2SiO_3 added to the alkaline solution means that more hydration products are formed.

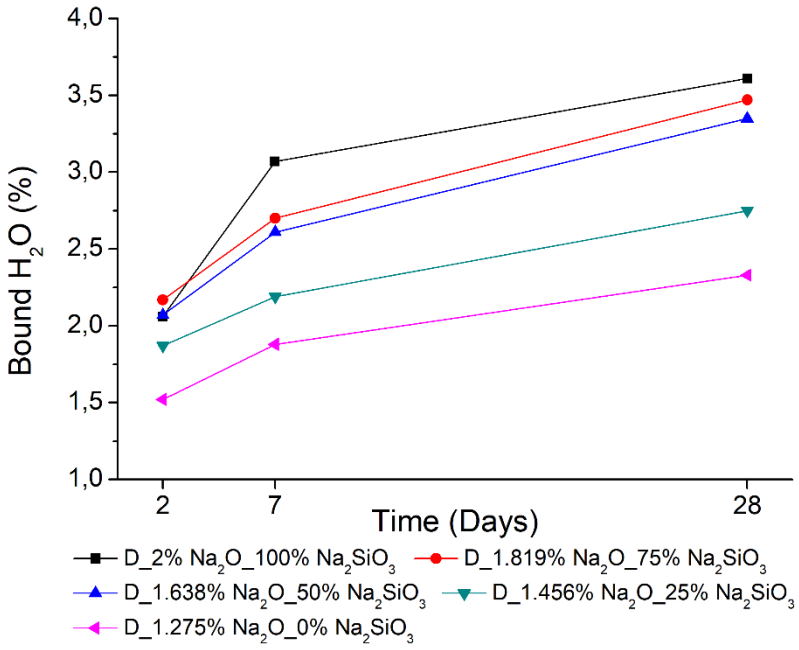

Figure 54 – Amount of bound water over the time of hydration in pastes with different amounts of Na_2SiO_3.

Figure 55 displays the development of the amount of bound water over the time of hydration for paste samples prepared with NaOH and 50% Na_2SiO_3 (blue symbols), as a reference, and samples activated with NaOH and 50% Na_2SiO_3 mixed with Na_2SO_4 (green symbols) or $CaSO_4$ (orange symbols), respectively.

Sample prepared with only NaOH and 50% Na_2SiO_3 and sample prepared with NaOH and 50% Na_2SiO_3 mixed with Na_2SO_4 show a quite similar development in the amount of bound water at all ages, indicating that the amount of hydration products formed in these two samples are identical. Sample prepared with NaOH and 50% Na_2SiO_3 mixed with $CaSO_4$ shows lower amounts of bound water at all ages, especially at 7 and 28 days, meaning that the amount of hydration products formed, namely C–S–H, are much smaller in this sample.

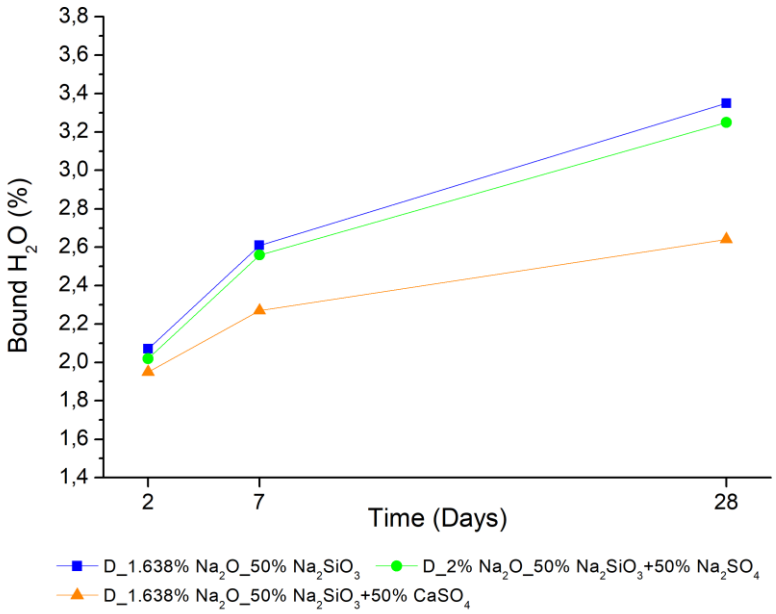

Figure 55 – Amount of bound water over the time of hydration in pastes activated with NaOH + 50% Na_2SiO_3 mixed with Na_2SO_4 or $CaSO_4$.

5.2.1.5. Fourier Transform Infrared Spectroscopy (FTIR)

The FTIR spectrum for the anhydrous binder D and its hydrated pastes prepared with different amounts of Na_2SiO_3 in the alkaline activation solution at 2, 7 and 28 days of hydration is presented in Figure 56. All samples were analysed following the experimental procedure described in section 3.6.

At all ages, the evolution of the FTIR spectrum of each sample seems to occur in a similar way, except for the sample with 0% Na_2SiO_3, whose deformations are less noticeable in relation to its anhydrous spectrum in bands (c) and (e), indicating a lower amount of C–S–H formed in this sample.

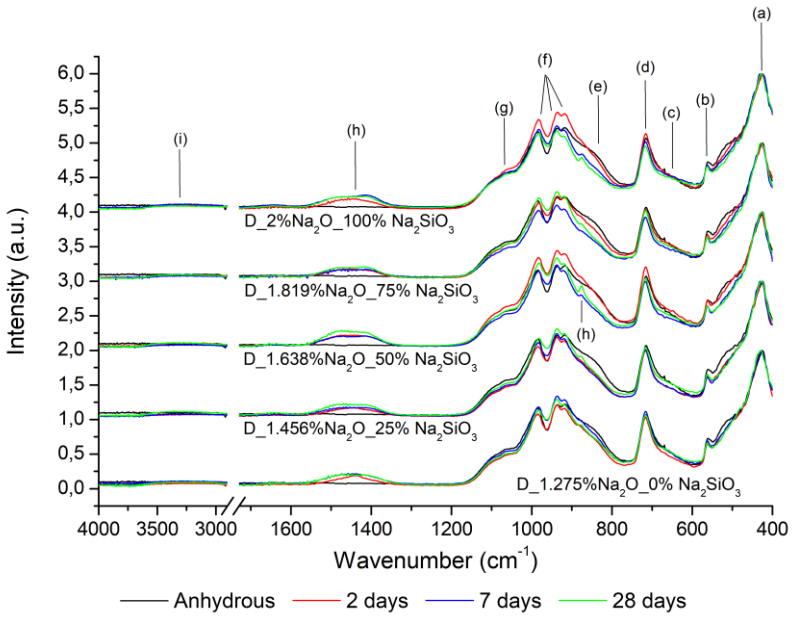

Figure 56 – FTIR spectra of anhydrous binder D and its hydrated samples with different amounts of Na_2SiO_3.

Figure 57 shows the FTIR spectrum for the anhydrous binder D and the hydrated samples prepared with NaOH and 50% Na_2SiO_3, and with NaOH and 50% Na_2SiO_3 mixed with Na_2SO_4 or $CaSO_4$, respectively.

As hydration progresses, the FTIR spectrum of each sample develops identically, bands (e) and (f) contract, more evidently in samples *D_1.638%Na_2O_50%Na_2SiO_3* and *D_2%Na_2O_50%Na_2SiO_3+50%Na_2SO_4*, representing the consumption of Q^0 and Q^1 species, respectively. Also, band (c) deforms, which is related with the Si-O-Si bonds in tobermorite-type C–S–H structures, and band (h) expands due to the carbonation of each sample.

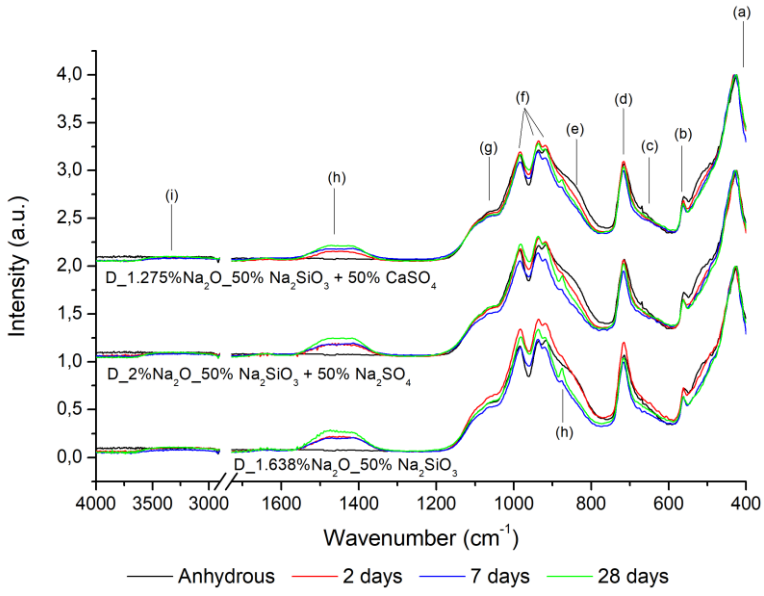

Figure 57 – FTIR spectra of anhydrous binder D and its hydrated samples with mixtures of Na_2SiO_3 with Na_2SO_4 and $CaSO_4$.

5.2.2. Effect of sodium sulphate (Na_2SO_4) as an activator in the alkaline activation

5.2.2.1. X-ray Diffraction with Rietveld Analysis

In Table 20 it is presented the development of phase quantification through Rietveld analysis of XRD measurements of samples in the anhydrous state and their hydrated samples prepared with Na_2SO_4 as a replacement to Na_2SiO_3 at different hydration ages. XRD measurements were performed as described in section 3.5.

Table 20 – Rietveld analysis quantification of paste samples prepared with Na_2SO_4 as a replacement to Na_2SiO_3.

		Rietveld analysis (% Phase quantification)			
Sample	**Time (days)**	**Amorphous**	**Pseudo-Wollast.**	**Tobermorite**	**Calcite**
D	**Anhyd.**	**82,5**	**17,5**	**–**	**–**
D_2%Na_2O_1.66%wt.Na_2SO_4	2	81,4	16,5	1,7	0,4
	7	77,3	18,9	3,3	0,5
	28	75,0	19,5	4,7	0,8
D_3.275%Na_2O_4.58%wt.Na_2SO_4	2	79,5	19,0	1,2	0,4
	7	76,7	20,3	2,5	0,5
	28	75,3	20,2	4,0	0,6
E	**Anhyd.**	**88,3**	**11,7**	**–**	**–**
E_2%Na_2O_1.66%wt.Na_2SO_4	2	88,9	8,2	2,7	0,2
	7	90,5	6,4	2,8	0,4
	28	84,1	9,6	5,4	0,9
F	**Anhyd.**	**90,0**	**10,0**	**–**	**–**
F_2%Na_2O_1.66%wt.Na_2SO_4	2	91,9	5,6	2,2	0,3
	7	88,9	6,9	3,8	0,4
	28	88,5	6,2	4,7	0,6

The higher degree of heterogeneity of binder D in the anhydrous state, due to their higher amount of crystalline structures, led to some discrepant values in the quantification of the Amorphous and Pseudo-Wollastonite phases.

It is possible to see that an alkaline activation with Na_2SO_4 allowed for a continuous formation of C–S–H, in a crystalline structure such as Tobermorite. It is also noticeable the formation of calcite in the samples. However, the increase of Na_2SO_4 did not lead to an increase in the amount of Tobermorite formed.

5.2.2.2. Compressive Strength Tests

Figure 58 shows the development of compressive strength over the time of hydration for paste samples of binder D, E and F (red, blue and dark cyan columns, respectively) prepared with Na_2SO_4 as a replacement to Na_2SiO_3. It is also shown the compressive strength evolution for a paste sample of binder D prepared with a higher concentration of Na_2SO_4 (magenta columns) and, as a reference, the compressive strength development of a paste prepared with 100% Na_2SiO_3 (black columns). The compressive strength tests were performed according to the experimental procedure reported in section 3.9.

Paste samples with Na_2SO_4 from binder D and F show identical and higher compressive strengths at all ages than the paste samples with binder E. Moreover, at 28 days, the paste prepared with binder D with higher concentration of Na_2SO_4 showed slightly better mechanical performance than pastes prepared with binders D and F with equal concentration, which could indicate that the increase in concentration of Na_2SO_4 in the alkaline solution resulted in an improvement, although not impressive, of the mechanical performance. Nonetheless, all samples with Na_2SO_4 tested showed significantly lower mechanical performances than the reference paste with Na_2SiO_3, excluding at 2 days.

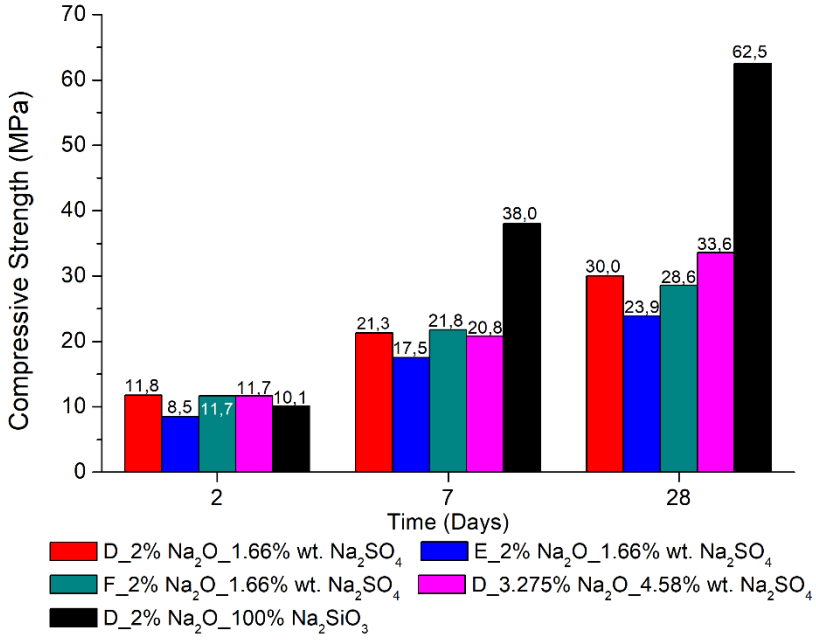

Figure 58 – Compressive strength evolution over time of hydration for paste samples with Na_2SO_4 as activator.

5.2.2.3. Thermogravimetric Analysis (TGA)

Figure 59 displays the evolution of the amount of bound water over time of hydration for the paste samples prepared with Na_2SO_4 as a replacement to Na_2SiO_3 and for the Na_2SiO_3 reference. Thermogravimetric measurements were conducted as described in section 3.8.

All pastes prepared with Na_2SO_4, except for sample from binder D with lower concentration of Na_2SO_4, present similar amounts of bound water at all ages, which indicates that hydration is developing

identically between these samples, producing identical amounts of hydration products. This fact can support the idea that the increase in Na_2SO_4 concentration did promote a slight formation of more hydration products. Nevertheless, sample from binder D with lower concentration presented smaller amounts of bound water at 7 and 28 days than the other samples, which should suggest smaller amounts of hydration products, namely C–S–H, which is not verified by the compressive strength results, section 5.2.2.2, indicating that some TGA measurements of pastes prepared with binder D may be compromised.

Compared with the amount of bound water present in the pastes prepared with 100% Na_2SiO_3, the reference, all pastes prepared with Na_2SO_4 showed smaller amounts of bound water, and therefore, hydration products, which is in agreement with the compressive strength results that showed better mechanical performance for the Na_2SiO_3 pastes.

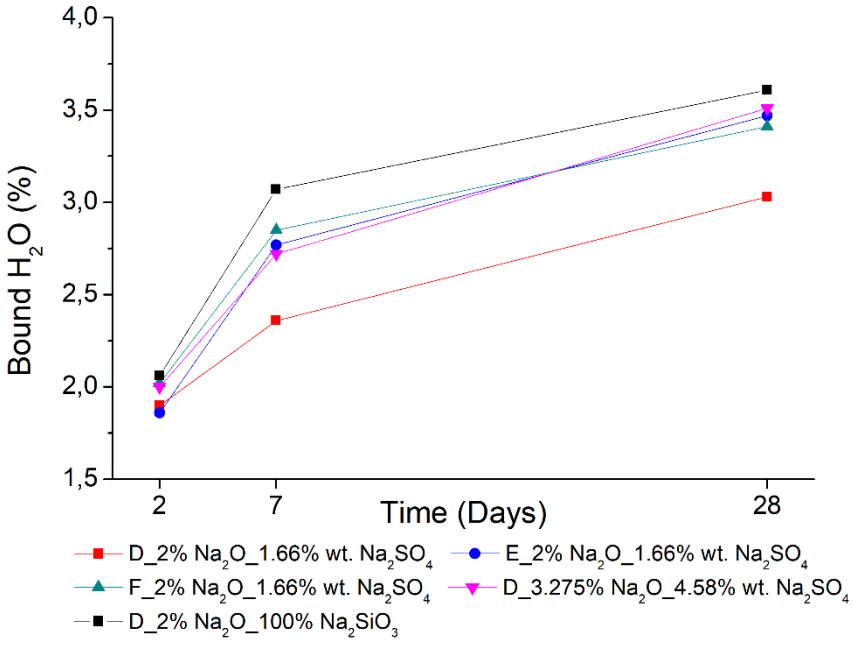

Figure 59 – Amount of bound water through time of hydration in paste samples with Na_2SO_4 as activator.

5.2.2.4. Fourier Transform Infrared Spectroscopy (FTIR)

Figure 60 shows the FTIR spectra for binders in the anhydrous state and their hydrated samples prepared with Na_2SO_4 as a replacement to Na_2SiO_3 at different hydration ages. All samples were analysed following the experimental procedure described in section 3.6.

The most perceptible changes between the samples are visible between their anhydrous spectra, where binder D present more intense (b), (d) and (f) bands, for example. This is evidence of a greater amount of pseudowollastonite in this binder, as confirmed by XRD results in section 5.2.2.1. Also, binders E and F present a greater amount of Q^0 species in the anhydrous state, band (e), which prompted the formation of a more ordered structure than samples from binder D, as seen by the deformation of the beforementioned band.

Furthermore, sample *D_3.275%Na_2O_4.58%wt.Na_2SO_4* presents a peak in band (c) and also, a shift of band (g) to higher wavenumbers, not visible in the other samples, that may be related to the higher presence of the sulphate-based activator. Band (c) presents a peak at ~610 cm^{-1} related to the bending vibration of S-O bonds and band (g) shifts towards ~1100 cm^{-1} associated to the stretching vibration of S-O bonds [84] [85].

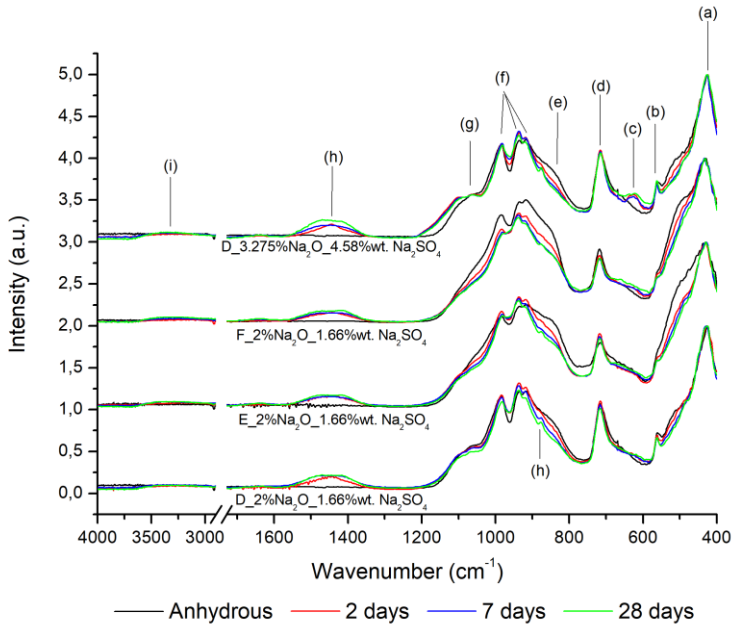

Figure 60 – FTIR spectra of anhydrous binders and their hydrated samples with Na_2SO_4 at 2, 7 and 28 days.

5.2.3. Effect of calcium sulphate ($CaSO_4$) as an activator in the alkaline activation

5.2.3.1. X-ray Diffraction with Rietveld Analysis

In Table 21 it is presented the development of phase quantification through Rietveld analysis of XRD measurements of samples in the anhydrous state and their hydrated samples prepared with $CaSO_4$ as a replacement to Na_2SiO_3 at different hydration ages. XRD measurements were performed as described in section 3.5.

The higher degree of heterogeneity of binder D in the anhydrous state, due to their higher amount of crystalline structures, led to some discrepant values in the quantification of the Amorphous and Pseudo-Wollastonite phases.

The results show that alkaline activation with $CaSO_4$ also prompted the formation of hydration products, mainly C–S–H, both in a crystalline structure an in a more amorphous structure. The formation of calcite is also visible from XRD measurements. Lastly, the increase of $CaSO_4$ concentration did not result in an increase in the amount of C–S–H formed.

Table 21 – Rietveld analysis quantification of paste samples prepared with $CaSO_4$ as a replacement to Na_2SiO_3.

		Rietveld analysis (% Phase quantification)			
Sample	**Time (days)**	**Amorphous**	**Pseudo-Wollast.**	**Tobermorite**	**Calcite**
D	**Anhyd.**	**82,5**	**17,5**	**–**	**–**
D_1.275%Na_2O_1.59%wt.$CaSO_4$	2	81,5	16,4	2,1	–
	7	77,3	18,7	3,6	0,4
	28	75,0	19,5	4,7	0,8
D_1.275%Na_2O_4.39%wt.$CaSO_4$	2	70,7	27,9	1,2	0,2
	7	75,8	22,0	1,5	0,7
	28	79,4	17,9	2,0	0,7
E	**Anhyd.**	**88,3**	**11,7**	**–**	**–**
E_1.275%Na_2O_1.59%wt.$CaSO_4$	2	88,8	9,0	1,7	0,5
	7	90,3	7,3	1,9	0,5
	28	88,1	8,2	3,3	0,4

5.2.3.2. Compressive Strength Tests

The evolution of compressive strength over the time of hydration for paste samples prepared with $CaSO_4$ as a replacement to Na_2SiO_3 with binder D and E (red and blue columns) is displayed in Figure 61. The compressive strength development is also shown for a paste sample of binder D prepared with a greater concentration of $CaSO_4$ (magenta columns) and, as a reference, the compressive strength development of a paste prepared with 100% Na_2SiO_3 (black columns). The compressive strength tests were performed according to the experimental procedure reported in section 3.9.

Paste samples with $CaSO_4$ from binder D and E display similar compressive strengths at early ages, however at 28 days, sample *D_1.275%Na_2O_1.59%wt.$CaSO_4$* presents a lower compressive resistance than sample *E_1.275%Na_2O_1.59%wt.$CaSO_4$*, due to its lower amorphous content in the anhydrous state, as seen in XRD measurements, in section 5.2.3.1. From the results of sample *D_1.275%Na_2O_4.39%wt.$CaSO_4$*, it is possible to see that the increase in $CaSO_4$ concentration resulted in a decrease in mechanical performance at early ages, compared with the other sample from binder D, *D_1.275%Na_2O_1.59%wt.$CaSO_4$*. In addition, all pastes prepared with $CaSO_4$ compared to the pastes prepared with Na_2SiO_3, showed significantly lower mechanical performances at all ages.

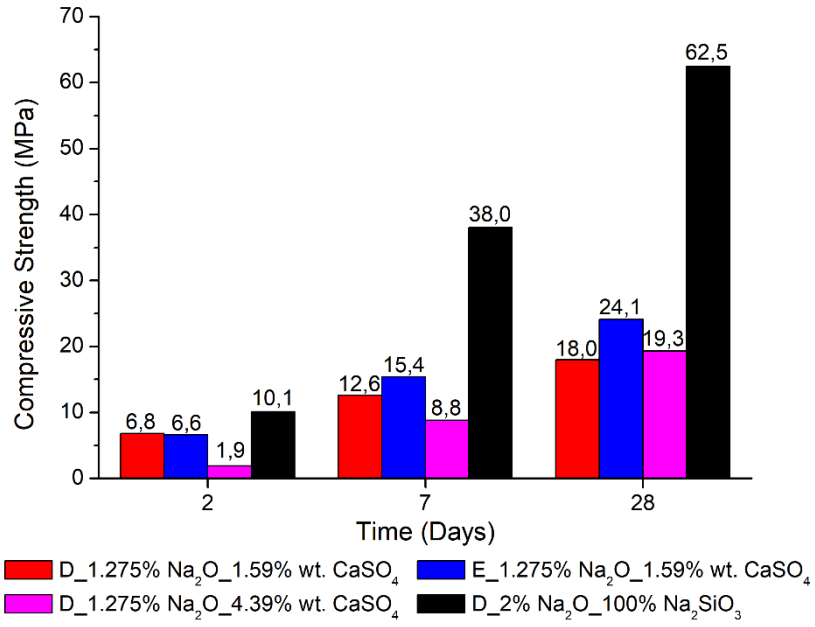

Figure 61 – Compressive strength evolution over time of hydration for paste samples with $CaSO_4$ as activator.

5.2.3.3. Thermogravimetric Analysis (TGA)

The evolution of the amount of bound water over time of hydration for the paste samples prepared with $CaSO_4$ as a replacement to Na_2SiO_3 and for the Na_2SiO_3 reference are shown in Figure 62. Thermogravimetric measurements were conducted as described in section 3.8.

Sample *D_1.275%Na_2O_4.39%wt.$CaSO_4$* showed a slower development of bound water than sample *D_1.275%Na_2O_1.59%wt.$CaSO_4$* that has a smaller $CaSO_4$ concentration, indicating that the reaction kinetics was slowed down by the increased concentration of $CaSO_4$.

Compared with the amount of bound water present in the pastes prepared with 100% Na_2SiO_3, the reference, all pastes prepared with $CaSO_4$ showed smaller amounts of bound water, and therefore, hydration products, which is in agreement with the compressive strength results that showed better mechanical performance for the Na_2SiO_3 paste.

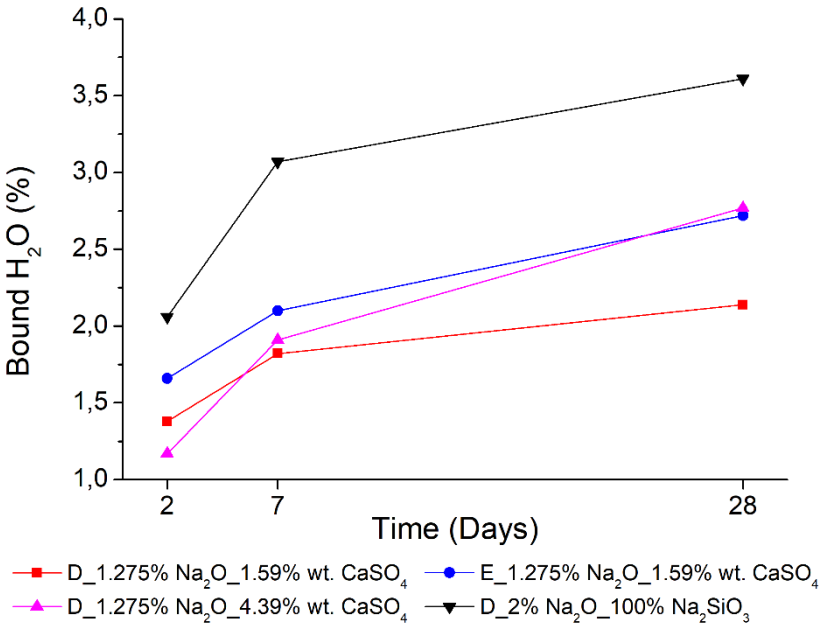

Figure 62 – Amount of bound water through time of hydration in paste samples with $CaSO_4$ as activator.

5.2.3.4. Fourier Transform Infrared Spectroscopy (FTIR)

Figure 63 displays the FTIR spectra for binders in the anhydrous state and their hydrated samples prepared with $CaSO_4$ as a replacement to Na_2SiO_3 at different hydration ages. All samples were analysed following the experimental procedure described in section 3.6.

The most perceptible changes between the samples are visible between their anhydrous spectra, where binder D present higher (b), (d) and (g) bands than binder E, for example. This is evidence of a greater amount of pseudowollastonite in this binder.

Furthermore, binders E presents a greater amount of Q^0 species in the anhydrous state, bands (e), which encouraged the formation of a more ordered structure than samples from binder D, as seen by the deformation of the aforementioned bands.

Also, sample *_1.275%Na_2O_4.39%wt.$CaSO_4$* presents a peak in band (c) as well as a shift of band (g) to higher wavenumbers, not visible in the other samples, which may be related to the higher presence of the sulphate-based activator. Band (c) presents a peak at ~610 cm^{-1} related to the bending vibration of S-O bonds and band (g) shifts towards ~1100 cm^{-1} associated to the stretching vibration of S-O bonds [84] [85].

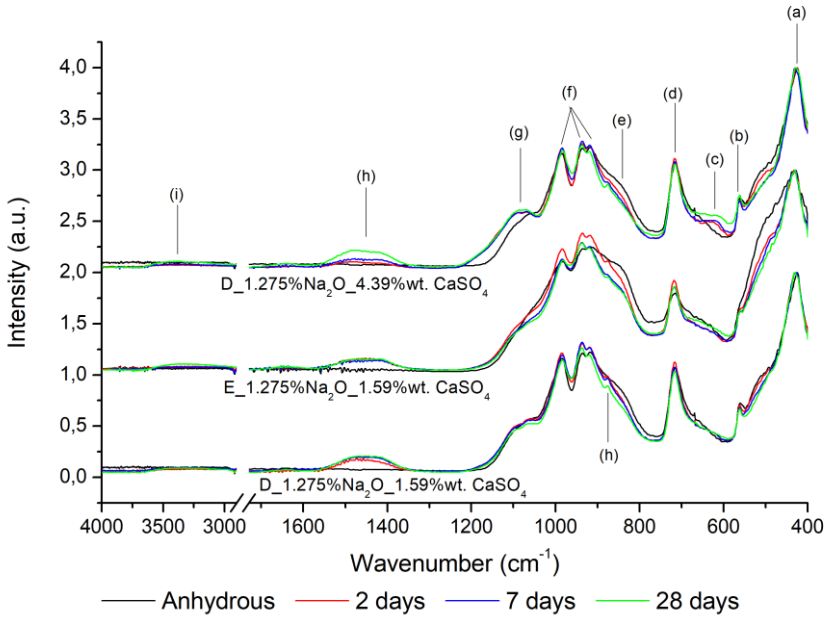

Figure 63 – FTIR spectra of anhydrous binders and their hydrated samples with $CaSO_4$ at 2, 7 and 28 days.

5.2.4. Optimization of W/C ratio in mortars

5.2.4.1. Workability Tests

Workability measurements were performed as described in section 3.11.

Table 22 shows the results for the workability tests for mortar with different W/C ratios. As expected, increasing the W/C ratio also increases the workability of the mortar.

Table 22 – Workability results of mortars with different W/C ratios.

A/C	Workability (%)
0,38	61
0,365	47
0,35	28
0,335	18

5.2.4.2. Compressive Strength Tests

Figure 64 shows the development of compressive strength at 2, 7 and 28 days of hydration for mortar samples with different W/C ratios. The compressive strength tests were performed according to the experimental procedure reported in section 3.9.

The results show that the best mechanical performance in mortars is achieved for the sample with W/C = 0.365, which achieved higher compressive strengths than the other samples at all ages.

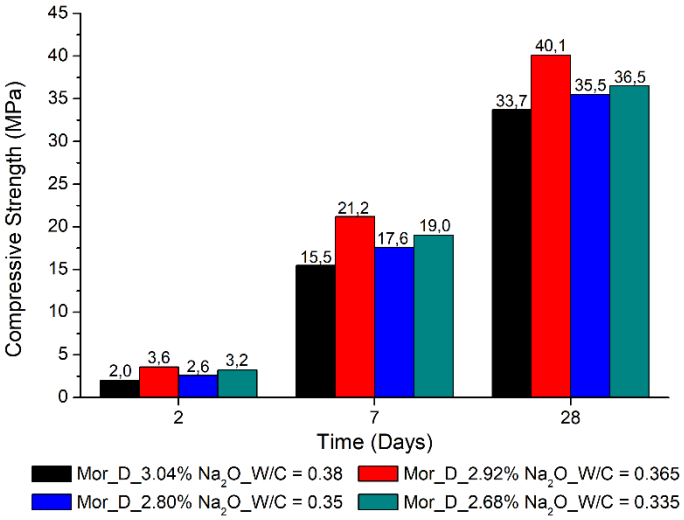

Figure 64 – Compressive strength evolution over time of hydration for mortar samples with different W/C ratios.

5.2.4.3. Thermogravimetric Analysis (TGA)

Figure 65 shows the evolution of the amount of bound water over the time of hydration for mortar samples with different W/C ratio. Thermogravimetric measurements were conducted as described in section 3.8.

All samples show a similar development of the amount of bound water over time, with quite similar values of bound water, except for the sample *Mor_D_2.92%Na_2O_W/C = 0.365*, that presents higher values of bound water at 7 and 28 days. This increased amount of bound water for mortar sample prepared with W/C = 0.365 can be explained by the fact that the TGA measurements of this mortar sample were performed according to a different method than the other samples, which led to these discrepant values. Nonetheless, it was expected that the amount of bound water of sample *Mor_D_2.92%Na_2O_W/C = 0.365* would be higher than all other mortar samples, considering the compressive strength results in section 5.2.4.2.

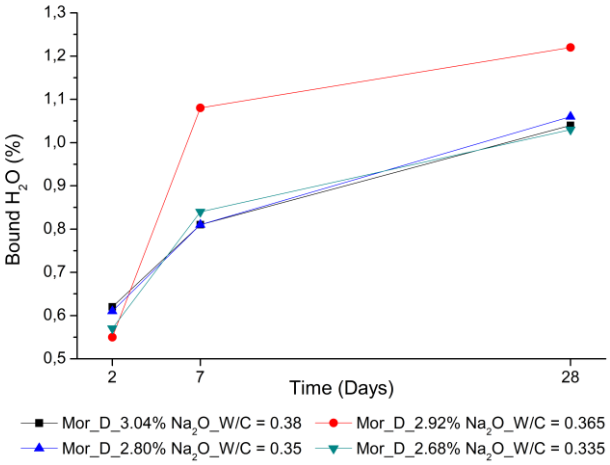

Figure 65 – Amount of bound water over time of hydration for mortar samples with different W/C ratios.

5.3. Discussion

In this section it is presented the discussion of the results in the studies of alternative activators, Na_2SO_4 and $CaSO_4$, the reduction of Na_2SiO_3 in the alkaline solution, mixtures of alternative activators with Na_2SiO_3 and the optimization of W/C ratio in mortars.

Both alkaline activation with Na_2SO_4 (Figure 58) and alkaline activation with $CaSO_4$ (Figure 61) show much lower compressive strengths than alkaline activation with Na_2SiO_3 (Figure 52), at all ages. The best mechanical performances achieved by activations with Na_2SO_4 and $CaSO_4$ roughly equal the performances achieved by an activation with only 25% Na_2SiO_3 of the amount normally used, which defeats the purpose of using these alternative activators.

In both cases, activation with Na_2SO_4 and $CaSO_4$, the increase in the concentration of each activator did not result in improvements in mechanical performance, and in the case of $CaSO_4$, the increase in concentration even worsened the compressive strengths, so it is not expected that the results of these alkaline activations improve significantly with another increase in concentrations of each activator.

According to Richardson [28], a model for the C–S–H found in samples with C/S lower than 1.4, which is the case for this amorphous binder, is given by Equation 7, based on the Tobermorite structure of severely dried samples.

$$\frac{H_2O}{Si} = \frac{19}{17} \times \frac{Ca}{Si} - \frac{7}{17} \tag{7}$$

In the present thesis, the binder under study presents a C/S around 1.1. For this reason, the chemical formula for the C–S–H formed in the samples of this thesis is $C_{1.1}SH_{0.82}$. Knowing the chemical formula of the C–S–H and the amount of bound water for each sample, determined by TGA measurements, the amount of C–S–H can be determined.

Figure 66 shows the results of compressive strength as a function of the amount of C–S–H of each sample activated with NaOH + Na_2SiO_3, NaOH + Na_2SO_4 and NaOH + $CaSO_4$. It is possible to see that pastes activated with Na_2SO_4 or $CaSO_4$ require a lower amount of C–S–H (8.9% and 8.8%, respectively) than Na_2SiO_3 (14.0%) to start developing compressive strengths, however, the activation with Na_2SiO_3 provides the formation of a more effective C–S–H, reaching significantly higher compressive strengths for the same amount of C–S–H.

Taking these results into account, both the alkaline activation with NaOH + Na_2SO_4 and the alkaline activation with NaOH + $CaSO_4$, cannot be considered as viable alternatives to the alkaline activation NaOH + Na_2SiO_3.

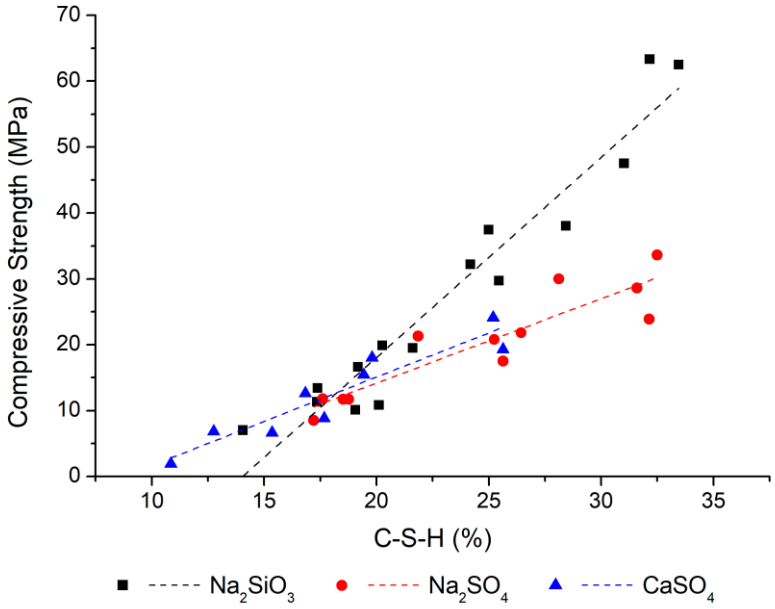

Figure 66 – Compressive strength in function of the amount of C–S–H formed in pastes for the different activators.

From the observation of Figure 51, which shows the calorimetry results for the samples with different amounts of Na_2SiO_3, it was clear that the peak of hydration was successively delayed as the amount of Na_2SiO_3 increased, allowing the appearance of an induction period. This induction period appears and becomes more evident as more Na_2SiO_3 is added. The addition of more Na_2SiO_3 increases the amount of soluble Si in the paste, which causes a very low undersaturation of Si in the reaction medium. Low Si undersaturation means that there is not enough energy to remove activation energy barriers for the dissolution of Si from the amorphous binder. As the soluble Si that comes from the activator is consumed to form C–S–H, the level of undersaturation increases, until there is enough driving force to remove the activation energy barriers, and then, the dissolution of Si from the binder starts to take place. Thus, the greater the amount of Na_2SiO_3 in the activation solution, the greater the amount of soluble Si, so the longer it takes to start dissolving Si in the binder, which leads to a longer induction time and a later peak of reaction [86].

According to Zuo *et al.* [86] and Ben Haha *et al.* [87], the increased amount of soluble Si also affects the microstructure formation, allowing for the formation of a homogeneous microstructure instead of a heterogeneous microstructure that is formed in the activation with only NaOH. This homogeneous microstructure is formed due to the delay in the dissolution of the binder, which gives sufficient time for the reaction products to form uniformly in the amorphous.

From the calorimetry results it is also possible to see that, as the amount of Na_2SiO_3 in the alkaline solution increases, so does the amount of heat released after 7 days, as expected given that as the amount of Na_2SiO_3 increases, the greater the amount of soluble Si that can act as a nucleation site.

Figure 52 shows the compressive strengths achieved for each sample with different amounts of Na_2SiO_3, in which samples with at least 50% Na_2SiO_3 stand out, reaching acceptable strengths for all

ages. Within these, it is still possible to see that the sample with 75% Na_2SiO_3 achieves results essentially equal to the sample with 100% Na_2SiO_3. Thus, it is possible to reduce the amount of Na_2SiO_3 that was previously used by about 25% without compromising the mechanical performance, allowing to lower the cost of alkaline activation required for this binder.

The addition of Na_2SO_4 and $CaSO_4$ to the activating solution of NaOH + 50% Na_2SiO_3 did not improve the mechanical performances, as shown in Figure 53. Sample D_2%Na_2O_50%Na_2SiO_3+50%Na_2SO_4 developed similar strengths to those of sample D_1.638%Na_2O_50%Na_2SiO_3, while sample D_1.638%Na_2O_50%Na_2SiO_3+50%$CaSO_4$ revealed considerably lower resistances, as a result of lower amounts of C–S–H formed, as indicated by TGA measurements (Figure 55) and Rietveld analysis (Table 18). The worse performance achieved by the activation with the mixture with $CaSO_4$ may be explained by the greater amount of Ca present in the reaction medium, coming from the activating solution, delays the dissolution of Ca from the binder, resulting in a slower growth of C–S–H and, consequently, lower compressive strengths.

Regarding mortars, the results showed that, as expected, as W/C ratio increased, so did the workability, since the increase of water favours the physical separation between particles. Nonetheless, mortar samples prepared with W/C = 0.38 and W/C = 0.365, whose workability is still far from the values typically reached by a traditional OPC with W/C = 0.5, around 83%, showed acceptable workability and a behaviour similar to that of a cement based adhesives, an essential property, which allows the saving of substantial amounts of water, an increasingly scarce resource.

Also, Figure 64 shows that the best mechanical performance in mortars is achieved for a W/C = 0.365, developing higher compressive strengths at all ages than all other samples, due to higher amount of C–S–H formed in this sample, as revealed by Figure 65. This particular result may indicate that below this W/C value, there is not enough water available to proceed with a said regular hydration reaction.

In Figure 67, it is represented the compressive strengths in function of the amount of C–S–H for all mortar samples prepared with the amorphous binder studied in this thesis. It is also shown the compressive strengths in function of the amount of C–S–H for a traditional OPC, CEM I 52.5R, mortar, used as a reference. From the trend line drawn for each data set, it is possible to see that amorphous mortars begin to develop compressive strengths with approximately the same amount of C–S–H (~ 4.8%) of a traditional OPC (~ 5.1%), revealing that below a given percentage of C–S–H formation, there is not enough “glue” to join all the pieces in order to obtain a full three-dimensional interconnected structure. When looking at the slope of the trendlines drawn in Figure 67, it is also possible to see that the hydration products formed during the hydration of this amorphous binder are a more effective material in the conversion of C–S–H to compressive strengths. However, at this moment, amorphous mortars are still unable to reach quantities of C–S–H comparable to those of an OPC mortar, thus cannot reach competitive strengths to those of OPC, especially at younger ages (2 and 7 days). On the bright side, at 28 days, it has been possible to obtain competitive compressive strengths with the amorphous mortar, activated with NaOH + Na_2SiO_3, with a 2.92% Na_2O concentration and a W/C ratio = 0.365, reaching 63.4 MPa, while the reference OPC, CEM I 52.5R, reached 69.0 MPa.

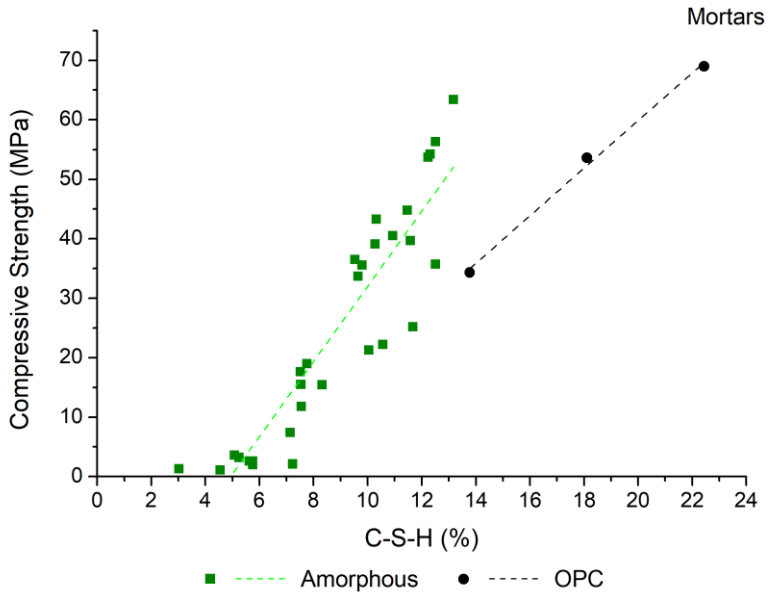

Figure 67 – Comparison of compressive strengths in function of amount of C–S–H of amorphous and OPC mortars.

Figure 68 shows the compressive strengths in function of the amount of C–S–H for all paste samples prepared with the amorphous binder, activated with NaOH + Na_2SiO_3 and a W/C ratio = 0.25, studied in this thesis. It is also shown the compressive strengths, at 2, 7 and 28 days, in function of the amount of C–S–H for a traditional OPC paste, CEM I 52.5R, used as a reference. Like mortars, amorphous pastes show a better conversion of C–S–H to compressive strengths than OPC, requiring less C–S–H (~ 13.2% in amorphous vs ~ 35.8% in OPC) to start developing compressive strength, and for the same amount of C–S–H, for example 50%, amorphous pastes develop almost three times (~ 90 MPa) the compressive strengths of pastes with OPC (~ 33 MPa).

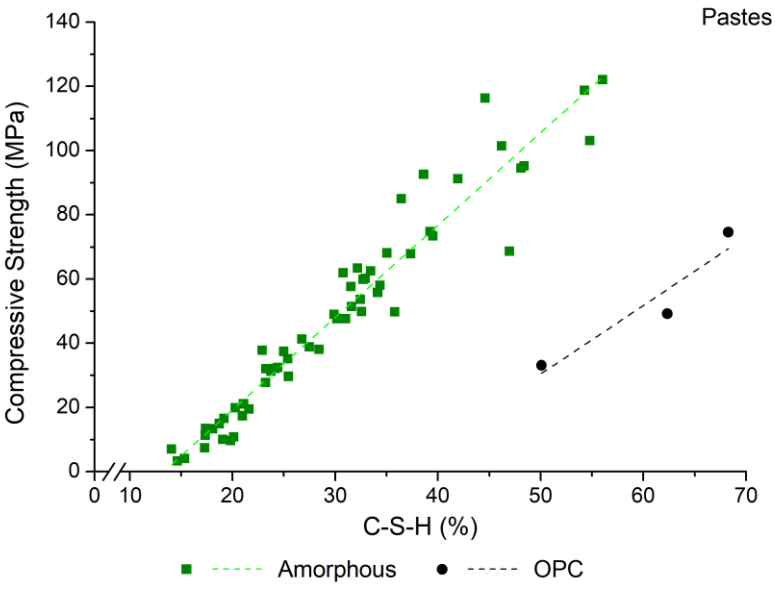

Figure 68 – Comparison of compressive strengths in function of amount of C–S–H of amorphous and OPC pastes.

Comparing the results in mortars and pastes of the amorphous binder obtained in this work and schematized in Figures 67 and 68, respectively, it is possible to verify that, in the upscale from pastes to mortar formulations, the resistances decreased considerably, mainly at young ages, due to the lower content of binder in the formulation (100% wt. in pastes vs. 25% wt. in mortars) and to the increase of the W/C ratio that occurs when changing from paste with W/C = 0.25, for mortar with W/C around 0.365, indicating that it might be helpful to search for a plasticizer that allows to significantly reduce the W/C and that can withstand the alkaline conditions of the binder activation in mortar and concrete formulations. However, this should be investigated in the future since this work showed that, in the case of the mortar formulations, the W/C of 0.365 is very close to the limit of the water needed to promote as effective hydration.

The amount of heat released at 2 and 7 days was plotted with the respective compressive strength for each amorphous and OPC paste with calorimetry results studied in this thesis and a trendline was drawn for each data set, shown in Figure 69. A linear relationship was found between the compressive strength and the amount of heat released until that moment for the amorphous pastes. This relationship can be used to estimate the compressive strength of a paste based only on its cumulative heat release. The negative intercept of the trendline suggests that some heat release is necessary in order to create a group of connected hydrated amorphous particles, providing the support for continuous growth and to begin the development of compressive strength [82].

Furthermore, compared to OPC, to achieve similar compressive strength, the amorphous binder requires significantly less heat than OPC, and also, the amorphous releases substantially less heat of hydration than OPC, making it a low heat binder, a very advantageous feature for large constructions for example, that require more energy efficient materials, capable of not generate massive amounts of heat and thus maintaining a low temperature, even when poured in large quantities.

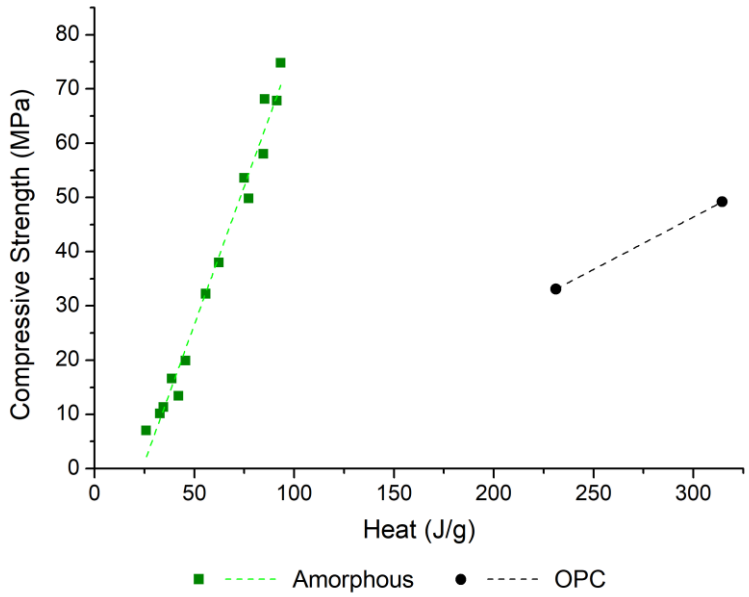

Figure 69 – Comparison of compressive strengths in function of amount of heat released between amorphous pastes and OPC pastes.

6. Conclusions

In this work, low calcium amorphous hydraulic binders with a C/S ratio of 1.1 were produced and chemical and mineralogically characterized. The effect of fineness, the type of mill used in grinding and the storage time after grinding on the binder's hydraulic reactivity were studied. In addition, this thesis also presents the effect of sodium silicate content in the alkaline activation solution and the effect of alternative activators, such as sodium sulphate and calcium sulphate, in the alkaline activation with the purpose of improving, or at least, maintaining a competitive mechanical performance while reducing the costs associated with alkaline activation. Lastly, an optimization of the W/C ratio in mortars was performed to improve the mechanical performance of mortars prepared with the amorphous binder. Paste samples were followed at 2, 7, 28 and 90 days of hydration through different experimental techniques, such as XRD, isothermal calorimetry, compressive strength tests, TGA and FTIR. Mortar samples were followed at 2, 7 and 28 days of hydration through compressive strength tests and TGA. The main conclusions of this thesis are as follows:

In the study of fineness, it was found that pastes prepared with binders with higher fineness (around 6000 cm^2/g of Blaine value) achieved by grinding in the ring mill for 3 minutes reach higher mechanical performances at young ages than pastes prepared with binders with lower fineness (around 4000 cm^2/g of Blaine value, a typical value in the current OPC), achieved by grinding for 1 minute in the ring mill. Pastes prepared with binders with higher fineness showed higher compressive strengths at 2 and 7 days in all samples, as can be seen in Figures 24, 25 and 26. At older ages, 28 and 90 days of hydration, the effects of greater fineness seem to dissipate for the binders with higher amorphous content, section 4.2.1.4, as seen in the pastes prepared with the binder with higher amorphous content, binder B, which showed similar compressive strengths between samples with different fineness (Figure 24). Pastes prepared with binders with lower amorphous content, binder C and D, still revealed some differences in mechanical performance between pastes prepared with different fineness (Figures 25 and 26). Consequently, the amorphous content is a very important property to control, since maintaining an amorphous content above 85% helps to maintain compressive strengths that are competitive with those of the OPC and allows the use of a smaller fineness, reducing the grinding costs without compromising the mechanical performance.

In the study of the type of mill, results showed that pastes prepared with binders ground in different mills, ring mill or ball mill, to a similar fineness, (around 4000 cm_2/g of Blaine value, a typical value in the current OPC) do not show significant differences in mechanical performance, differing by 11% in compressive strengths at 28 days between pastes prepared with binders ground in different mills (Figures 36 and 37) nor in the amount of hydration products formed, diverging at most 5 % (Figures 39 and 40). These results indicate that the microstructure formed during hydration is similar between pastes prepared with binder ground in different mills, suggesting that the type of mill used for grinding the amorphous binder does not have a significant effect on the hydraulic reactivity of the amorphous.

In the storage time study, it was found that the paste prepared with amorphous stored for 7 days showed a slower reaction kinetics than the paste prepared with freshly ground amorphous. The slower

kinetics may be due to some carbonation that occurs on the amorphous surface after being ground. However, after 7 days, this effect is dissipated, as both samples, with and without storage time, released similar amounts of heat of hydration, with the sample with 7 days of storage time releasing 91,3 J/g of heat of hydration and the sample prepared with freshly ground binder releasing 85,4 J/g of heat of hydration (Figure 46). The compressive strengths results were also found to be similar for all ages (Figure 47). Thus, it can be inferred that a storage time of up to 7 days does not have a significant effect on the overall reactivity of the binder, only on the initial kinetics of the reaction of hydration.

In the study of the Na_2SiO_3 content, it was found, by the results of calorimetry (section 5.2.1.2), that the successive decrease of silicate content accelerates the reaction kinetics, but decreases the amount of heat released, indicating that the amount of hydration products formed is lower, which is confirmed by the TGA results in section 5.2.1.4. The results of compressive strength are in agreement with the results of calorimetry and TGA, indicating better mechanical performance for pastes with higher Na_2SiO_3 content after 7 days of hydration (Figure 52). In addition, it is possible to verify that the paste prepared with 75% Na_2SiO_3 shows better mechanical performance than the paste prepared with the concentration used previously in this project, 100% Na_2SiO_3, which allows a reduction in the costs of Na_2SiO_3 in the alkaline activation of this binder.

In the study of Na_2SO_4 and $CaSO_4$ as activators, it was found that pastes prepared with alkaline activation of Na_2SO_4 (section 0) or with alkaline activation of $CaSO_4$ (section 5.2.3.2) develop considerably lower compressive strengths to those developed by pastes activated with Na_2SiO_3, with their mechanical performance being comparable with those of the paste activated with 25% Na_2SiO_3 (Figure 52), which defeats the purpose of using these less expensive activators.

In the study of the optimization of the W/C ratio in alkali-activated mortars, it was concluded, as expected, that the workability is dependent on the amount of water, thus the mortar prepared with W/C = 0.38 showed better workability, and as W/C was reduced, the workability worsened (section 5.2.4.1). Even so, mortars prepared with W/C = 0.38 and W/C = 0.365 showed acceptable workability and a behaviour similar to that of a cement based adhesive. As for the compressive strengths (Figure 64), the best mechanical performances were achieved for W/C = 0.365, with a of 2.92% Na_2O concentration, reaching 63.4 MPa at 28 days, an acceptable result when compared with a mortar prepared with reference OPC, that reaches 69.0 MPa. However, at younger ages, namely 2 and 7 days, alkali-activated mortars are still unable to achieve acceptable mechanical strengths that can be competitive with those of traditional OPC.

Last but not least, it is important to note that this hydraulic binder with low calcium content is capable of developing significantly higher compressive strengths in pastes than those achieved by traditional OPC at all ages and, in mortars, it can already achieve mechanical performance comparable to that of the traditional OPC after 28 days of hydration. These mechanical results coupled with the fact that this binder allows a reduction of about 25% in the amount of CO_2 emitted, reveals the enormous potential of this new binder, providing a solution to answer the environmental problems related to the production of traditional OPC cement.

7. Future work

In order to continue the work done so far on the Nanocimento project, it would be of the greatest interest to further develop the study of this amorphous hydraulic binder. To this end, this chapter suggests some points to be developed in future studies, namely:

- Sample preparation in triplicate, at least, to minimize sample preparation errors and ensure more reliable results.
- Optimization of the chemical composition of the raw meal, prepared with the most common raw materials in the cement industry and from CIMPOR's quarries, mainly its iron and alumina content.
- Study the utilisation of calcium based aggregates in mortar formulations instead of siliceous aggregates like sand, to answer possible drawbacks that may arise from alkali-silica reactions (ASR) between siliceous aggregates and alkaline species.
- Study the mechanical performance of this binder in concrete formulations.
- Development of a plasticizer that can withstand the alkaline medium of the alkaline activation of this binder, a crucial point to reduce the total amount of water needed and, thus, improve the mechanical strengths in the mortar and concrete studies of this binder.
- Improvement of the production conditions, namely the study of a new refractory material for the covering of the silicon carbide crucible and the improvement of the cooling conditions of the melt to increase the amorphous content in the binders produced on a larger scale.

8. Bibliography

1. IEA, *Cement – Tracking Industry*, 2019. [Accessed on 6/06/2020]; Available from: https://www.iea.org/reports/tracking-industry-2019.
2. Hasanbeigi, A., L. Price, and E. Lin, "Emerging energy-efficiency and CO2 emission-reduction technologies for cement and concrete production: A technical review"*, Renewable and Sustainable Energy Reviews*, vol. 16, no. 8, pp. 6220-6238, 2012.
3. Habert, G., "Assessing the environmental impact of conventional and 'green' cement production", in *Eco-efficient Construction and Building Materials*, F. Pacheco-Torgal, et al., Editors, Woodhead Publishing, 2014, pp. 199-238.
4. Andrew, R.M., "Global CO2 emissions from cement production"*, Earth Syst. Sci. Data*, vol. 10, no. 1, pp. 195-217, 2018.
5. Jean-Louis Cohen, G.M.M., *Liquid Stone : New Architecture in Concrete*, 1st ed, Princeton Architectural Press, 2006.
6. *Cement production worldwide from 1995 to 2019*. [Accessed on 14/03/2020]; Available from: https://www.statista.com/statistics/1087115/global-cement-production-volume/.
7. Taylor, H.F.W., *Cement Chemistry*, 2nd ed, Thomas Telford, 1997.
8. Antoni, M., et al., "Cement substitution by a combination of metakaolin and limestone"*, Cement and Concrete Research*, vol. 42, no. 12, pp. 1579-1589, 2012.
9. Staněk, T. and P. Sulovský, "Active low-energy belite cement"*, Cement and Concrete Research*, vol. 68, pp. 203-210, 2015.
10. Provis, J.L. and S.A. Bernal, "Geopolymers and Related Alkali-Activated Materials"*, Annual Review of Materials Research*, vol. 44, no. 1, pp. 299-327, 2014.
11. Santos, R.L., et al., "Novel high-resistance clinkers with 1.10<CaO/SiO2<1.25: production route and preliminary hydration characterization"*, Cement and Concrete Research*, vol. 85, pp. 39-47, 2016.
12. Santos, R.L., et al., "Alkali activation of a novel calcium-silicate hydraulic binder with CaO/SiO2 = 1.1"*, Journal of the American Ceramic Society*, vol. 101, no. 9, pp. 4158-4170, 2018.
13. Hewlett, P. and M. Liska, *Lea's Chemistry of Cement and Concrete*, 5th ed, Elsevier Science, 2019.
14. Bye, G.C., *Portland Cement: Composition, Production and Properties*, 2nd ed, Thomas Telford, 1999.
15. Frauke Schorcht, I.K., Bianca Maria Scalet, Serge Roudier, Luis Delgado Sancho, "Best Available Techniques (BAT) Reference Document for the Production of Cement, Lime and Magnesium Oxide", 2013.
16. CIMPOR, "Declaração Ambiental Alhandra", 2018.
17. Hewlett, P.C., *Lea's Chemistry of Cement and Concrete*, 4th ed, Elsevier Butterworth-Heinmann, 2004.
18. Zhang, Y.M. and T.J. Napier-Munn, "Effects of particle size distribution, surface area and chemical composition on Portland cement strength"*, Powder Technology*, vol. 83, no. 3, pp. 245-252, 1995.
19. Freitas, A.A., et al., "From lime to silica and alumina: systematic modeling of cement clinkers using a general force-field"*, Physical Chemistry Chemical Physics*, vol. 17, no. 28, pp. 18477-18494, 2015.
20. Iacobescu, R.I., et al., "Valorisation of electric arc furnace steel slag as raw material for low energy belite cements"*, Journal of Hazardous Materials*, vol. 196, pp. 287-294, 2011.

21. Koumpouri, D. and G.N. Angelopoulos, "Effect of boron waste and boric acid addition on the production of low energy belite cement"*, Cement and Concrete Composites*, vol. 68, pp. 1-8, 2016.

22. Scrivener, K.L. and A. Nonat, "Hydration of cementitious materials, present and future"*, Cement and Concrete Research*, vol. 41, no. 7, pp. 651-665, 2011.

23. Bullard, J.W., et al., "Mechanisms of cement hydration"*, Cement and Concrete Research*, vol. 41, no. 12, pp. 1208-1223, 2011.

24. Desch, C.H., "The setting of cements and plasters. A general discussion. The mechanism of the setting process in plaster and cement" in *Transactions of the Faraday Society*, 1919, pp. 1-7.

25. Juilland, P., et al., "Dissolution Theory Applied to the Induction Period in Alite Hydration"*, Cement and Concrete Research*, vol. 40, no. 6, pp. 831-844, 2010.

26. Chen, J.J., et al., "Solubility and structure of calcium silicate hydrate"*, Cement and Concrete Research*, vol. 34, no. 9, pp. 1499-1519, 2004.

27. Pellenq, R. and H. Van Damme, "Why Does Concrete Set?: The Nature of Cohesion Forces in Hardened Cement-Based Materials"*, MRS Bulletin*, vol. 29, no. 5, pp. 319-323, 2004.

28. Richardson, I., "Model structures for C-(A)-S-H(I)"*, Acta Crystallographica Section B*, vol. 70, no. 6, pp. 903-923, 2014.

29. Allen, A.J., J.J. Thomas, and H.M. Jennings, "Composition and density of nanoscale calcium–silicate–hydrate in cement"*, Nature Materials*, vol. 6, no. 4, pp. 311-316, 2007.

30. Pellenq, R., et al., "A Realistic Molecular Model of Cement Hydrates"*, Proceedings of the National Academy of Sciences of the United States of America*, vol. 106, no. 38, pp. 16102-16107, 2009.

31. Abdolhosseini Qomi, M.J., et al., "Combinatorial molecular optimization of cement hydrates"*, Nature Communications*, vol. 5, no. 4960, pp. 1-10, 2014.

32. Taylor, H.F.W., "Proposed Structure for Calcium Silicate Hydrate Gel"*, Journal of the American Ceramic Society*, vol. 69, no. 6, pp. 464-467, 1986.

33. Mahasenan, N., S. Smith, and K. Humphreys, "The Cement Industry and Global Climate Change: Current and Potential Future Cement Industry CO2 Emissions" in *Greenhouse Gas Control Technologies - 6th International Conference*, 2003, pp. 995-1000.

34. Fonta, P., "The “Paris agreement” on climate change: An opportunity for cement sector to further reduce its CO2 emissions" in *2017 IEEE-IAS/PCA Cement Industry Technical Conference*, 2017, pp. 1-8.

35. Supino, S., et al., "Sustainability in the EU cement industry: the Italian and German experiences"*, Journal of Cleaner Production*, vol. 112, pp. 430-442, 2016.

36. Gartner, E. and H. Hirao, "A review of alternative approaches to the reduction of CO2 emissions associated with the manufacture of the binder phase in concrete"*, Cement and Concrete Research*, vol. 78, pp. 126-142, 2015.

37. Naqi, A. and J.G. Jang, "Recent Progress in Green Cement Technology Utilizing Low-Carbon Emission Fuels and Raw Materials: A Review"*, Sustainability*, vol. 11, no. 537, pp. 1-18, 2019.

38. Danish, A., M. Salim, and T. Ahmed, "Trends and developments in green cement "A sustainable approach""*, Sustainable Structures and Materials*, vol. 2, no. 1, pp. 45-60, 2019.

39. Samad, S. and A. Shah, "Role of binary cement including Supplementary Cementitious Material (SCM), in production of environmentally sustainable concrete: A critical review"*, International Journal of Sustainable Built Environment*, vol. 6, no. 2, pp. 663-674, 2017.

40. Imbabi, M.S., C. Carrigan, and S. McKenna, "Trends and developments in green cement and concrete technology"*, International Journal of Sustainable Built Environment*, vol. 1, no. 2, pp. 194-216, 2012.

41. Scrivener, K.L., "Options for the future of cement"*, Indian Concr. J*, vol. 88, no. 7, pp. 11-21, 2014.

42. Scrivener, K., et al., "Calcined clay limestone cements (LC3)", *Cement and Concrete Research*, vol. 114, pp. 49-56, 2018.

43. Gartner, E. and T. Sui, "Alternative cement clinkers", *Cement and Concrete Research*, vol. 114, pp. 27-39, 2018.

44. Scrivener, K.L., V.M. John, and E.M. Gartner, "Eco-efficient cements: Potential economically viable solutions for a low-CO2 cement-based materials industry", *Cement and Concrete Research*, vol. 114, pp. 2-26, 2018.

45. Gartner, E., "What are BYF cements, and how do they differ from CSA cements", *Proceedings of the Future of Cement*, vol. 200, pp. 1-9, 2017.

46. Samarakoon, M.H., et al., "Recent advances in alkaline cement binders: A review", *Journal of Cleaner Production*, vol. 227, pp. 70-87, 2019.

47. Juenger, M., et al., "Advances in alternative cementitious binders", *Cement and concrete research*, vol. 41, no. 12, pp. 1232-1243, 2011.

48. Luukkonen, T., et al., "One-part alkali-activated materials: A review", *Cement and Concrete Research*, vol. 103, pp. 21-34, 2018.

49. Santos, R.L., "New Hydraulic Binders with Low Calcium Content", Ph.D dissertation, Instituto Superior Técnico, Univ. de Lisboa, Lisboa, Portugal, 2016.

50. Santos, R.L., et al., "Microstructural control and hydration of novel micro-dendritic clinkers with CaO/SiO2=1.4", *Cement and Concrete Research*, vol. 76, pp. 212-221, 2015.

51. Paradiso, P., et al., "Formation of nanocrystalline tobermorite in calcium silicate binders with low C/S ratio", *Acta Materialia*, vol. 152, pp. 7-15, 2018.

52. Santos, D., et al., "Influence of Pseudowollastonite on the Performance of Low Calcium Amorphous Hydraulic Binders", *Materials*, vol. 12, no. 3457, pp. 1-13, 2019.

53. Horta, R.S.B., et al., "Amorphous low-calcium content silicate hydraulic binders and methods for their manufacturing", CIMPOR - Cimentos de Portugal, SGPS, S.A.; Instituto Superior Técnico, 2019.

54. IPQ, *EN196-1 - Métodos de ensaio de cimentos. Parte 1: Determinação das resistências mecânicas*, 2017.

55. *X-ray Diffraction (XRD)*. [Accessed on 19/03/2020]; Available from: http://web.pdx.edu/~pmoeck/phy381/Topic5a-XRD.pdf.

56. *X-ray Powder Diffraction (XRD)*. [Accessed on 19/03/2020]; Available from: https://serc.carleton.edu/research_education/geochemsheets/techniques/XRD.html.

57. Misture, S.T. and R.L. Snyder, "X-ray Diffraction", in *Encyclopedia of Materials: Science and Technology*, K.H.J. Buschow, et al., Editors, Pergamon, 2001, pp. 9799-9808.

58. Scrivener, K.L., et al., "Quantitative study of Portland cement hydration by X-ray diffraction/Rietveld analysis and independent methods", *Cement and Concrete Research*, vol. 34, no. 9, pp. 1541-1547, 2004.

59. Zhao, P., et al., "Error Analysis and Correction for Quantitative Phase Analysis Based on Rietveld-Internal Standard Method: Whether the Minor Phases Can Be Ignored?", *Crystals*, vol. 8, no. 110, pp. 1-11, 2018.

60. Dwivedi, C., et al., "Electrospun Nanofibrous Scaffold as a Potential Carrier of Antimicrobial Therapeutics for Diabetic Wound Healing and Tissue Regeneration", in *Nano- and Microscale Drug Delivery Systems*, A.M. Grumezescu, Editor, Elsevier, 2017, pp. 147-164.

61. Stuart, B., *Infrared spectroscopy : fundamentals and applications*, 1st ed, J. Wiley, 2004.

62. Subramanian, A. and L. Rodriguez-Saona, "Fourier Transform Infrared (FTIR) Spectroscopy", in *Infrared Spectroscopy for Food Quality Analysis and Control*, D.-W. Sun, Editor, Academic Press, 2009, pp. 145-178.

63. Pane, I. and W. Hansen, "Investigation of blended cement hydration by isothermal calorimetry and thermal analysis", *Cement and Concrete Research*, vol. 35, no. 6, pp. 1155-1164, 2005.

64. Alarcon-Ruiz, L., et al., "The use of thermal analysis in assessing the effect of temperature on a cement paste"*, Cement and Concrete Research*, vol. 35, no. 3, pp. 609-613, 2005.

65. Katsioti, M., et al., "Characterization of various cement grinding aids and their impact on grindability and cement performance"*, Construction and Building Materials*, vol. 23, no. 5, pp. 1954-1959, 2009.

66. IPQ, *EN 196-6 - Métodos de ensaio de cimento. Parte 6: Determinação da finura*, 2019.

67. Sathonsaowaphak, A., P. Chindaprasirt, and K. Pimraksa, "Workability and strength of lignite bottom ash geopolymer mortar"*, Journal of Hazardous Materials*, vol. 168, no. 1, pp. 44-50, 2009.

68. Haach, V.G., G. Vasconcelos, and P.B. Lourenço, "Influence of aggregates grading and water/cement ratio in workability and hardened properties of mortars"*, Construction and Building Materials*, vol. 25, no. 6, pp. 2980-2987, 2011.

69. CEN, *Methods of test for mortar for masonry - Part 3: Determination of consistence of fresh mortar (by flow table)*, 1999.

70. Moon, G.D., et al., "Effects of the fineness of limestone powder and cement on the hydration and strength development of PLC concrete"*, Construction and Building Materials*, vol. 135, pp. 129-136, 2017.

71. Sitarz, M., W. Mozgawa, and M. Handke, "Vibrational spectra of complex ring silicate anions — method of recognition"*, Journal of Molecular Structure*, vol. 404, no. 1, pp. 193-197, 1997.

72. Yu, P., et al., "Structure of Calcium Silicate Hydrate (C-S-H): Near-, Mid-, and Far-Infrared Spectroscopy"*, Journal of the American Ceramic Society*, vol. 82, no. 3, pp. 742-748, 1999.

73. Bhat, P.A. and N.C. Debnath, "Theoretical and experimental study of structures and properties of cement paste: The nanostructural aspects of C–S–H"*, Journal of Physics and Chemistry of Solids*, vol. 72, no. 8, pp. 920-933, 2011.

74. Matson, D.W., S.K. Sharma, and J.A. Philpotts, "The structure of high-silica alkali-silicate glasses. A Raman spectroscopic investigation"*, Journal of Non-Crystalline Solids*, vol. 58, no. 2, pp. 323-352, 1983.

75. Lecomte, I., et al., "(Micro)-structural comparison between geopolymers, alkali-activated slag cement and Portland cement"*, Journal of the European Ceramic Society*, vol. 26, no. 16, pp. 3789-3797, 2006.

76. Paluszkiewicz, C., et al., "Nucleation of hydroxyapatite layer on wollastonite material surface: FTIR studies"*, Vibrational Spectroscopy*, vol. 48, no. 2, pp. 263-268, 2008.

77. Colomban, P., et al., "Raman identification of ancient stained glasses and their degree of deterioration"*, Journal of Raman Spectroscopy*, vol. 37, no. 5, pp. 614-626, 2006.

78. El-Didamony, H., A.A. Amer, and H. Abd Ela-ziz, "Properties and durability of alkali-activated slag pastes immersed in sea water"*, Ceramics International*, vol. 38, no. 5, pp. 3773-3780, 2012.

79. Ismail, I., et al., "Microstructural changes in alkali activated fly ash/slag geopolymers with sulfate exposure"*, Materials and Structures*, vol. 46, no. 3, pp. 361-373, 2013.

80. Puertas, F., et al., "A model for the C-A-S-H gel formed in alkali-activated slag cements"*, Journal of the European Ceramic Society*, vol. 31, no. 12, pp. 2043-2056, 2011.

81. Garcia-Lodeiro, I., et al., "Compatibility studies between N-A-S-H and C-A-S-H gels. Study in the ternary diagram Na2O–CaO–Al2O3–SiO2–H2O"*, Cement and Concrete Research*, vol. 41, no. 9, pp. 923-931, 2011.

82. Bentz, D., et al., "Relating Compressive Strength to Heat Release in Mortars"*, Advances in Civil Engineering Materials*, vol. 1, no. 1, pp. 1-14, 2012.

83. DeCristofaro, N. and S. Sahu, "CO2 – Reducing Cement"*,* Solidia Technologies® – World Cement, 2014.

84. Gong, K. and C.E. White, "Nanoscale Chemical Degradation Mechanisms of Sulfate Attack in Alkali-activated Slag"*, The Journal of Physical Chemistry C*, vol. 122, no. 11, pp. 5992-6004, 2018.

85. Scholtzová, E., et al., "Structural and spectroscopic characterization of ettringite mineral – combined DFT and experimental study"*, Journal of Molecular Structure*, vol. 1100, pp. 215-224, 2015.

86. Zuo, Y. and G. Ye, "Preliminary Interpretation of the Induction Period in Hydration of Sodium Hydroxide/Silicate Activated Slag"*, Materials*, vol. 13, no. 21, pp. 4796, 2020.

87. Ben Haha, M., et al., "Influence of activator type on hydration kinetics, hydrate assemblage and microstructural development of alkali activated blast-furnace slags"*, Cement and Concrete Research*, vol. 41, no. 3, pp. 301-310, 2011.

9. Annexes

Table 23 – Compilation of results for each sample of paste and mortar in the fineness study.

	XRD	Fineness	Calorimetry results			Compressive strength (MPa)				Bound water (%)			
Sample	Amorphous (%)	Blaine (cm^2/g)	Peak (Hours)	QH 2D (J/g)	QH 7D (J/g)	2 days	7 days	28 days	90 days	2 days	7 days	28 days	90 days
A_145min_Ball	90,4	3874	33,8	33,4	75		53,6				3,50		
A_3min_Ring	90,4	4097	9,1	56,8	85,4		68,1	116,3			3,78	4,81	
A_145+0.5min_Ball+Ring	90,4	4360	24,4	46,5	84,9		58,0	122,1			3,71	6,05	
B_1min_Ring	85,5		23,4	42,5	77,1		49,8	91,2	101,4		3,51	4,53	4,99
B_3min_Ring	85,5		9,1	65,4	93,3		74,8	95,2	103,0		4,24	5,22	5,91
C_1min_Ring	76,8	4120				3,3	27,7	51,4		1,58	2,51	3,41	
C_3min_Ring	76,8	5973				17,4	59,8	73,3		2,26	3,53	4,26	
D_1min_Ring	82,5	4054				9,7	38,9	55,7		2,14	2,96	3,69	
D_3min_Ring	82,5	6517				35,1	60,1	92,5		2,74	3,55	4,17	
Mor_A_145min_Ball	90,4	3874				2,6	25,2	53,7		0,62	1,26	1,32	
Mor_A_145+0.5min_Ball+Ring	90,4	4360				7,4	35,7	63,4		0,77	1,35	1,42	

Table 24 – Compilation of results for each sample of paste and mortar in the mill study.

	XRD	Fineness	Calorimetry results			Compressive strength (MPa)				Bound water (%)			
Sample	Amorphous (%)	Blaine (cm^2/g)	Peak (Hours)	QH 2D (J/g)	QH 7D (J/g)	2 days	7 days	28 days	90 days	2 days	7 days	28 days	90 days
C_1min_Ring	76,8	4120				3,3	27,7	51,4		1,58	2,51	3,41	
C_180min_Ball	76,8	4085				4,1	32,0	57,6		1,66	2,51	3,40	
D_1min_Ring	82,5	4054				9,7	38,9	55,7		2,14	2,96	3,69	
D_220min_Ball	82,5	4351	25,8	32,8	62,2	10,1	38,0	62,5		2,06	3,07	3,61	
Mor_C_1min_Ring	76,8	4120				1,3	15,4	43,3		0,33	0,90	1,11	
Mor_C_180min_Ball	76,8	4085				1,0	11,0	36,8	54,2	0,49	0,81	1,11	1,33

Table 25 – Compilation of results for each sample of paste in the storage time study.

	XRD	Fineness	Calorimetry results			Compressive strength (MPa)				Bound water (%)			
Sample	Amorphous (%)	Blaine (cm^2/g)	Peak (Hours)	QH 2D (J/g)	QH 7D (J/g)	2 days	7 days	28 days	90 days	2 days	7 days	28 days	90 days
A_3min_Ring_1dayST	90,4	4097	9,1	56,8	85,4		68,1	116,3			3,78	4,81	
A_3min_Ring_7daysST	90,4		21,8	55,9	91,3		67,8	68,6	118,7		4,03	5,07	5,86

Table 26 – Compilation of results for each paste sample in the Na_2SiO_3 study.

Sample	XRD	Fineness	Calorimetry results			Compressive strength (MPa)				Bound water (%)			
	Amorphous (%)	Blaine (cm^2/g)	Peak (Hours)	QH 2D (J/g)	QH 7D (J/g)	2 days	7 days	28 days	90 days	2 days	7 days	28 days	90 days
D_2%Na_2O_100%Na_2SiO_3	82,5	4351	25,8	32,8	62,2	10,1	38,0	62,5		2,06	3,07	3,61	
D_1.819%Na_2O_75%Na_2SiO_3	82,5	4351	19,9	35,8	60,3	10,8	37,4	63,3		2,17	2,70	3,47	
D_1.638%Na_2O_50%Na_2SiO_3	82,5	4351	14,2	38,8	55,8	16,6	32,2	47,5		2,07	2,61	3,35	
D_1.456%Na_2O_25%Na_2SiO_3	82,5	4351	6,5	34,5	45,7	11,3	19,9	29,7		1,87	2,19	2,75	
D_1.275%Na_2O_0%Na_2SiO_3	82,5	4351	4,2	25,9	42,1	7,0	13,4	19,5		1,52	1,88	2,33	

Table 27 – Compilation of results for each paste sample in the Na_2SiO_3 mixtures study.

Sample	XRD	Fineness	Calorimetry results			Compressive strength (MPa)				Bound water (%)			
	Amorphous (%)	Blaine (cm^2/g)	Peak (Hours)	QH 2D (J/g)	QH 7D (J/g)	2 days	7 days	28 days	90 days	2 days	7 days	28 days	90 days
D_1.638%Na_2O_50%Na_2SiO_3	82,5	4351	14,2	38,8	55,8	16,6	32,2	47,5		2,07	2,61	3,35	
D_2%Na_2O_50%Na_2SiO_3+50 %Na_2SO_4	82,5	4351				15,0	31,2	47,6		2,02	2,56	3,25	
D_1.638%Na_2O_50%Na_2SiO_3 +50%$CaSO_4$	82,5	4351				13,4	21,1	32,3		1,95	2,27	2,64	

Table 28 – Compilation of results for each paste sample in the Na_2SO_4 study.

	XRD	Fineness	Calorimetry results			Compressive strength (MPa)				Bound water (%)			
Sample	Amorphous (%)	Blaine (cm^2/g)	Peak (Hours)	QH 2D (J/g)	QH 7D (J/g)	2 days	7 days	28 days	90 days	2 days	7 days	28 days	90 days
D_2%Na_2O_1.66%wt.Na_2SO_4	82,5	4351				11,8	21,3	30,0		1,90	2,36	3,03	
E_2%Na_2O_1.66%wt.Na_2SO_4	88,3	5471				8,5	17,5	23,9		1,86	2,77	3,47	
F_2%Na_2O_1.66%wt.Na_2SO_4	90					11,7	21,8	28,6		2,02	2,85	3,41	
D_3.275%Na_2O_4.58%wt.Na_2SO_4	82,5	4012	3,3	40,2	61,3	11,7	20,8	33,6		2,00	2,72	3,51	

Table 29 – Compilation of results for each paste sample in the $CaSO_4$ study.

	XRD	Fineness	Calorimetry results			Compressive strength (MPa)				Bound water (%)			
Sample	Amorphous (%)	Blaine (cm^2/g)	Peak (Hours)	QH 2D (J/g)	QH 7D (J/g)	2 days	7 days	28 days	90 days	2 days	7 days	28 days	90 days
D_1.275%Na_2O_1.59%wt.$CaSO_4$	82,5	4351				6,8	12,6	18,0		1,38	1,82	2,14	
E_1.275%Na_2O_1.59%wt.$CaSO_4$	88,3	5471				6,6	15,4	24,1		1,66	2,10	2,72	
D_1.275%Na_2O_4.39%wt.$CaSO_4$	82,5	4012	22,1	15,5	38,8	1,9	8,8	19,3		1,17	1,91	2,77	

Table 30 – Compilation of results for each mortar sample in the W/C ratio study.

	XRD	Fineness	Compressive strength (MPa)				Bound water (%)			
Sample	Amorphous (%)	Blaine (cm^2/g)	2 days	7 days	28 days	90 days	2 days	7 days	28 days	90 days
Mor_D_3.04%Na_2O_W/C = 0.38	82,5	4012	2,0	15,5	33,7		0,62	0,81	1,04	
Mor_D_2.92%Na_2O_W/C = 0.365	82,5	4351	3,6	21,2	40,1	56,3	0,55	1,08	1,22	1,35
Mor_D_2.80%Na_2O_W/C = 0.35	82,5	4012	2,6	17,6	35,5		0,61	0,81	1,06	
Mor_D_2.68%Na_2O_W/C = 0.335	82,5	4012	3,2	19,0	36,5		0,57	0,84	1,03	